Année 2010 **N° d'ordre : 40352**

Université Lille 1 Sciences et Technologies

Laboratoire Génie Civil et géo-Environnement Lille Nord de France (EA 4515)

École Doctorale Sciences Pour l'Ingénieur (SPI 072)

THESE

Pour obtenir le grade de

Docteur de l'Université de LILLE 1

Spécialité : Génie Civil

Présentée par

AJORLOO Ali Mohammad

Characterization of the Mechanical Behavior of Improved Loose Sand for Application in Soil-Cement Deep Mixing

Caractérisation du comportement mécanique d'un sable lâche amélioré avec du ciment - Application à la technique du « Deep Mixing »

Soutenue publiquement le 20 septembre 2010

Devant le jury composé de :

I. SHAHROUR, Professeur, Université Lille 1	**Président du Jury**
J.C ROBINET, Professeur, INSA Rennes	**Rapporteur**
D. DIAS, Maitre de Conférences HDR-INSA Lyon	**Rapporteur**
H. MROUEH, Maitre de Conférences HDR, Université Lille 1	**Directeur de thèse**
L. LANCELOT, Maitre de Conférences, Université Lille 1	**Invité**

Année 2010 **N° d'ordre : 40352**

Université Lille 1 Sciences et Technologies

Laboratoire Génie Civil et géo-Environnement Lille Nord de France (EA 4515)

École Doctorale Sciences Pour l'Ingénieur (SPI 072)

THESE

Pour obtenir le grade de

Docteur de l'Université de LILLE 1

Spécialité : Génie Civil

Présentée par

AJORLOO Ali Mohammad

Characterization of the Mechanical Behavior of Improved Loose Sand for Application in Soil-Cement Deep Mixing

Caractérisation du comportement mécanique d'un sable lâche amélioré avec du ciment - Application à la technique du « Deep Mixing »

Soutenue publiquement le 20 septembre 2010

Devant le jury composé de :

I. SHAHROUR, Professeur, Université Lille 1	**Président du Jury**
J.C ROBINET, Professeur, INSA Rennes	**Rapporteur**
D. DIAS, Maitre de Conférences HDR-INSA Lyon	**Rapporteur**
H. MROUEH, Maitre de Conférences HDR, Université Lille 1	**Directeur de thèse**
L. LANCELOT, Maitre de Conférences, Université Lille 1	**Invité**

Résumé

Les technologies de mélange de sol en profondeur (« deep mixing ») pour le soutènement des excavations sont de plus en plus utilisées dans le monde. Le mélange de sol en profondeur devient une alternative plus économique aux systèmes traditionnels de soutènement pour les travaux d'excavation, pour la conception des fondations superficielles, l'analyse de la stabilité des talus et de la liquéfaction des sols. Ceci nécessite un développement plus poussé des modèles décrivant le comportement mécanique des sols ainsi améliorés, comme base pour accroitre la sécurité et diminuer les coûts économiques.

Cette thèse est basée sur l'étude en laboratoire des caractéristiques de résistance au cisaillement d'un sable siliceux modifié avec du ciment de Portland, seul ou en combinaison avec des liants à réactions lentes (pouzzolaniques) comme des fumées de silice et de la chaux. Les effets de la cimentation sur la résistance, la rigidité et le comportement contractant-dilatant du sable cimenté sont étudiés au cours d'essais de compression simple, de traction, de cisaillement direct et de compression triaxiale drainée pour des éprouvettes maturées jusqu'à 180 jours. Plus précisément, les relations contrainte-déformation, les modes de rupture, les paramètres de résistance au cisaillement pour le sable lâche et dense, le module de cisaillement et de compression, les réponses volumétriques, l'état critique des sols cimentés sont décrits et discutés. En outre, cette étude vise à développer une formulation « Ready Mix », où le type de liant utilisé et le rapport eau/ciment ou eau/liant jouent un rôle fondamental dans l'évaluation de la résistance visée pour une utilisation en « deep mixing » de sols granulaires de type SM (resp SP) dans la classification LPC (resp USCS).

Le comportement contrainte-déformation des sables cimentés est non linéaire avec une alternance contractance-dilatance. Les résultats montrent que la réponse contrainte-déformation est fortement influencée par la pression de confinement et la teneur en ciment. La raideur et la résistance sont grandement améliorées par l'augmentation de la teneur en liant. Un comportement plus fragile a été démontré à faible pression de confinement et avec de hautes teneurs en ciment. Une augmentation de l'angle de résistance au cisaillement et de la cohésion avec l'augmentation de la teneur en ciment a été observée de façon uniforme. Pour le sable sans ciment, la résistance au pic correspond au taux maximum d'expansion volumétrique, alors que pour le sable cimenté elle représente une condition où la sommation de toutes les composantes prend son intensité maximale. Finalement, la corrélation entre la résistance à la compression simple et l'indice lié à la réaction pouzzolaniques de la chaux et de la fumée de silice a été discutée.

Mots-clés : sol-ciment, mélange en profondeur, sable siliceux, dilatance, fumées de silice, réactions pouzzolaniques, triaxial, état critique, comportement fragile

Abstract

The use of deep soil mixing technology for excavation support is growing worldwide. As soil deep mixing becomes a more economical alternative to traditional support systems for excavation, shallow foundation design and analysis of slope stability and liquefaction of soil, the amelioration of models describing the mechanical behavior of improved soil is required, as a basis for cost-effectiveness and a safer design.

This work features a laboratory study of shear strength of a loose silica sand modified with Portland cement only or in combination with high curing time binders (due to pozzolanic reactions) such as lime and silica fume. The effects of cementation on the stress–strain behavior, stiffness and strength of treated sand are investigated through unconfined compression tests, tensile strength tests, direct shear tests and drained triaxial compression tests, for curing times up to 180 days. More precisely, stress-strain relationships, failure modes, shear strength parameters for loose and dense sand, compressibility and volumetric responses, critical state of cemented sand are described and discussed. In addition, this study attempts to develop a « ready mix » design procedure, where the type of binder, water/cement or water/ binder ratios play a major part in the assessment of the targeted strength in deep soil mixing applications for loose granular soils (SP in the unified classification).

The results show that the stress–strain behavior of cemented sands is nonlinear with contractive–dilative stages. The stress-strain response is strongly influenced by effective confining pressure and cement content. Stiffness and strength were greatly improved by an increase in binder content. An increase of the angle of shearing resistance and cohesion intercept with increasing cement content was observed consistently. Brittle behavior was observed at low confining pressure and high cement content. For uncemented sand, the peak strength occurs for a maximum rate of volumetric expansion, whereas for cemented sand it represents a condition where the summation of all components the maximum intensity become. Finally, the correlation of unconfined compression strength with the index of pozzolanic reaction of lime and silica fume is discussed.

Keywords**:** soil-cement, deep mixing, silica sand, strength–dilatancy, silica fume, pozzolanic reactions, triaxial, critical state, brittle behavior

Acknowledgement

This thesis would not have been prepared without God blessing and extremely hard work of Professors and Colleagues as well as patience and encouragement of my Family.

My special thanks are directed to the President and all the personnel of ***The University of Science and Technology of Lille (USTL)*** *and* ***The Power and Water University of Technology of Tehran (PWUT)*** *who helped me to do my research by all means.*

I wish to express my best gratitude and sincere thanks to my supervisors in this research, ***Prof. H. MROUEH*** *and* ***Dr. L. LANCELOT*** *who did their best to guide me from different points of view. They not only directed me but also supported me patiently through their kind advice and comments.*

I would like to express my sincere gratitude to ***Prof. I. SHAHROUR*** *who guided me through different discussion and comments on the research.*

My thanks are also directed to all reporters and examiners of the thesis for their review and comments.

Last but certainly not least, I would like to express my deepest gratitude for the continuous support, caring, understanding and love that I received from my wife, daughter and son, without whom this work would not have been conducted. Similar appreciation is extended to my late father, sisters and brothers. Thank you all.

Table of Contents

List of Tables

GENERAL INTRODUCTION

General Introduction

Scope

Poor soil conditions can impair the integrity of existing structures, thus special soil treatment methods can be required during the construction phase in order to allow the project to proceed. The beneficial effects of a cementing agent on the performance of geotechnical structures have been widely documented (Dupas and Pecker 1979; Clough and Sitar 1981; Clough et al. 1988).The work of Leroueil and Vaughan (1990) unambiguously showed that similar patterns of behavior are observed irrespective of the origin and strength of the cementation. Major purposes of treatment are to eliminate, the danger of excessive settlement, to increase the strength, to ensure the safety and the stability of surrounding buildings, to reduce the permeability (Shroff and Shah, 1999). Cementing agents such as cement, lime, or fly ash may also be introduced *in situ* to weaker soils with specialized ground improvement technologies such as the deep mixing method (Porbaha 1998).

Recent research work has demonstrated that cemented soil can be modeled by the effective stress principle (Cuccovillo and Coop 1997; Gens and Nova 1993). It has been extensively reported that a cementing agent will increase the effective cohesion. Experimental evidence suggesting the destruction of bonding between soil grains at low strain was reported by Saxena and Lastrico (1978). The failure surface of the cemented soil was found to be considerably curved relative to the parent soil. Lade and Overton also showed that the higher strength of the cemented samples was related partly to the higher dilatancy rate at failure. The higher stiffness of cemented soils has been successfully explained by a number of researchers (Malandraki and Toll 1994 and Cuccovillo and Coop 1997). The precise properties obtained reflect the characteristics of the native soil, the construction variables (principally the mixing method), the operational parameters, and the binder characteristics (Bruce and Bruce, 2003). Different types of binder like lime and lime-cement have been used for deep mixing in Sweden (Ahnberg, 2006). The strength and stiffness properties of stabilized soil, with the use of low curing binder like lime and silica fume, have been found to change considerably with time, mainly due to different chemical reactions taking place. Studies of the influence of these

factors are needed in order to improve the models describing the mechanical behavior of improved soil as a basis for safer and more cost-effective design of soil improvement by deep mixing.

Objectives

This work aims at studying experimentally the mechanical behavior of an improved loose silica sand with the addition of Portland cement only or with a lime and silica fume mixture in a slurry form. This type of cementing agent is considered to be representative of that used in cement-stabilized construction and is also capable of reflecting the roles of other cementing agents. Besides, there still exists no dosage methodologies based on rational criteria as in the case of the concrete technology, where the water/cement ratio or water/ binder ratio plays a fundamental role in the assessment of the targeted strength. This is why this study attempts to develop a ready mix design method for deep soil-cement mixing and to detect correlations between unconfined and triaxial behavior of the soil-cement mix, for a fine silica sand similar to Hostun-RF, well studied in the French research community, to propose improvement coefficients that can be factored into the calculation works.

Layout of the thesis

Following this general introduction, the dissertation is organized in five chapters. **Chapter 1** proposes a literature review is presented to attempt a state-of-the-art in ground improvement studies, focussing on the deep mix method. It also describes the means used to control the uniformity of treatment before, during and after soil mixing. The general background theory for the behavior of sands and cemented soils is also presented: stress-strain behavior, shear strength, volumetric responses, large deformations and critical state, and finally engineering properties of grouted sands in unconfined, tensile strength and triaxial compression.

Chapter 2 deals with the materials and testing methods: a description of the silica sand used in this study, together with the binders and other additions are presented, and details of the experimental procedures are given. The preparation processes used for the formation of the different types of samples tested are explained. A full description of the testing procedures

used is given: drained triaxial tests, permeability measurement in a triaxial cell, direct shear tests, unconfined compression tests, tensile strength tests.

Chapter 3 consists of a synthesis of experimental results. The chapter starts off by discussing the effects of binders on improved soil properties**,** linking binders' reactions and changes in basic geotechnical properties. It is shown that the increase in strength with time after improvement is governed by a number of factors. Most of the chapter is dedicated to presenting, discussing and assessing the behavior of cemented sand, based on all the triaxial tests data. Then a study of stress dilatancy and bond breakages is presented. Finally the use of the pozzolanic reaction index due the lime and silica fume in the cemented sand is summarized and discussed.

The report ends with a general discussion and a conclusion.

Chapter 1:

LITERATURE REVIEW

1 LITERATURE REVIEW

1.1 Introduction

Mostly, the intent of soil improvement by addition of binders is to modify the soil so that its properties become similar to that of a soft rock such as clay shale or lightly cemented sandstone. Mixing various binders into a soil will bring about significant changes in most of the soil properties. The strength properties of cemented soil are affected by different factors. The factors regarded as being important in this research are the type of soil, the type and quantity of binder and the curing conditions, for various stress conditions.

A hypothesis in studying the strength behavior was that the improved soils would exhibit strength and deformation properties similar to over consolidated natural soils, making it possible to describe the strength and deformation properties with the same set of parameters as those normally used for natural soils.

Findings from previous researchers are cross-compared and examined in an attempt to present a general background to the mechanics of sands and cemented sand against which the behavior of this kind of sand will be examined in Chapters 2 and 3.

1.2 Ground Improvement by the Deep Mix Method (DMM)

1.2.1 A Deep Mix Example

Deep mixing has become a general term to describe a number of soil improvement/soil mixing techniques. The US Federal Highway Administration (FHWA) has suggested that these techniques be classified based on:

- The method of additive injection (i.e.dry vs. wet injection),
- The method by which the additive is mixed (i.e. high pressure jet or rotary/mechanical energy),
- The location of the mixing tool/paddles (i.e. along a portion or at the end of the drilling rods).

The stabilizing agent is usually a slurry mixture of cement, water, and sometimes bentonite. The material resulting from this mixing operation with small amounts of cement has the advantage of improved strength and stiffness. Figure 1.1 gives examples values of the strengths of soil, soil cement and concrete and the typical arrangement of soil cement columns for excavation support.

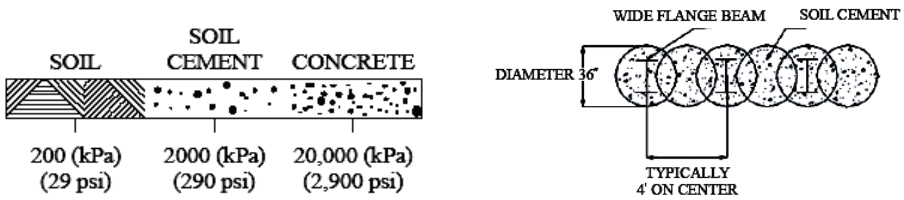

Figure 1.1 *Strength Comparison and typical Soil Cement Columns (Ratherford, 2004)*

The Fort Point Channel DMM project used three different water cement (w/c) ratios (0.7, 0.8, and 0.9) and five different cement factors (CF) of Portland Type I/II cement (2.2, 2.3, 2.5, 2.6 and 2.9 kN/m^3) throughout the duration of the project (McGinn and O'Rourke, 2003). Analysis of the unconfined compressive test results showed a statistically significant relationship between increased compressive strength and rising w/c and CF. The compressive strength of soil cement increased by a factor of 2.5 as CF increased from 1.93 to 2.91 kN/m^3 for a w/c=0.7. Improved mixing and blending of cement with in situ soils allowed for increased water content in the field, contributing to a more homogenous soil cement product with increased compressive strength.

1.2.2 Existing Data for DMM Design

The main focus of the geomaterial design is that a quality product (continuously mixed soil cement with no openings or joints) must be achieved to satisfy the minimum strength and other design requirements. It is thus important for the design engineer to understand the factors contributing to the strength and permeability of the soil cement. For instance, the unconfined compression strength specified for an excavation support cutoff wall is usually greater than 700 kPa and the hydraulic conductivity usually ranges from 10^{-5} to 10^{-6} cm/s (Taki and Yang, 1991). Variations in soil conditions, mixing process and sampling

procedures contribute to the variability of the data. Treated soil properties have been studied by Bruce (2003) and are summarized in Table 1.1.

Table1.1 *Typical data on soil treated by deep mixing (Bruce,.2003)*

WET METHODS	
PROPERTY	**TYPICAL RANGE**
Unconfined Compresion Strength UCS (typically at 28 days)	0.2 - 5.0 MPa (0.5 - 5 MPa in granular soils) (0.2 - 2 MPa in cohesive soils)
Permeability K	1×10^{-6} to 1×10^{-9} m/s (lower if bentonite is used)
E_{50}	350 to 1000 times U.C.S. for lab samples and 150 to 500 times U.C.S. for field samples
Shear strength (direct shear, no normal stress)	40 to 50% of U.C.S. at U.C.S. values < 1 MPa, but this ratio decreases gradually as U.C.S. increases.
Tensile strength	Typically 8 - 14% U.C.S.
28-day U.C.S.	1.4 to 1.5 times the 7-day strength for silts and clays. 2 times the 7-day strength for sands
60-day U.C.S.	1.5 times the 28-day U.C.S., while the ratio of 15-year U.C.S. to 60-day U.C.S. may be as high as 3:1. In general, grouts with high w/c ratios have lower long-term strength gain beyond 28 days.
DRY METHODS	
Undrained shear strength, c_u	10 to 50 times c_u of soil (150 to 1000 kPa)
Young's Modulus	50 to 200 times c_u 50 to 200 times q_u of treated soil (cement only)
Strain at failure	< 2%
Permeability (lime cement) Permeability (lime)	About the same as for *in situ* soils Increases 100 to 1000 times

There is a lack of information on drained shear strength of treated soils, especially when compared to the abundance of data for unconfined compressive testing.

1.2.3 Advantages of DMM

There are many advantages of DMM compared to other soil improvement methods and traditional techniques. The placement of DMM columns causes little disturbance to

surrounding soil, therefore allowing installation close to an adjacent building's foundation. The construction is also typically faster than other traditional methods. The ability to create soil cement columns to stabilize the base against deep rotational failure is also an important advantage. The strength of the soil cement columns can be changed based on project requirements by varying the ratio of cement and water to the in situ soil. This allows the designer to control deformations through soil cement specifications and system stiffness (Ratherford, 2004).

1.2.4 Applicability of DMM

The various DMM techniques can be used to produce a wide range of treated soil structures on both land and marine projects. The particular geometry chosen is dictated by the purpose of the DMM application, and reflects the mechanical capabilities and characteristics of the particular method used. The main groups of applications are reported by Bruce and Bruce (2003) as follows: hydraulic cut-off walls (Japan, U.S.), excavation support walls (Japan, China, and U.S.), liquefaction mitigation (Japan, U.S.), environmental remediation (U.S., Western Europe). In general, DMM is most attractive in projects where:

- The ground is neither very stiff nor very dense, nor contains boulders or other obstructions,
- Treatment depths of less than about 40 m are required,
- Treated ground strengths have to be closely engineered (typically 0.1 to 5 MPa).

Earthquakes are one of the major natural hazards that threaten human life while damaging high-cost infrastructures. Yasuda (1993) reported hundreds of soil improvement projects for liquefaction mitigation in Japan during 1985–1990, including the use of deep mixing. In selecting soil improvement methods for preventing liquefaction, priority is usually given to construction efficiency, reliability, and cost-effectiveness. For improving the engineering characteristics of the liquefiable ground, the loose soil at the bottom and/ or periphery of the structure is replaced by an underground solid body, comprising overlapped columns,

that aims at restraining shear deformation below the structure. The overlapped units are shaped to produce a block, lattice (or grid), wall, and group of columns, as studied by Porbaha (1998) for various patterns of deep mixing (schematically illustrated in Fig. 1.2a). However, due to the high cost of improvement, the basic idea is to create a solid skeleton with adequate stiffness to resist shearing deformation. In this regard, the lattice-type improvement has been the most common configuration used for liquefaction mitigation, as shown in Fig. 1.2b.

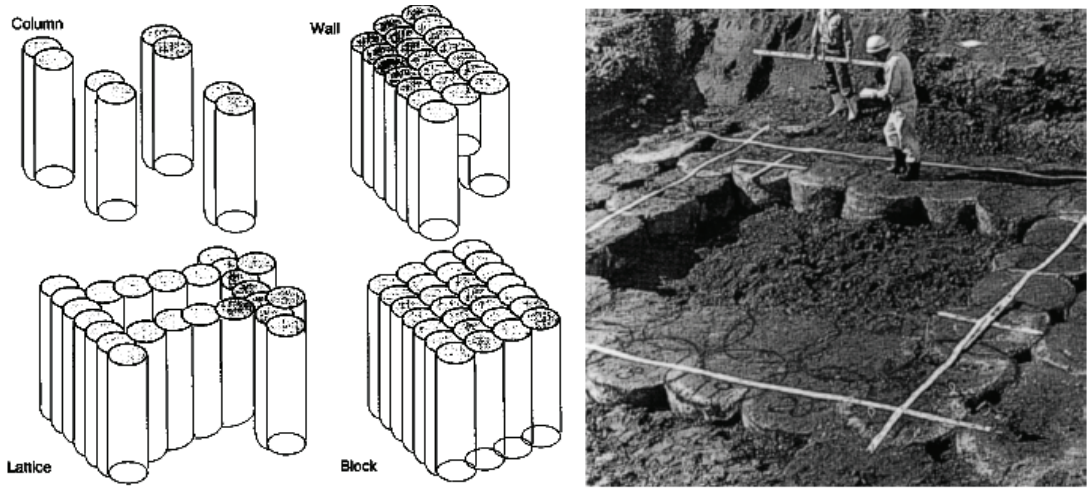

Figure 1.2 *(a) Various Patterns of Deep Mixing, (b) Lattice-Type Improved Ground (Porbaha, 1998)*

The feasibility of the application of DMM to excavations as studied by Ratherford (2004) depends on site conditions and economics. Sites with ground settlement sensitivity, vibration sensitivity, high groundwater table, and/or soft soils are often good candidates for the use of DMM. Since the placement of DMM columns causes little disturbance to surroundings when rotation/extraction is controlled, the method can be used in soils close to a building's foundation.

Numerous projects have incorporated deep mixing for temporary excavation support and base stability (Pearlman and Himick, 1993; Yang and Takeshima, 1994; O'Rourke and O'Donnell, 1997; Bahner and Naguib, 1998; Bruce, 2000; McMahon et al. 2001; Yang 2003).

1.3 Laboratory experiments for lime – cement columns

The following results are based on Jacobson (2002) and focus on important factors affecting strength gain in lime-cement columns and on laboratory procedures for preparing test specimens and determining the strength of lime-cement-soil mixtures.

1.3.1 Important factors affecting strength gain in lime-cement columns

The laboratory results studied by Ahnberg (1996) show that most fine-grained soils have the potential for improvement, given the right combination of lime and cement. Strength gain in lime-cement columns is primarily due to particle bonding induced by the cement, as well as reactions taking place between the lime and the surrounding soil.

The added binder produces free calcium cations (Ca^{++}), which replace dissimilar adsorbed cations on the colloidal surface. Practically all fine-grained soils display rapid cation exchange and flocculation-agglomeration reactions when treated with lime and/or cement in the presence of water. Pozzolans are materials that react with water and calcium to produce a cementing effect. A pozzolan is defined by ASTM as "*a silicious or aluminous material, which in itself possesses little or no cementation value, but will, in finely divided form and in the presence of moisture, chemically reacts with calcium hydroxide at ordinary temperatures to form compounds possessing cementitious properties*". Pozzolans that provide silica as a result of mineralogical breakdown in a high pH environment, with the addition of lime and silicious minerals in clay and soils, will react with the lime to produce calcium silicates and aluminates that bond the particles together. Pozzolanic reactions are time and temperature dependant, with lime hydration requiring more hydration time than cement.

For clay soils, Miura *et al.* (2002) suggest that the prime factor governing the engineering parameters of cement-stabilized soil is the clay-water/cement ratio, *wc/c*. This is defined as the ratio of initial water content of the soil (%) to the cement content (%). The cement content is the ratio of cement to clay by weight in their dry state. For wet–mixing processes, the additional water input into the soil is taken into account in the numerator of

the *wc/c* ratio. This parameter helps to control the input of cementing agent to attain strength development with curing time and clay water content, and also aids in understanding the subsequent engineering behavior.

1.3.2 Types of Stabilization Agents, Dosage Rates and Proportions

Stabilizers used in lime-cement columns are of course lime and cement. Lime is produced from natural limestone, and the particular type of lime formed depends on the parent material and the production process (Lambe, 1969). The most widely used and best performing limes in soil stabilization are the high calcium quick limes and hydrated (slaked) limes. Of these two, research has shown that quicklime usually produces a better stabilization effect. In clays with high organic and/or high sulfide content, experience has shown that large proportions of cement are required in combination with lime additive to achieve sufficient strength (Ahnberg *et al.,* 1989). Eades and Grim (1966) suggest that for 100 percent lime mixes; the optimum lime content for most soils is between 2 and 5 percent of the dry soil by weight. In a laboratory mix design study by Ahnberg *et al.* (1999) where several binder types are used, the ratios used are those listed in Table 1.2, with a typical ratio being 25:75 lime/cement for a dosage rate of 150 kg/m^3:

Table1.2 *Typical Binder Types and Proportions, Ahnberg et al. (1999)*

Binder 1	Binder 2	Binder 3	Binder ratio
Cement Std	Lime		80:20
Cement Std	Lime		50:50
Cement SH	Lime		50:50
Cement Std	Slag		50:50
Cement Std	Fly ash		50:50
Cement Std	Fly ash	gypsum	40:40:20
Slag	Fly ash	gypsum	40:40:20
Cement Std	Slag	gypsum	40:40:20
Cement Std	Slag	silica dust	45:45:10

1.3.3 Effect of curing condition and confining pressure in strength gain of lime-cement

Esrig (1999) stated that most strength gain occurs within the first 28 days after mixing, and strength continues to increase at a slower rate thereafter. When normalized by the 28-day

strength, the results show that all binder mixtures produced essentially the same rate of strength gain. Generally, long-term strength increase is more pronounced in lime stabilization than cement stabilization due to the longer time required to complete the pozzolanic reactions in that case. As curing temperature increases, the rate of pozzolanic reactions also increase resulting in an increased rate of strength gain. Another issue that affects the curing process is the ambient ground temperature, which can range from 8° to 14° C or more (Esrig 1999).

Confining pressure can be applied to samples in order to mimic overburden stresses. Pousette *et al.* (1999) found that for peat samples, increasing the load during curing time from 10 to 40 kPa, increased strength by 85%. The density of the peat samples after consolidation increased significantly, indicating that higher load leads to a larger consolidation, a higher density, and a more stable sample. Ahnberg (1994) reported that an increase in confining pressure produced an increase in the drained shear strength and in that respect triaxial tests were more suitable for simulating in-situ conditions

1.3.4 Strength and Secant Modulus of Elasticity for Lime-Cement Treated Soils

The variation of the 14-day undrained shear strengths of lime-cement columns studied by Kivelo (1998) and determined by unconfined compression tests ranges from 0 to more than 500 kPa, as shown in Figure 1.3. It is shown to vary significantly with the soil type and the lime and cement content. The shear strength, which is half the unconfined compressive strength, decreases in general with increasing water content and with increasing organic content. Investigations by Kukko and Ruhomaki (1995) and by Ahnberg *et al.* (1994) indicate that the dosage rate, the lime-cement ratio and the water content of the soil are the main factors affecting shear strength. The deformation of soil improved with lime-cement under an axial load is governed by the stiffness, or modulus of elasticity, of the columns and of the base soil between the columns (Kivelo 1998).

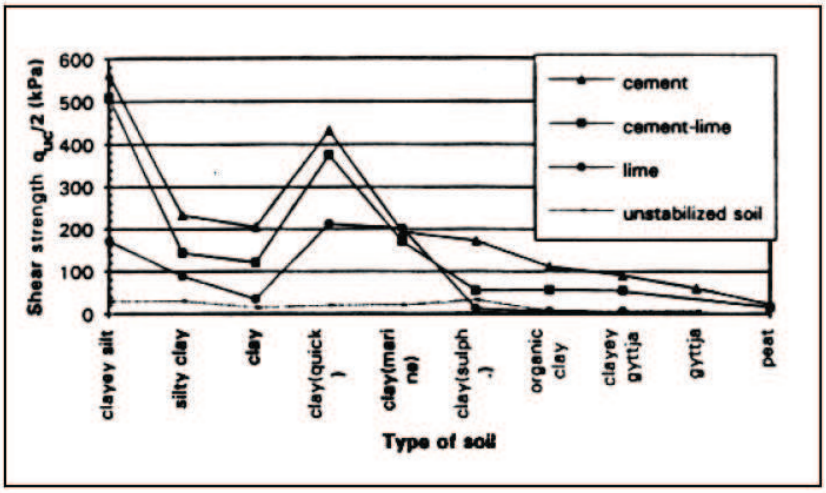

Figure 1.3 *Effect of Cement, Lime-cement (25:75), and Lime 14 days after stabilization of different types of soils in the laboratory (Ahnberg et al., 1994)*

The modulus of elasticity of lime-cement columns has been investigated by Ekstrom (1994) in unconfined compression tests, triaxial tests, and in-situ load tests. Figure 1.4 shows E_{50}, or secant modulus, versus half the unconfined compressive strength, obtained from both in-situ lime-cement columns and on samples prepared in the laboratory.

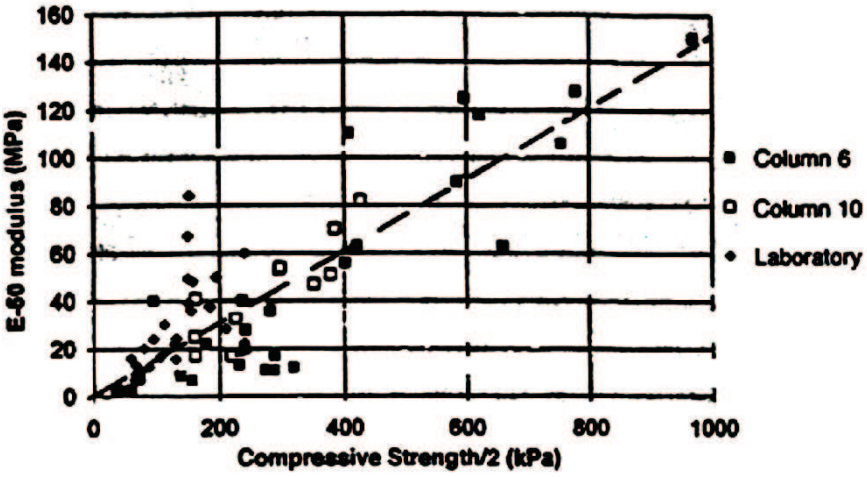

Figure 1.4 *Relation between unconfined compressive strength of lime-cement columns and modulus of elasticity E_{50} (Ekstrom 1994)*

The results show that the ratio of the undrained E_{50} modulus to the unconfined compressive strength is normally 50 to 150. The line corresponding to a ratio of 75 is plotted in the figure.

1.4 Elements on Mechanical Behavior of Soils and Soil-Cement Mix

1.4.1 Generalities on soils mechanical behavior

The physical theories relating to the mechanical behavior of soils when they are subjected to shearing or compression will be recalled hereafter. The emphasis here is on soil behavior in the saturated condition.

In an elastic material the deformation resulting from the imposition of a stress is a function of that stress, and the effect is fully reversible. If the relationship between strain and stress is linear over a certain range, Hooke's law is applicable within that range. The elastic parameters used in stress analysis, and the conditions to which they relate, are summarized in figure 1.5

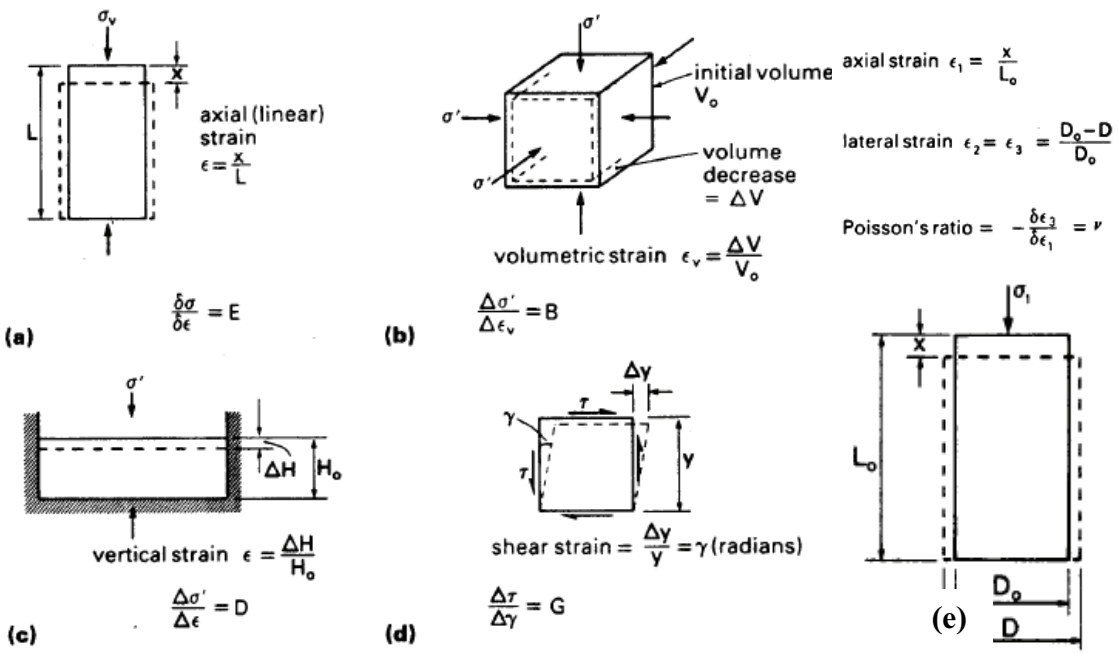

Figure 1.5 *Representation of elastic parameters: (a) Young's modulus (E), (b) bulk modulus (B), (c) constrained modulus (D), (d) shear modulus (G) ,(e) Poisson's ratio (ν) , (Head. k.h., 1988)*

In a given soil, the parameters vary according to conditions such as stress level, previous stress history, depth and orientation.

However the stress-strain behavior of soils is known to be non linear, and can take many different forms between the idealized 'elastic' and 'plastic' relationships. Fig. 1.6 (a) is

typical of the 'brittle' behavior of dense sands and over consolidated clays, and Fig.1.6 (b) represents the 'ductile' behavior of very loose sands and normally consolidated clays. Elastic parameters assigned to soils are linear approximations over a limited range of stress.

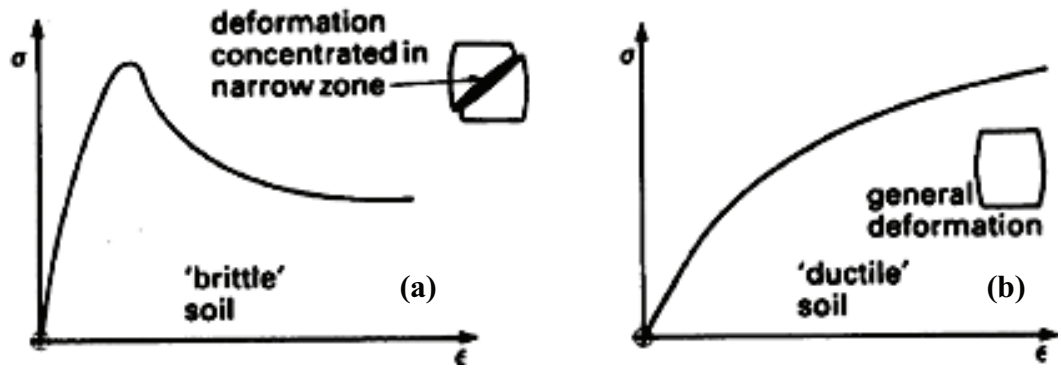

Figure 1.6 *Stress-strain relationships for: (a) typical 'brittle' soil, (b) typical 'ductile' soil, (after Head, 1988)*

For the specified failure criterion it is necessary to be able to relate the shear strength τ on a potential failure surface to the stress normal to that surface, denoted by σ_n (total stress) or σ'_n (effective stress). The effective stresses on a plane of failure are given by the Coulomb equation, which can be written in effective stress as:

$$\tau'_f = c' + \sigma'_n \tan\phi' \quad (1.1)$$

The angle of shearing resistance ø', relating to effective stresses, is a measure of internal friction between the grains, which is present in all soils. The shear strength parameters c' and ø' can be obtained from a set of triaxial compression tests by plotting the Mohr circles of effective stress representing the selected failure condition and drawing the envelope to them. The shear stress on the failure plane at failure, τ_f for a particular test, can be derived as shown in Fig. 1.7. The value of τ_f is given by the ordinate of the point P at which the Mohr circle of failure touches the strength envelope, denoted by:

$$\tau'_f = \frac{1}{2}(\sigma'_1 - \sigma'_3)_f \cos\phi' \quad (1.2)$$

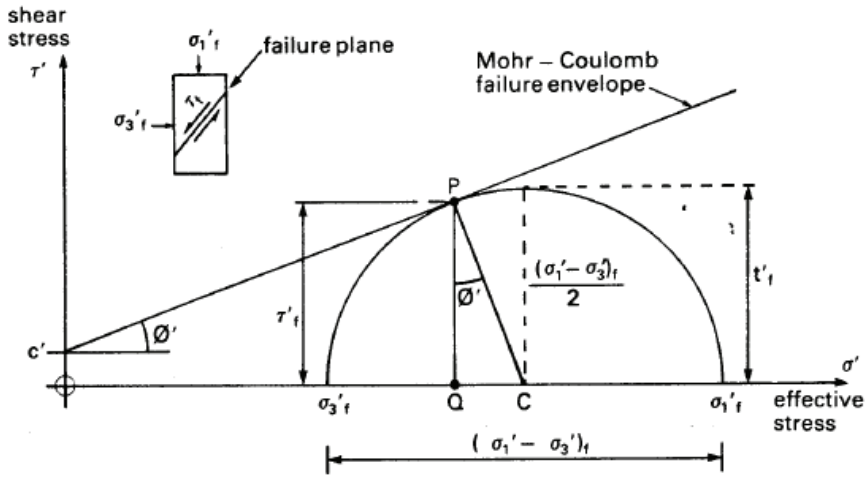

Figure 1.7 *Derivation of soil shear strength parameters, (Head, 1988)*

1.4.2 Criteria for Determining the Shear Strength in Loose and Dense Sands

Typical curves relating shear stress, volume change and void ratio to displacement in a shear test are drawn in Fig. 1.8b, 1.8e and 1.8d, for loose (L) and dense sand (D). In the Coulomb plot relating shear resistance to normal stress (Fig. 1.8a), the sharp rise to the peak strength at P for dense sand is represented by DP, giving a peak angle of shear resistance φ'_p .The shear strength then falls to C and the angle reduces to φ'_c. In contrast, the angle of shear resistance of the loose sand rises slowly to a maximum value φ'_c after a very large displacement without first attaining a peak value. For both samples, the condition at C is marked by a flattening of the volume change or void ratio curves (Fig. 1.8e and 1.8d), indicating that shearing is then taking place at constant volume. Both samples have reached the same density, and therefore the same void ratio (*critical* void ratio): the state at C is known as the *critical state* for that applied normal stress.

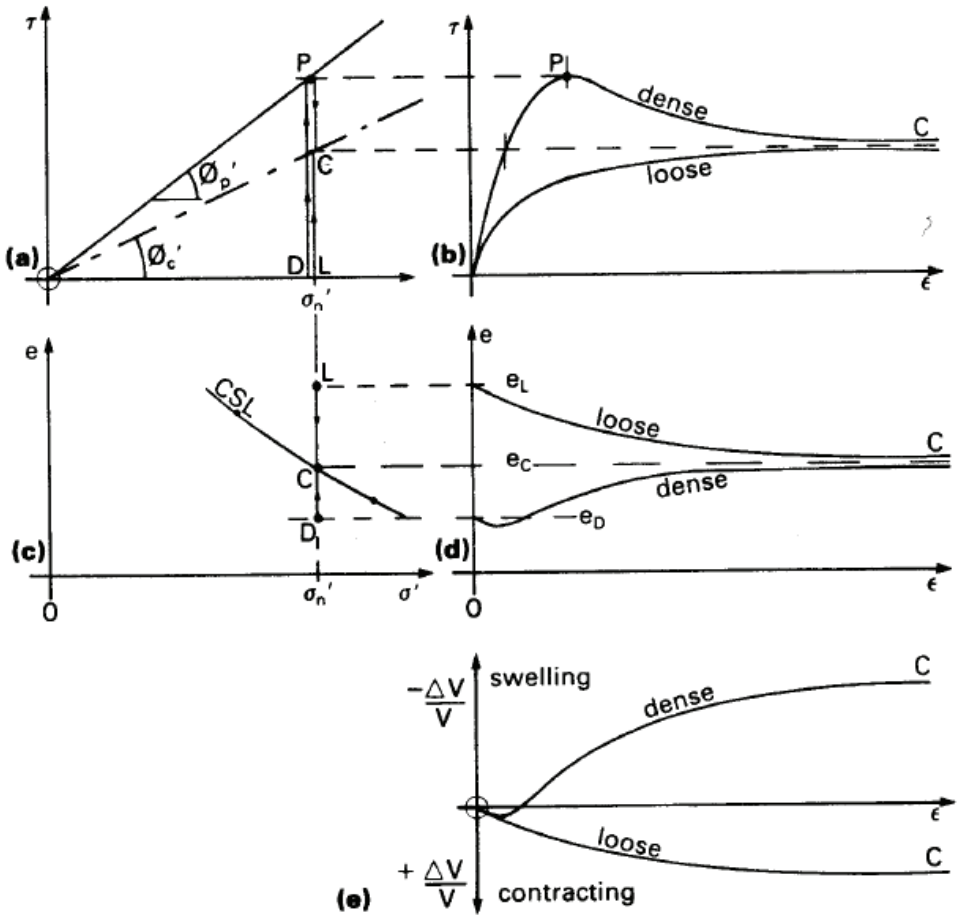

Figure 1.8 *Shear characteristics of dense and loose sands : (a) Coulomb-plot, (b) shear stress against displacement, (c) voids ratio changes during shear, (d) voids ratio changes against displacement, (e) volume change against displacement, (Head et al, 1988)*

The shear strength at the critical state is a fundamental property of a particular soil and depends only on the effective stress. In contrast, the 'peak' strength is dependent on the initial density (or void ratio). The angle of shear resistance at peak is made up of two components: the frictional constant value φ'_c and a variable dilatancy component related to initial void ratio. The latter is positive for sands that are initially denser than the critical density (e_o less than e_c) and negative for sands that are less dense (e_o greater than e_c).

It has been shown that shear strength, principal stresses and deformations in cemented soils under drained conditions are similar to the relationships referred to above for dense sands.

1.4.3 Compression Behavior of Sands

Fig 1.9 was found in Dano (2001) and illustrates the response of loose and dense sand samples under monotonic triaxial compression. Two main parameters control the evolution of the deviator stress q and the volumetric strain ε_v: the compactness of the granular structure and the stress state. Initially, the sand undergoes a contraction of volume called contractancy accompanying an increase in deviator stress more or less quickly depending on the initial soil compactness and the average stress applied. This contraction, reflecting a tangle of grains, fades gradually to eventually vanish, either definitively in the case of loose sand, or occasionally in the case of dense sand.

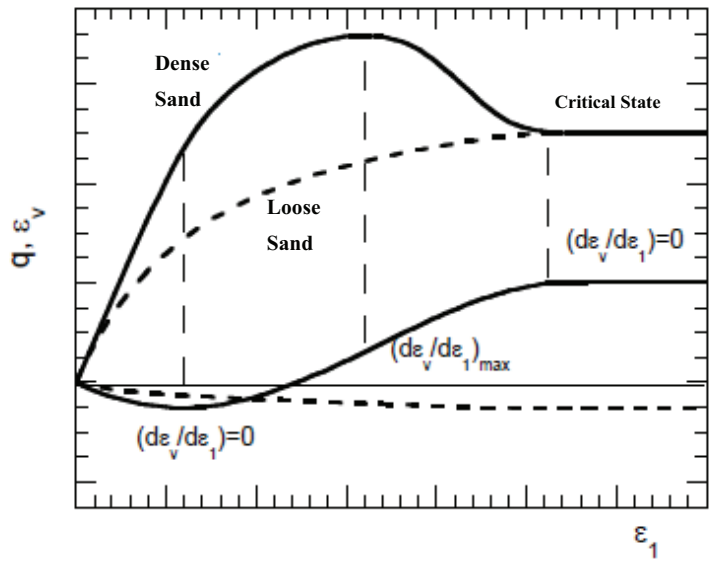

Figure 1.9 *Triaxial test on loose or dense sand, (Dano, 2001)*

For larger deformations in the case of loose sand, it tends to a constant volume deformation simultaneous to shear with a constant deviator characteristic of perfect plasticity, independent of the initial density.

In the case of dense sand, the contraction phase is followed by a phase of dilatancy linked to a disentanglement of the granular structure. The dilatancy is more important when the grains are initially closely packed and when the average stress is low. The maximum expansion ratio, represented by the inflection point of the volumetric deformation versus axial strain curve, is reached for the maximum value of the deviator. In addition, the

deviator decreases thereafter to reach eventually a state of perfect shear plasticity characterized by a constant volume.

The behavior of sands in isotropic compression can be presented from a range of initial specific volumes v (v is defined as v=e+1). As the tests progress and a high enough pressure is reached, all the different compression curves for the different initial densities converge to a unique line that is defined as the Normal Compression Line (NCL). The equation of the NCL in a specific volume v versus log of average pressure p' space is as follows:

$$v = N - \lambda \ln p' \quad (1.3)$$

Where, N is the value of v if the NCL is projected to an effective stress p' = 1 kPa and λ is its gradient. By conducting a series of tests and combining all the final critical state points in q-p' space, the slope M of the Critical State Line (CSL) can be derived. In Fig.1.10 a schematic stress – strain behavior of sands for various stress levels is reported by Coop (1999). In a v-lnp' space, the behavior can be directly associated with the starting point of the test relative to the location of the CSL.

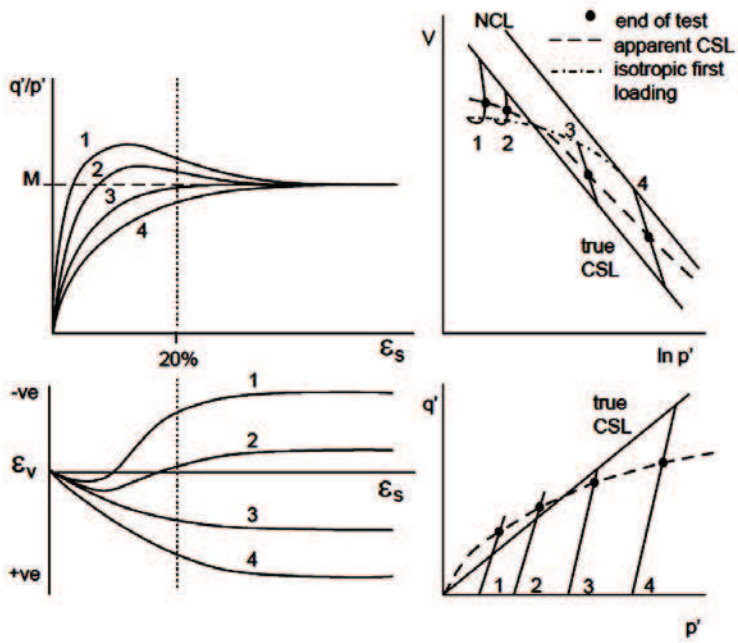

Figure 1.10 *Effects of incomplete testing on the identification of the CSL (Coop, 1999)*

The isotropic NCL and the CSL are parallel having the same inclination with different

offsets at p' = 1 kPa, so that the equation for the CSL is as follows (Ventouras, 2005):

$$v = \Gamma - \lambda \ln p' \quad (1.4)$$

Where, Γ is the specific volume at p' = 1 kPa and λ is the slope of the line.

At large strains a linear relationship between the stress ratio q/p' and the rate of dilation $\delta\varepsilon_v/\delta\varepsilon_s$ exists (Fig. 1.11) and the representative equation is as follows:

$$\frac{q}{p'} = M - a\left[\frac{\delta\varepsilon_v}{\delta\varepsilon_s}\right] \quad (1.5)$$

Where, *a* is a constant. According to Equation 1.5, when $\delta\varepsilon_v/\delta\varepsilon_s = 0$ it is expected that q/p'=M.

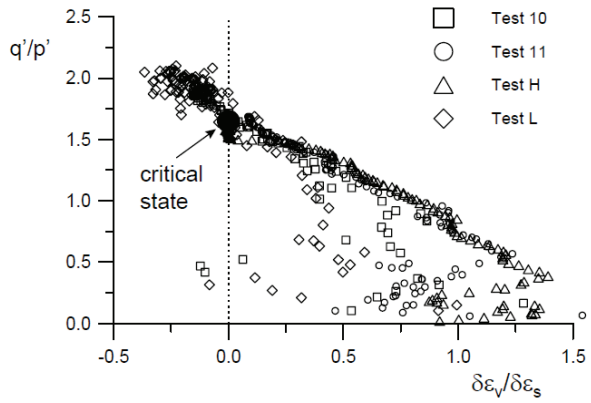

Figure 1.11 *Stress dilatancy data for Dogs Bay sand (after Coop, 1990)*

Creswell and Powrie (2004) showed a clear difference in behavior between the intact and reconstituted samples (Fig.1.12): the intact samples are associated with much higher dilation rates compared to the reconstituted samples.

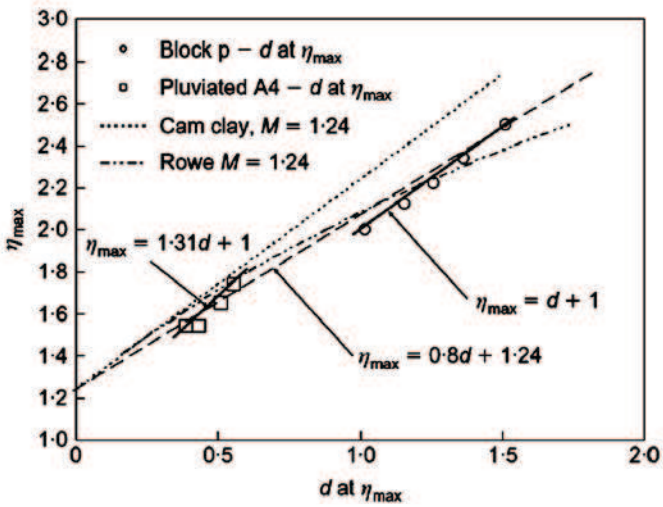

Figure 1.12 *Rate of dilation d, at the maximum stress ratio, η_{max}, for tests on both intact and pluviated A4 sand at different cell pressures (after Cresswell & Powrie, 2004)*

Fig.1.13 reported by Ventouras (2005) shows that the end-points lie on the same line regardless of sample type or sampling method. In addition it shows the CSL from all tests based on an average value of M=1.3, which corresponds to a φ'_{cs} of 32.3°.

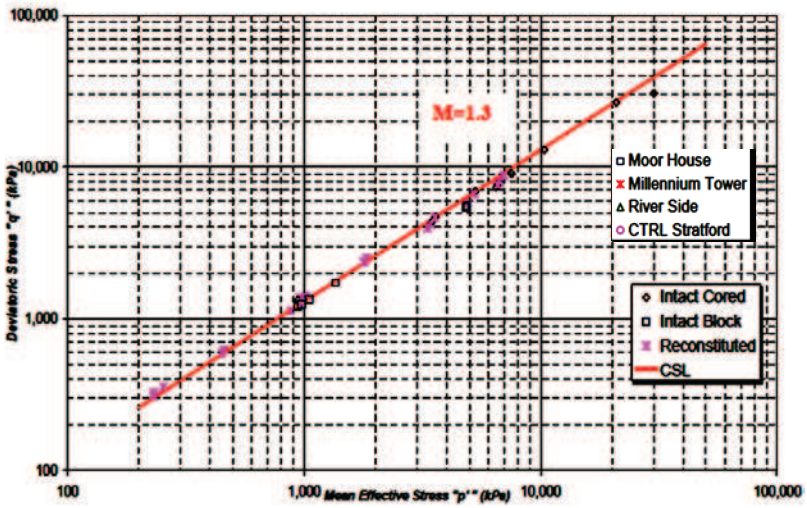

Figure 1.13 *Sample type comparison for critical states in the q-p' plane, including the chosen CSL (Ventouras, 2005)*

1.4.4 Mechanical Behavior and Engineering Properties of Grouted Sands

1.4.4.1 Unconfined Compression Strength

Unconfined uniaxial compression tests were performed by Dano (2004) to assess the effect of certain parameters on the strength of grouted sands. It was noted that, for most soil–

cement mixtures, the strength depends mainly on the cement content of the grout and on the grain-size distribution, the mineralogy, and the relative density of the granular skeleton. Fig.1.14a represents the evolution of the unconfined compressive strength, R_c, of the pure microfine cement grout (IJ) and the evolution of the unconfined compressive strength, R_c of the Fontainebleau sand (FS) at Dr =78%.

Based on these results R_c is related to relative density D_r and the cement-to-water ratio C/W by the equation:

$$R_c = A_0 *(C/W)^N \qquad (1.6)$$

The values of the two parameters A_0 and N are determined by fitting the experimental data. According to Fig.1.14b in the case of the microfine cement grout (IJ), we have:

$$R_c = 40.0*(C/W)^2 \qquad (1.7)$$

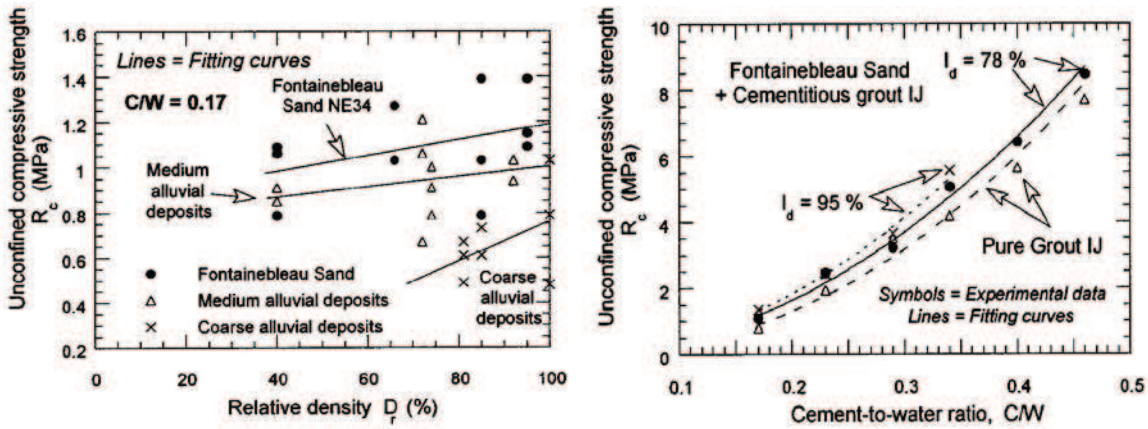

Figure 1.14 *Effect of cement to water ratio and relative density, D_r on unconfined compressive strength R_C of grouted sands: (a) effect of relative density, D_r; and (b) evolution of unconfined compressive strength R_c with cement to water ratio. (Dano, 2004)*

1.4.4.2 Tensile Strength

The bonds produced by the hydration and the setting of the cement also provide a tensile strength for the soil–cement mixture. Dano (2004) reported that the unconfined compression strength R_c, and the direct tensile strength R_{TD} are related to the shear resistance parameters c' and ϕ' as follows:

$$R_{TD} = \frac{2c' \times \cos\varphi'}{1+\sin\varphi'} \qquad (1.8)$$

$$R_C = \frac{2c' \times \cos\varphi'}{1 - \sin\varphi'} \quad (1.9)$$

It was found that R_{TD} / R_c for standard values of the friction angle is approximately 20 %.

1.4.4.3 Triaxial Compression Strength

In Dano (2004), specimens of grouted sands were prepared in the laboratory by injection of very fine cement or mineral grouts, and the results of drained triaxial tests on grouted Fontainebleau sand are shown in Fig. 1.15. It shows the beneficial effect that the grout injection has on the strength and on the stiffness of soil. It also confirms general trends for cement-treated soils:

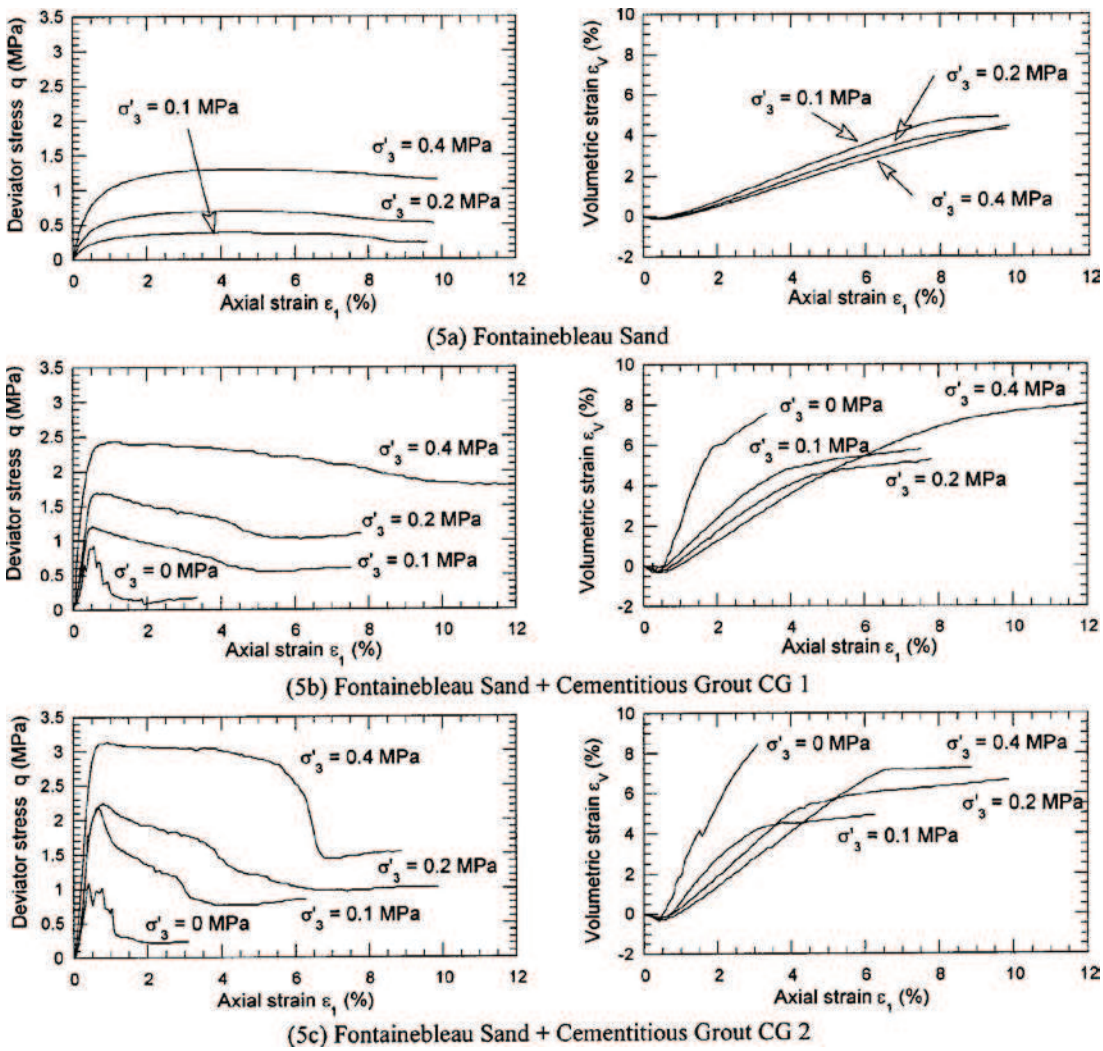

Figure 1.15 *Drained triaxial tests (NF P 94-074) on Fontainebleau sand where σ_3'= constant effective lateral stress during triaxial tests, Dano (2004)*

- a stiffness and strength increase as the binder content increases;

- a typically contractive–dilative volumetric behavior (for grouted sands, when compared to uncemented sands, the contractancy domain is slightly reduced and the slope of the volumetric strain variation in the dilatancy stage increases).
- a more brittle post peak behavior for cementitious grouts for low confining pressures and high cement contents (failure occurs with visible vertical cracks for high cement-to-water ratios and low confining pressures, whereas strain localization with inclined shear bands occurs for low cement-to-water ratios and high confining pressures).

Poisson's ratio v can be deduced from the initial slope of the curve in the contractancy domain (Eq. 1.10), whereas the dilation angle ψ is conventionally related to the maximum slope of the $\varepsilon_v - \varepsilon_1$ curve (Eq. 1.11) at the inflection point in the dilatant stage, as follows:

$$\left(\frac{\Delta\varepsilon_v}{\Delta\varepsilon_1}\right) = 1 - 2v \qquad (1.10)$$

$$\left(\frac{\Delta\varepsilon_v}{\Delta\varepsilon_1}\right)_{\max} = \left(\frac{-2\times\sin\psi}{1-\sin\psi}\right) \qquad (1.11)$$

However, the values of ψ should be considered with care for grouted sands for low confining pressures because of the strain localization effects mentioned earlier.

1.4.5 Engineering Properties of Stabilized Soft Soils

A study on two types of clay and two types of organic soil stabilized with different types of binders was performed by Ahnberg (2006). Cement, lime, blast furnace slag and fly ash in different combinations were used as binders. Unconfined compression tests and triaxial tests were used to investigate the strength of the various samples stabilized in the laboratory. The results reported by Babasaki *et al.* (1996) and Ahnberg (1996) showed that the increase in strength of soft soils with time after stabilization is governed by a number of factors such as the type and amount of binder, the mixing effort, the temperature and the stresses during curing. Fig.1.16 shows examples of the increase in unconfined compressive strength, for the two clays stabilized with various binders (Ahnberg, 2005).

The increase in unconfined compressive strength for the cement-stabilized soils, which were cured at 7° C from 7 to 800 days, is approximately described by the expression:

$$\frac{q_t}{q_{28}} \approx 0.3.\ln t \qquad (1.12)$$

Where, t is the time (days), and q_t and q_{28} are the unconfined compressive strengths after t days and 28 days, respectively (Figure 1.17).

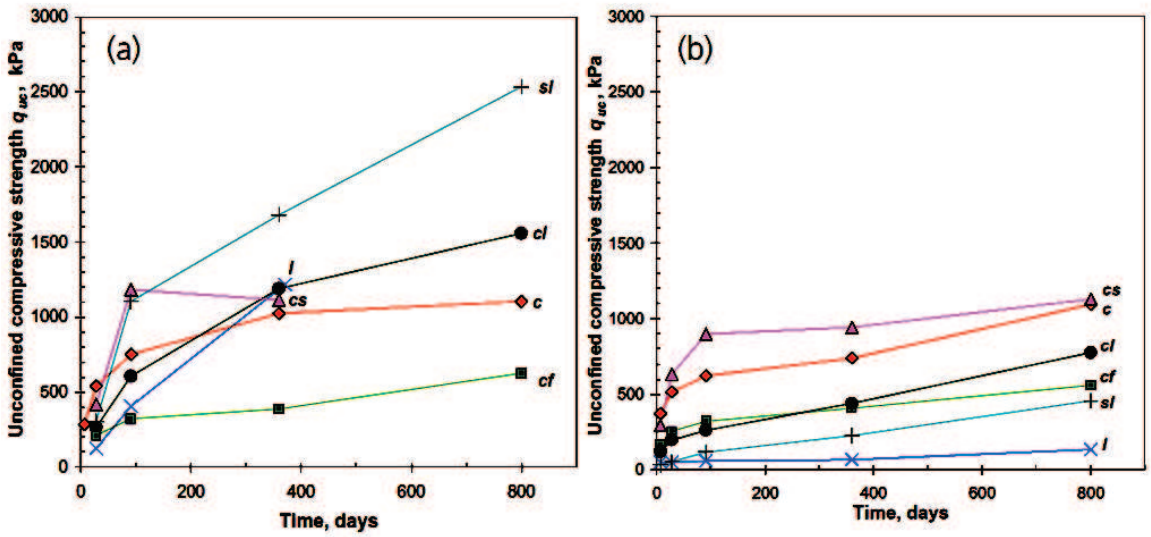

Figure 1.16 *Examples of variation of measured strength with time after mixing for (a) Loftabro clay and (b) Linkoping clay with cement, lime and various composite binders (50:50). c = cement, l = lime, s = slag, f = fly ash, Binder quantity100 kg/m^3 (Ahnberg, 2005)*

Equation (1.12) is similar to relationships reported previously for cement-stabilized soils (Porbaha *et al.* 2000, Horpibulsuk *et al.* 2003).

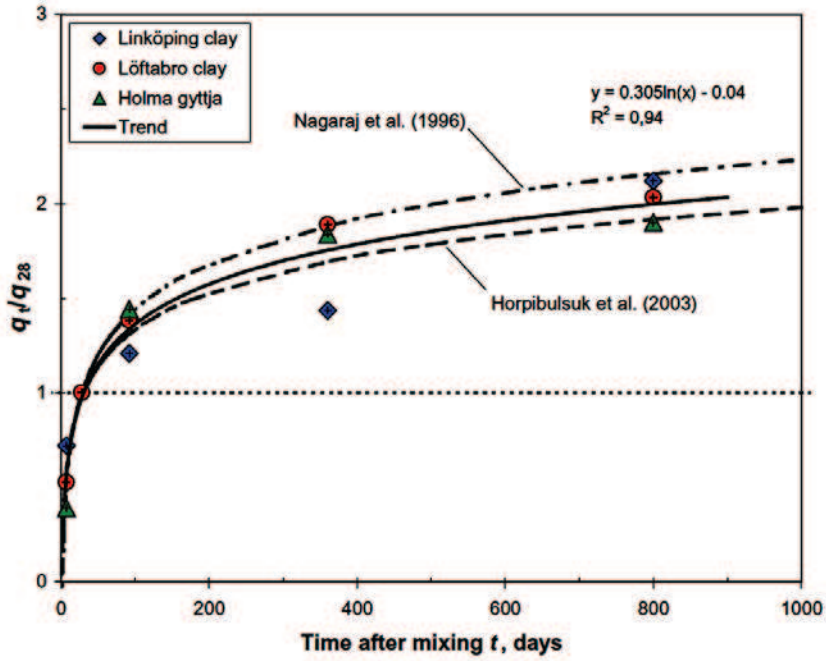

Figure 1.17 *Relative increases in unconfined compressive strength with time for cement-stabilized soft soils (Ahnberg, 2006)*

Estimated variations in the amount of reaction products that can be produced by common types of binders are presented by Ahnberg (2005) in Fig.1.18.

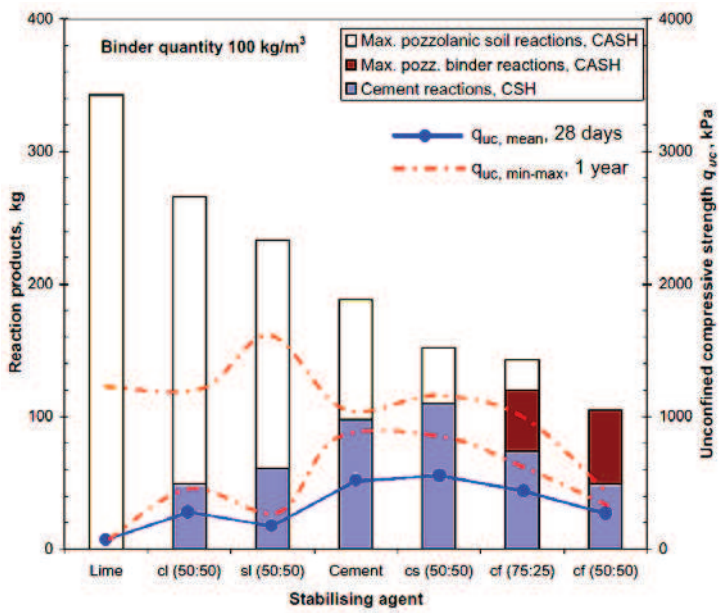

Figure 1.18 *Estimates of the amount of reaction products contributing to the strength of stabilized soils (bars) together with measured strength for one month (—•—) and one year (- - -) after mixing. c = cement, l = lime, s = slag, f = fly ash. (Ahnberg, 2005)*

The blue, or pale shaded, bars represent the more rapid cement reactions and the yellow or unshaded bars represent the more long-term pozzolanic reactions with the soil. The red or darker shaded, bars, for combinations of cement and fly ash, represent the pozzolanic reactions that may occur with the fly ash itself, since silica and alumina normally are more readily available in the fly ash than in the soil.

The measured effective stress paths in undrained tests together with failure and yield stresses evaluated from drained tests on stabilized clay, are presented by Ahnberg (2006) in a s´: t effective stress plane, where $s' = (\sigma'_1+\sigma'_3)/2$ and $t = (\sigma'_1 - \sigma'_3)/2$ (Fig.1.19). The test results include different binders, quantities and times after mixing. Lines are drawn indicating the evaluated effective strength parameters: friction angle ø´ and cohesion intercept c´ for the different mixtures.

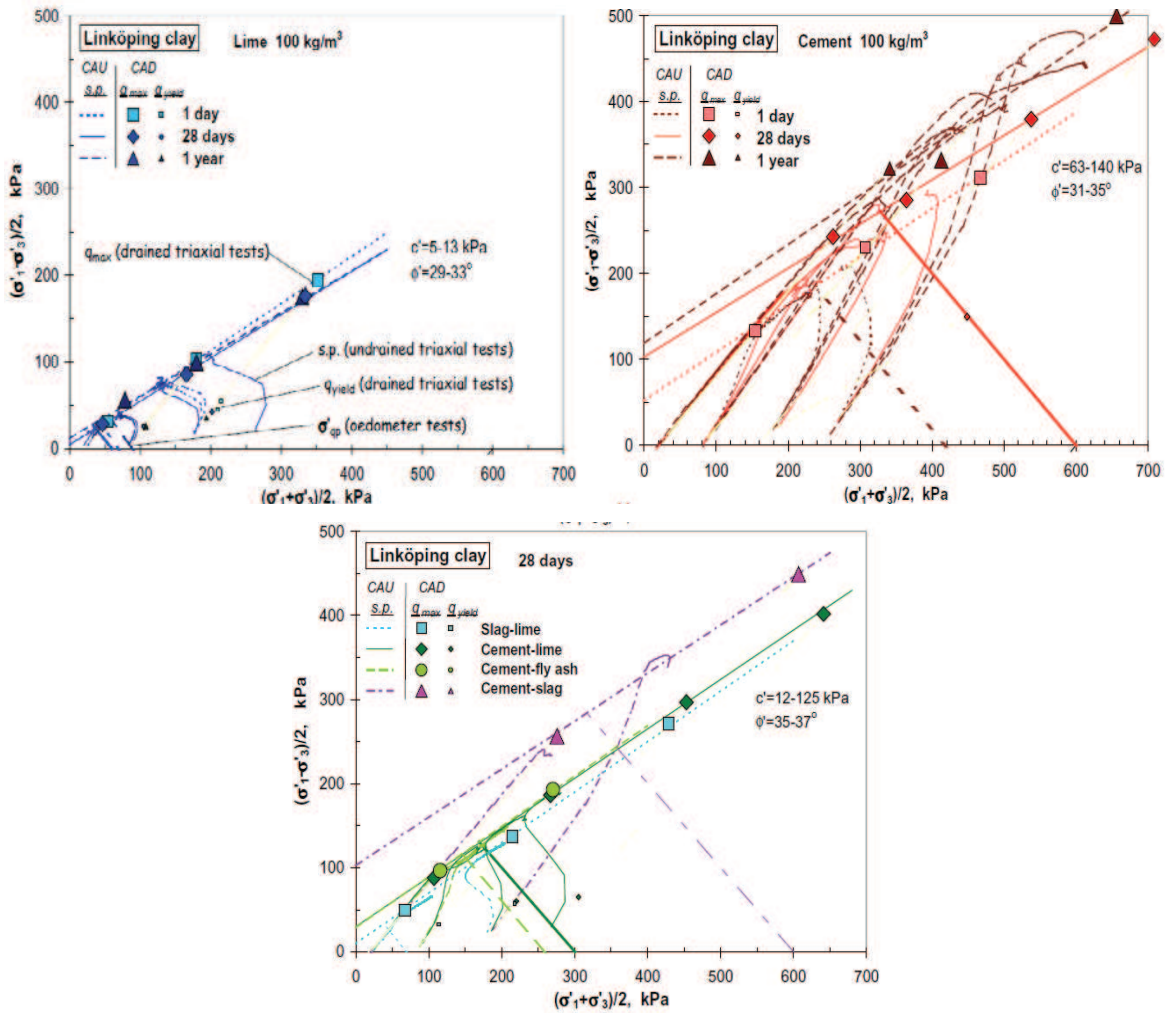

Figure 1.19 *Measured stress paths in the s´: t stress plane for stabilized clay (Ahnberg, 2006)*

1.5 Synthesis

Deep mixing technology can be effectively used for excavation support to increase bearing capacity, reduce movements, prevent sliding failure, control seepage by acting as a cut–off barrier, and as a measure against base heave. When used in conjunction with and in substitution to traditional techniques, DMM results in more economical and convenient solutions for the stability of the system and the prevention of seepage. Currently, an in-depth study of the properties resulting from mixing cement with various types of in situ soils has not been well documented. To accurately design the excavation support wall using deep mixing technology, the modulus and strength characteristic of the soil cement is required. Currently, only estimations of the modulus based on various assumptions are used in the design (Ratherford, 2004).

Based on the results of triaxial tests by Dano (2004) on grouted sands, the cohesion varies between 0.1 and 0.5 MPa depending on the cement content of the grout and the relative density of the soil. The grouted sands show a contractive–dilative response along a deviator stress path and the dilation angles of the grouted sands are at least equal to and usually higher than the dilation angle of the uncemented sands at the same dry density.

For the effect of soil treatment on the isotropic compression behavior, it can be observed from Ventouras (2005) studies that when compressing an intact sample, there is a smaller volumetric strain than for a reconstituted sample. In q-p' space, all experiments lay on the same linear trend, with a critical state stress ratio of M=1.3. When examining the shearing behavior of the soil, the intact samples have been shown to give higher peak stress-ratios during the test while at the end giving the same stress-ratio as the reconstituted samples.

For stabilized soft soils, studied by Ahnberg (2006), the use of cement, lime, slag and fly ash give varying increase in strength with time depending on the combination of binders chosen. The increase in strength was found to be roughly related to the type and quantity of possible reaction products. The results highlight the importance of taking into account a time factor in estimating the strength of stabilized soils in design.

Chapter 2:

MATERIAL AND TESTING METHODS

2 MATERIALS AND TESTING METHODS

In this part the materials and testing methods used in the different parts of the study are described in detail. The testing program is presented to facilitate comparisons of the tests referred to in the separate parts, and to provide a background to the test results presented in subsequent chapters.

2.1 Soil-cement mixtures used for the study

The aim of the experimental program was to investigate the effects of various levels of cement, lime and silica fume (SF) ratios including 0%, 40% and 80 % lime (note that for all mixes, SF to cement ratio of 0.1 and SF to lime ratio of 0.3 were taken constant), on shear strength, elastic parameters and permeability of a sandy soil-cement mix. As shown in Fig 2.1 and 2.2, and Table 2.1, 12 mixture proportions were tested, with different water to cement ratios (ranging from 1.61 to 2.45) and water to cementitious binders (cement + lime + SF) ratios (ranging from 0.75 to 2.22). Mixtures are referenced with C standing for cement, L for lime and S for sand. Numbers following the aforementioned codes refer to the factor of cementitious materials used, in kg for 1 cubic meter of silica sand.

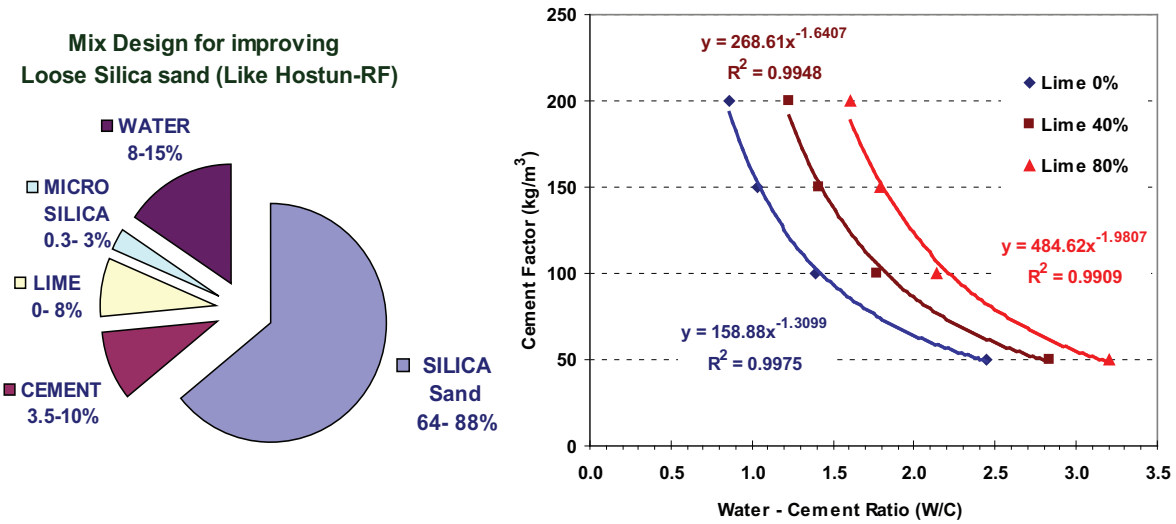

Figure 2.1 *General Pie Chart for Mix Design, and Cement factor versus water- cement ratio (w/c) and lime content for treated Silica sand*

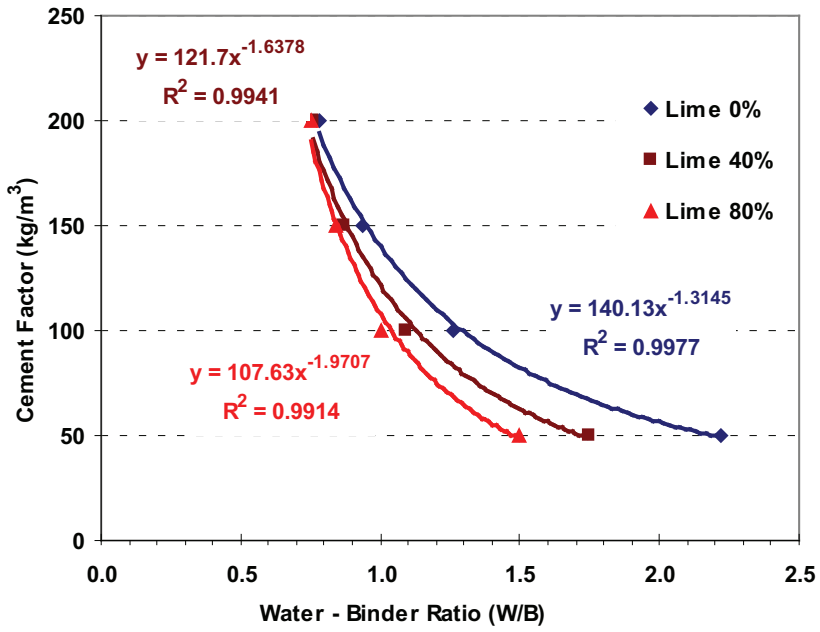

Figure 2.2 *Cement factor versus water- binder ratio (W/B) and lime content, for treated Silica sand*

Table 2.1 *Mixture proportions of studied deep mix sandy soil-cement mixes*

Mix Code	W/C	W/B	For 1 m^3 of sand				Silica Sand	C/S	B/S	L/C
			Water (kg/m^3)	Cement (kg/m^3)	Lime (kg/m^3)	Silica fume (kg/m^3)	(kg/m^3)	%	%	%
C50 L0	2.45	2.22	123.0	50	0	5.0	1336	3.7	4.1	0
C50 L20	2.83	1.75	141.5	50	20	5.6	1336	3.7	6.1	40
C50 L40	3.20	1.50	160.0	50	40	6.2	1336	3.7	8.0	80
C100 L0	1.39	1.26	139.0	100	0	10	1336	7.5	8.2	0
C100 L40	1.77	1.09	177.0	100	40	11.2	1336	7.5	12.2	40
C100 L80	2.14	1.00	214.0	100	80	12.4	1336	7.5	16.0	80
C150 L0	1.03	0.94	154.5	150	0	15	1336	11.2	12.4	0
C150 L60	1.41	0.87	211.5	150	60	16.8	1336	11.2	18.2	40
C150 120	1.79	0.84	268.5	150	120	18.6	1336	11.2	24.0	80
C200 L0	0.86	0.78	172.0	200	0	20	1336	15.0	16.5	0
C200 L80	1.23	0.76	246.0	200	80	22.4	1336	15.0	24.2	40
C200L160	1.61	0.75	322.0	200	160	24.8	1336	15.0	32.0	80

C=Cement, B=Binders (Cement+Lime+Silica Fume), S= Silica Sand, L= Lime

2.2 Silica sand properties

The parent soil used for this study was a silica sand with similar characteristic as RF-Hostun sand, a reference sand widely used in France. It is a quartz sand, with medium size and subangular grains ranging from 0.125 to 0.8 mm in average diameter. The grain-size distribution is shown in Fig.2.3

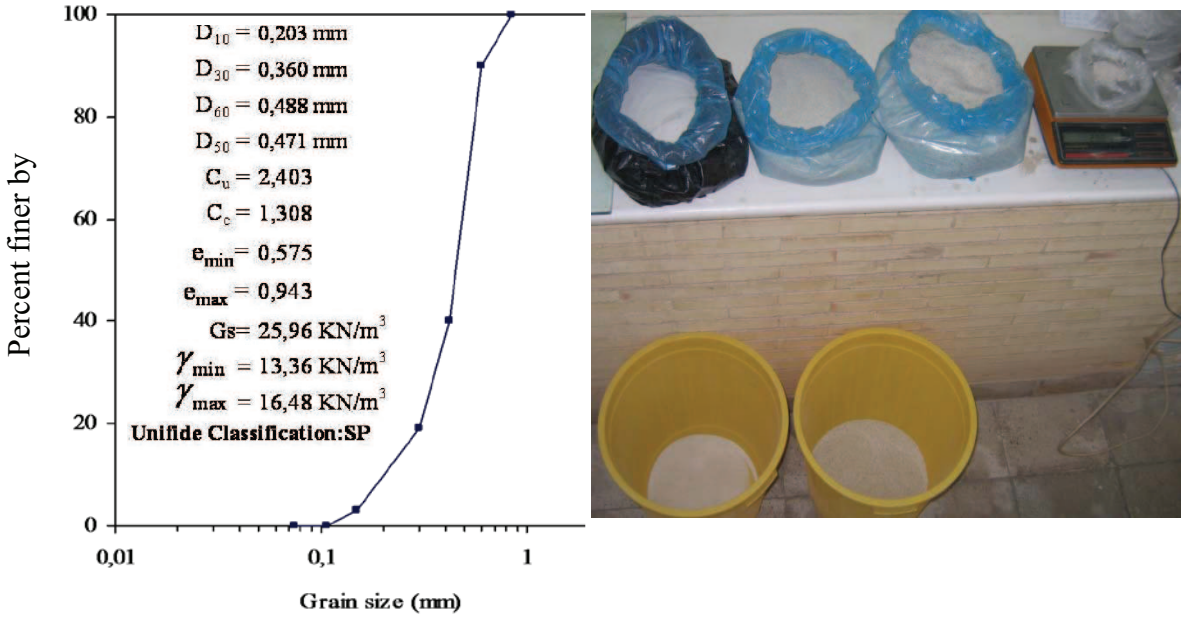

Figure 2.3 *Physical properties and grain-size distribution curve of the silica sand used in this study*

The principal physical characteristics are a mean diameter D_{50}=0.471 mm, a uniformity coefficient C_u=2.26, a unit weight of solid particles γ_s=25.96 kN/m^3, a minimum void ratio e_{min}=0.575, and a maximum void ratio, e_{max}=0.943.

2.3 Properties of binders and other additives

The main binder used to mix with silica sand was Portland cement, conforming to type II-Tehran, according to ASTM C150. The physical and chemical characteristics of cement are summarized in Tables 2.2 and 2.3.

Table 2.2 *Physical and mechanical properties of the main binders*

Characteristic	Cement Type II-Tehran	Lime	Silica Fume Iran-Ferroalloy
Specific surface area (m^2/kg)[1]	285	120	20(m^2/g)[2]
Initial setting time (min)	140	---	---
Final setting time (min)	180	---	---
Specific gravity (g/cm^3)	3.07	2.38	2.20
Compressive Strength (MPa), 7 days	17.5	---	---
Compressive Strength (MPa), 28 days	30.5	---	---
Water Consistency	0.26	0.83	0.616

1-Determined by the Blaine method, 2-Nitrogen absorption method (BET)

Table 2.3 *Composition of the main binders*

Binders / %Oxide	Cement Type II-Tehran	Lime	Silica Fume Iran Ferroalloy
SiO_2	20.71	1.4	93.6
Al_2O_3	4.09	0.6	1.32
Fe_2O_3	3.25	0.3	0.87
CaO	62.31	93.0	0.49
MgO	3.63	1.0	0.97
SO_3	1.6	0.1	0.1
Na_2O	0.31	0.1	0.3
K_2O	0.95	---	1.01

The reaction of cement with water causes a series of complex chemical compound. The main compounds in cement are dicalcium silicate and tricalcium silicate, and the physical behavior of these compounds is similar to that of cement during hydration. Highly crystalline portlandite $Ca(OH)_2$ and amorphous calcium-silicate-hydrate C-S-H are formed in the hydration of Portland cement (PC). The hydrated cement paste consists of approximately 70% C-S-H, 20% C-H,7% sulfoaluminate , and 3% secondary phase calcium hydroxide, which is

formed as a result of chemical reaction, is soluble in water and has a low strength. These properties affect the quality of cementation negatively. Adding mineral admixtures to cement decreases the amount of $Ca(OH)_2$. Cement paste containing silica fume (SF) produces amorphous C-S-H gel with high density and low Ca/Si ratio (Temiz, 2002). Silica fume replacement enhances the durability of mortar exposed to magnesium sulfate attack due to the lowering of the lime content, and therefore the increase of the initial compressive strength, on account of the pozzolanic reaction. Mortars containing a mass fraction of more than 8 % of silica fume are characterized by a good sulfate resistance and show lower expansion than a control sulfate-resisting mortar (Jelica & Zelic, 2006).

The type of lime used here was the most commonly used for civil foundation and construction in Iran, and silica fume was collected from the production of ferrosilicon (Iran Ferroalloys company), containing a mass fraction of SiO_2 of about 93.6 %, having a surface area of 20 m^2/g and an ignition loss of 1.42%.

2.4 Sample preparation

The quantities of Portland cement used correspond to 50 to 200 kg per m^3 of silica sand (cement/sand =3.8 to 15%) and the mortars were prepared from a mixture of Portland cement, silica-sand in its minimum dry density (13.36 kN/m^3) corresponding to soil condition after digging the ground in deep mix procedures, and mass fractions of lime of 0, 40 and 80%.

The water-to-cement ratio varied from 1.61 to 2.45 and the water-to-binders (C+L+SF) ratio varied from 0.778 to 2.22. The samples were prepared to have the same flow-table consistency (cement=0.26, lime=0.83, SF=0.616, Silica sand optimum moisture = 8%) and no super-plasticizer was added.

For unconfined, tensile and triaxial compression tests, cylindrical specimens of diameter D = 50 mm and height h = 100 mm mortar samples were prepared, according to ASTM D 1632-96 and ASTM D4767-95. After a setting period of 24-hour for high percentage cement (more than 100 kg/m^3) and 48-hour for low percentage cement, in a humid environment (20 °C, 90 % RH), the specimens were taken out of the moulds and immersed into tap water until time of testing (Fig.2.4).

Figure 2.4 *Sample preparation for silica soil-cement (see mix design table 2.1), cylindrical specimens with D=50 mm, h=100 mm, for unconfined, tensile and triaxial compression tests, according to ASTM D 1632-96 and ASTM D4767-95*

For direct shear tests in accordance with ASTM D-3080, prismatic specimens were produced with dimensions 60×60×300 mm , then cut for the direct shear box dimension 60 ×60 ×20 mm as shown in Fig.2.5.

Figure 2.5 *Sample preparation for silica soil-cement prismatic specimens of dimensions 60×60×300 mm (see mix design Table 2.1), then cut for direct shear box dimensions 60×60×20 mm, in accordance with ASTM D-3080.*

2.5 Apparatus Description and Experimental Procedures

2.5.1 Triaxial compression tests

2.5.1.1 Experimental equipment

In triaxial tests, a typical displacement-controlled triaxial cell was used (Fig. 2.6). Tests were done in strain control mode, with constant confining pressure during the test. The tests were fully computer controlled in data acquisition.

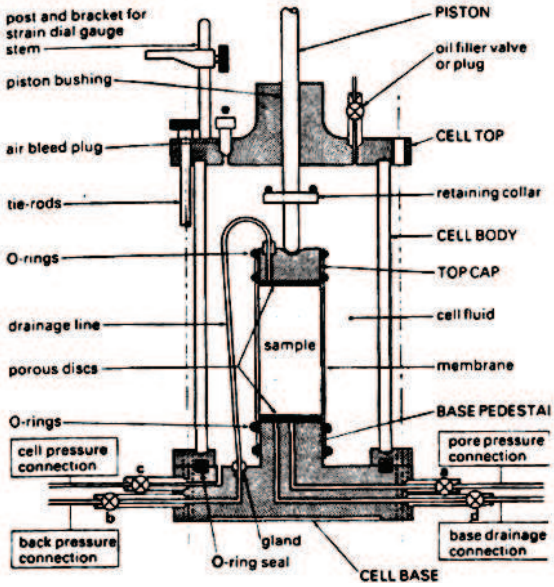

Figure 2.6 *Details of a typical triaxial cell (Head et al, 1988)*

The axial displacement was imposed by means of a controlled speed driven motor, with a compression force up to 100 kN and an axial movement control as low as 0.001 mm/min.

The strength of the samples was measured by unconfined tests according to ASTM D-2166. Before strength testing, the specimens were cut and smoothed to form parallel end surfaces. The end plates were lubricated with grease in order to minimize friction at the end surfaces.

The triaxial tests, which are somewhat more complex and time consuming, were used for the strength and deformation behavior by measurements of changes in stresses and volume, as well as strain, during loading in accordance with ASTM D-4767. Consolidated drained tests have been done to study the effective parameters of mechanical behavior of soil-cement. Cell pressure was generated by pressurized water and a high-pressure constant rate pump was used to produce it. Drained triaxial tests in cemented soils were done with confining pressures of 0,

100, 200 and 400 kPa. The samples were always saturated by vacuum flushing followed by application of back pressure to achieve a Skempton's *B* value of at least 0.96.

Before starting a test, freshly de-aired water was drawn into the constant pressure systems and flushed through the pipe work connections to the test apparatus.

The strain measurements were made by means of an external displacement transducer and a volume change rolling diaphragm transducer (Fig.2.7). During the deviatoric stage, the evolution of pore pressure was monitored and the strain rate was adjusted in such a manner to prevent the generation of excess pore pressure.

For unconfined compression and triaxial tests, samples were loaded vertically with a loading velocity of 0.25%/min (0.25 mm/min) until failure appeared. To investigate the strength increase of the samples, tests were performed 12, 28 and 180 days after mixing.

To gain a better understanding of the effects of binders on the behavior of the improved soil, a number of other tests were also performed. These included the determination of basic parameters such as the density and water content of the improved soil. A number of permeability tests in age 180 days samples were performed according to Darcy's law with the use of a triaxial system after saturation of each samples.

To obtain comparable reference data and to illustrate the effect of improvement on the strength and deformation behavior, triaxial tests were also performed on unimproved, natural silica sand.

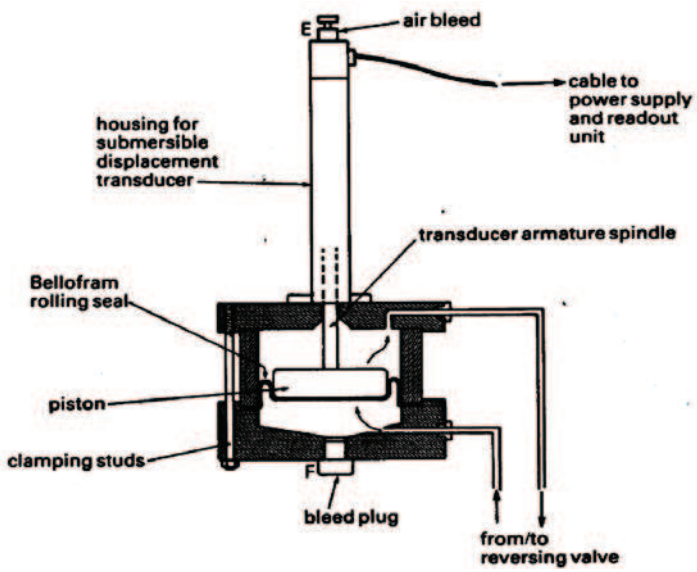

Figure 2.7 *Principle of rolling diaphragm volume-change transducer (Head et al, 1988)*

An advanced automatic system was used (ELE Data System 6). The system comprised an interface unit, a desktop computer with screen display. The key to this system was the programmable interface unit for scanning the transducers, which enabled the computer to be devoted to storage and analysis of test data. The computer initiated the programmed screen displays which guide the operator, and controlled the printer/plotter which reproduced the results in both tabular and graphical form. Once a test stage had been started, data were collected automatically without needing further attention until the stage had been completed.

Also used was the Autonomous Data-acquisition Unit (ADU). The interface unit which collected data had its own microprocessor and a large memory for storing test data. The host computer could recall stored data for processing, display and printing out when required. A typical arrangement is shown in Fig.2.8.

Figure 2.8 *The advanced automatic system comprises an interface unit (ADU), linked to an effective stress triaxial test and a desktop computer with screen display.*

2.5.1.2 Drained triaxial compression tests procedure

Testing of the parent soil was conducted to provide some benchmark data for reflecting the effects of the cementing agent. The principle of the drained triaxial compression test is

indicated in Fig.2.9a. The vertical and horizontal stresses σ'_1 and σ'_3 acting on the sample are shown in Fig.2.9b. Three sets of readings are made during this test (in addition to time): cell confining pressure (held constant), axial load (deviator stress), axial deformation (strain). For carrying out effective stress triaxial tests, two additional features are needed in the cell: provision for measurement of pore water pressure, and provision for drainage. Pore water pressure is generally measured at the base of the sample, which is therefore a non-drainage surface. It is assumed that drainage takes place from the top of the sample. The drainage line incorporates a volume-change gauge to measure the movement of water out of or into the sample.

The immediate connections to a sample set up in the triaxial cell are shown diagrammatically in Fig.2.10. Valve 'a' is connected to the apparatus for measuring pore pressure. Valve 'b' isolates the drainage line connected to the top end of the sample from the drainage or backpressure system when the 'drained' condition is required. Valve 'c' is connected to the cell chamber pressurizing system. Valve 'd' was a spare connection to the sample base. Valve 'e' was the cell chamber air bleed.

The sample, assumed to be of normally consolidated saturated soil, is consolidated under the cell pressure during the compression stage and further.

Triaxial testing of silica sand was conducted on effective confining stress σ'_3 in the range 200 to 400 kPa for loose sand (γ_{min}=13.36 kN/m^3, e_{max}=0.943) and in the range 100 to 300 kPa for dense sand (γ_{max}=16.48 kN/m^3, e_{min}=0.575).

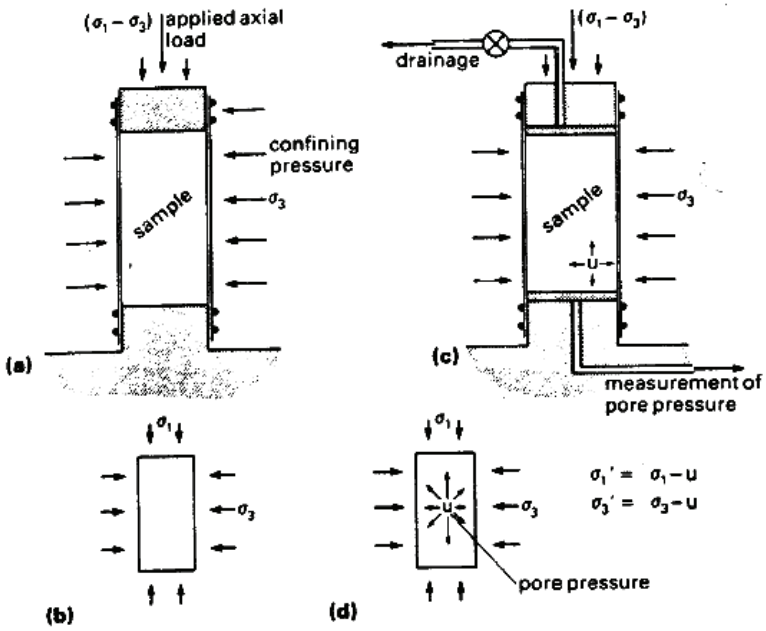

Figure 2.9 *Principles of triaxial compression tests: (a) application of stresses, (b) representation of principal stresses, (c) usual arrangement for effective stress tests. (d) Representation of total and effective stresses (Head et al, 1988)*

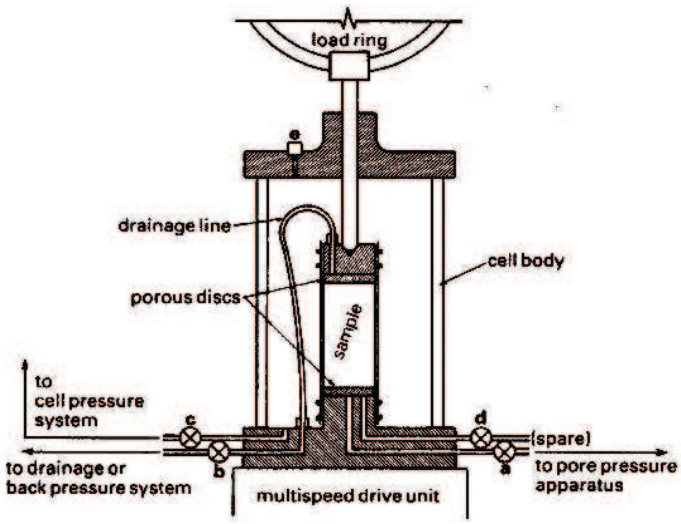

Figure 2.10 *Connections to a triaxial cell for effective stress tests (Head et al, 1988)*

2.5.2 Apparatus and Procedures used in Direct Shear Tests

This part deals with the measurement of the shear strength of cemented soil in the laboratory by shear box test, in which the relative movement of two halves of a square block of soil-cement takes place along a horizontal surface. Shear strength measured in the laboratory is

dependent upon the conditions imposed during the test and in some instances upon the duration of the test.

The consolidated-drained test by shear box is given in ASTM D-3080. In principle the shear box test is an 'angle of friction' test, in which one portion of soil is made to slide along another by the action of a steadily increasing horizontal shearing force, while a constant load is applied normal to the plane of relative movement. These conditions are achieved by placing the soil in a rigid metal box, square in plan, consisting of two halves. The lower half of the box can slide relative to the upper half when pushed (or pulled) by a motorized drive unit, while a yoke supporting a load hanger provides the normal pressure. The principle is shown in Fig.2.11. During the shearing process the relative displacement of the two portions of the specimen and the applied shearing force are both measured so that a load/displacement or shear stress/shear strain curve can be drawn.

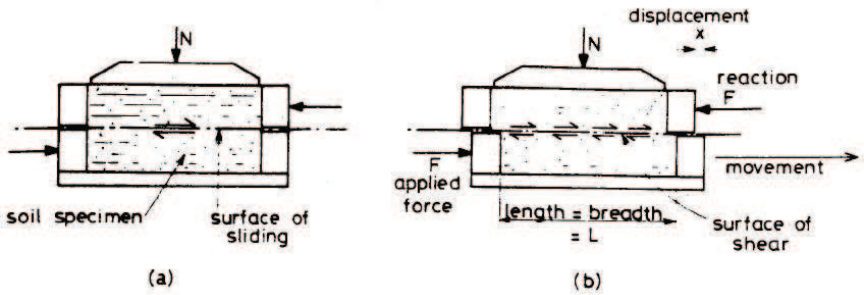

Figure 2.11 *Principle of shear box test: (a) start of test, (b) during relative displacement, (K.h.Head et al, 1988)*

The vertical movement of the top surface of the specimen, which indicates changes of volume, is also measured and enables changes in density and void ratio during shear to be evaluated. In order to carry out a slow 'drained' shear test, provision is made for the specimen to be consolidated before shearing and for further drainage to take place during shear at a suitably slow rate of displacement, so that the consolidated-drained shear strength parameters can be determined. The use of reversing attachments enabled a specimen to be re-sheared a number of times in order to determine the drained residual shear strength.

The most common type of apparatus accommodates a 60 mm square specimen, and is referred to here as the 'standard' apparatus which is described in detail. The normal pressures applied

to specimens in a set of tests should generally 'bracket' the maximum stress likely to occur in the ground. Normal pressures of about 50%, 100%, and 150-200% of these values are often appropriate. The shear box machine comprises a drive unit, shear box carriage, load hanger and other items detailed in Fig 2.12, which are supported on a bench or mounted in a steel-framed stand. A load ring for measuring the horizontal shear force with a 2 kN capacity was used, but a ring of 4.5 kN capacity may be required for measuring high shear strengths.

Figure 2.12 *Assembly of 60 mm standard shear box machine comprises a drive unit, shear box carriage, load hanger and load ring, details of 60 mm shear box.*

An electric motor and multi-speed drive unit typically provide 24 speeds ranging from 5 mm/min to about 0.0003 mm /min. The motor is reversible.

A micrometer dial gauge with a 12 mm travel and readings to 0.002 mm is used for measuring vertical movement of the top of the specimen. At the start of the test the motor is switched on and simultaneously the timer is started. At regular intervals, the horizontal dial, the load dial and the vertical movement dial readings are recorded with the time.

Tests were carried out on a set of specimens (see mix design Table 2.1) each at a different normal stress within 100, 200 and 400 kPa .The samples were first allowed consolidating under the selected normal pressure, until consolidation is completed. Shear displacement was

then applied slowly enough to allow the dissipation of any further pore water pressure which may develop due to shear, the rate of displacement being determined to be the same as the triaxial sample rate displacement 0.25 mm/min. Under these conditions the effective stresses were equal to the applied stresses.

2.5.3 Apparatus and procedure for permeability tests on silica sand-cement samples

2.5.3.1 Principle

The permeability of a soil is a measure of its capacity to allow the flow of a fluid through it. The degree of permeability is determined by applying a hydraulic pressure difference across a sample of soil, which is fully saturated, and measuring the consequent rate of flow of water. The method used for measuring permeability depends upon the characteristics of the material, but under the same physical law, known as Darcy's law, denoted as:

$$q = kiA \quad \text{or} \quad v = q/A = ki \qquad (2.1)$$

where q = discharge per unit time

A = total cross-sectional area of soil mass, perpendicular to the direction of flow

i = hydraulic gradient

k = Darcy's coefficient of permeability

v = velocity of flow, or average discharge velocity

In practice, if a soil sample of length L and cross-sectional area A is subjected to a differential head of water (h_1- h_2), then the hydraulic gradient will be given by i= (h_1-h_2)/L, and by substituting for i in equation (2.1):

$$q = k\,\frac{h_1 - h_2}{L}A \qquad (2.2)$$

When the hydraulic gradient is unity k=v. Thus the coefficient of permeability k is defined as the average velocity of flow that will occur through the total cross-sectional area of soil under a unit hydraulic gradient.

2.5.3.2 Permeability Test using a Triaxial Cell

This test method covers the procedure for determining the water permeability of soils using a triaxial cell, according to CRD-C 163-92.

This test method involves the establishment of a steady-state flow condition in a cylindrical cemented soil specimen housed in a standard triaxial cell, accommodating cylindrical specimens of 50 mm in diameter and 100 mm in length. A radial confining pressure is maintained around the specimen. Delivery of the drive pressure to the triaxial cell is obtained through the back pressure system and measured the volume of inlet de-aired water to sample. Drive pressure must be less than confining pressure. The volume of inlet de-aired water to sample is measured by the volume change device (see section 2.5.1.1).

A pressure gradient is maintained across the sample with one end exposed to ambient pressure and the opposite end at the test drive pressure. The effluent is collected and the volume flow rate is determined. Once steady-state flow conditions are obtained, the permeability is determined.

The permeability tests were done after the end of saturation stage of each sample, for 180 day aged samples.

Chapter 3:

EXPERIMENTAL RESULTS

3 Experimental Results

3.1 Mechanical Behavior of Silica Sand

3.1.1 Stress–Strain and Volumetric Response, Critical State

Results from triaxial tests on silica sand are shown in Fig 3.1. These results are typical of the experimental stress-strain behavior of most sands. A stress peak is observed for dense sand, however no shear band was observed and sample bulging remained unnoticeable until approximately 10 % axial strain. No stress peak occurs for loose samples and bulging appeared even later (10–12% axial strain). For the critical state to be reached, large strains were required, which usually exceed 20-30% shear strain on a triaxial sample. Fig 3.1b shows the critical state points in q-p' space and the gradient M of the critical state line (CSL) for loose sand is M_c=1.3, and peak strength state line for dense condition, M_p=1.8, where:

$$M_C = \frac{q_{cr}}{P'_C} \qquad (3.\ 1)$$

$$M_P = \frac{q_P}{P'_P} \qquad (3.2)$$

It is recalled that M can be connected to the angle of internal friction by the relation:

$$\sin\varphi' = \frac{3M}{6+M} \qquad (3.3)$$

The volumetric strain response is presented in Fig.3.1c. The ε_v– ε_1 curves (where ε_v is the volumetric strain and ε_1 is axial strain) in loose samples were manifesting a compressive response until failure. In dense samples, in the first stage of the test a compressive response was found, then dilatancy was observed. The dilatancy rate at failure was close to zero, and hence the failure condition was at or very close to critical state.

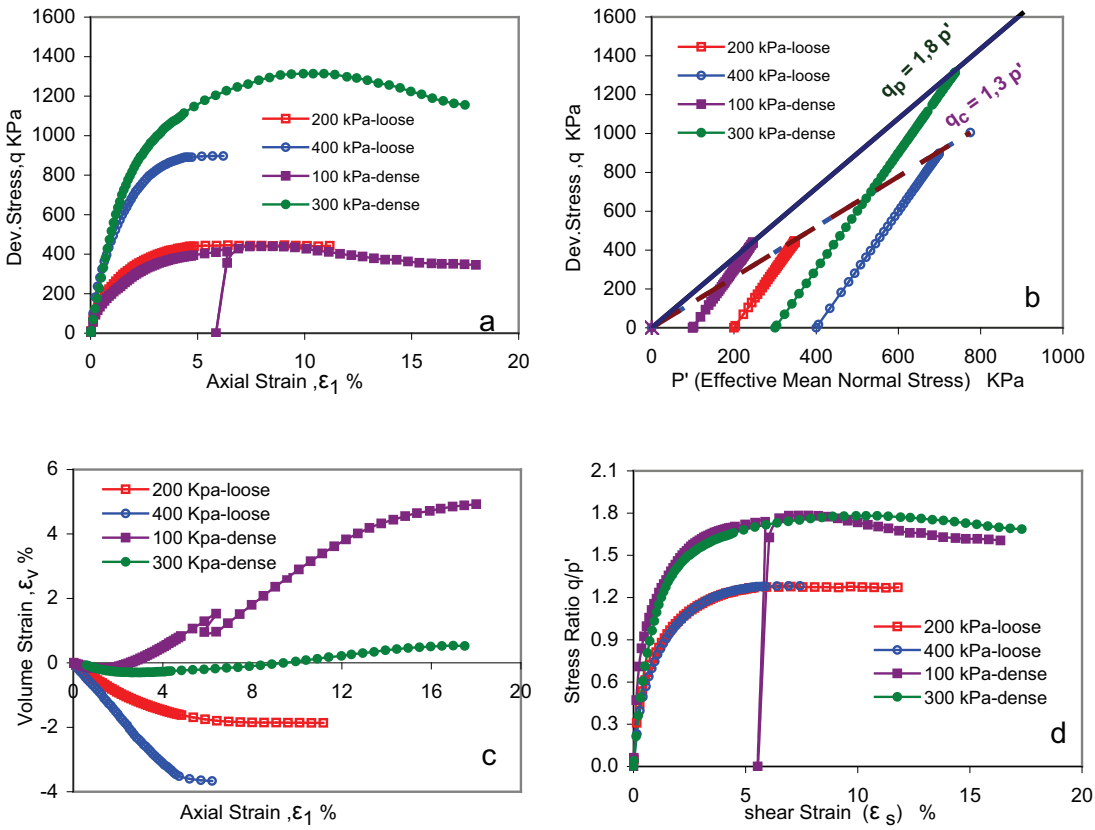

Figure 3.1 *Drained triaxial tests for Silica sand for confining pressures of 200 and 400 kPa for loose (open symbols), and 100 and 300 kPa for dense (closed symbols): (a) deviator stress q versus axial strain ε_1, (b) deviator stress q versus effective mean normal stress p', (c) ε_v versus ε_1 and (d) stress ratio q/p' versus shear strain ε_s.*

3.1.2 Shear Strength Parameters for loose and dense Silica sand

A set of identical specimens consolidated to different effective stresses gave a set of Mohr circles of effective stress at failure as shown in Fig. 3.2. The envelope to these circles inclined at an angle $ø'_P$=43.5°, for peak failure state, and $ø'_{cr}$=41.0° for ultimate state of dense sand and at an angle $ø'_p$=$ø'_c$=32.2° for peak failure and ultimate state of loose sand. The apparent cohesion intercept is C_d =0.

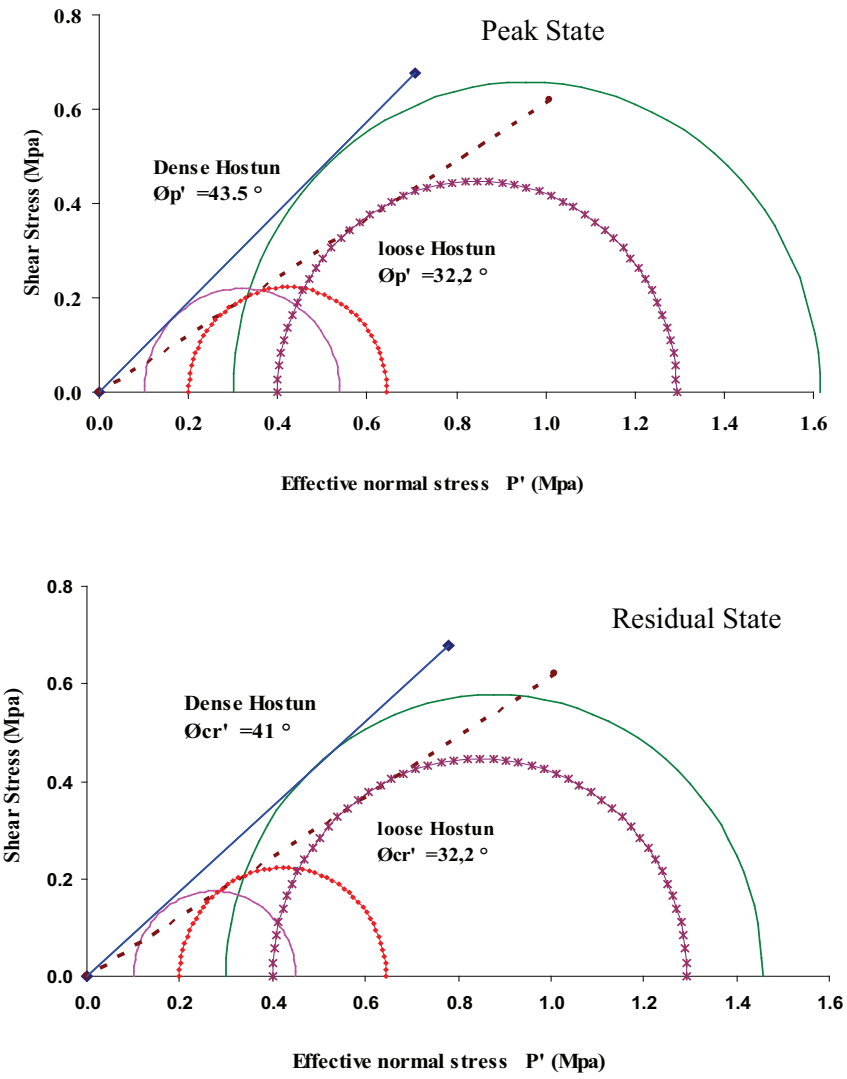

Figure 3.2 *Mohr circle diagram for drained triaxial compression tests in terms of effective stresses for peak and residual state of Silica sand: loose (dashed line) and dense (solid line).*

3.1.3 Isotropic Compression behavior

The results of a hydrostatic compression test on the parent soil used in this study are compared with results reported by Al Mahmoud (1997) and Lancelot (2006) on Hostun RF sand (I_D= 0.124) and shown in fig.3.3. These authors observed that the isotropic normal compression line for loose Hostun sand is reached for relatively high stresses, with a compression index C_c= 0.115, whereas "elastic rebound" index was C_s= 0.02. The preconsolidation pressure σ'_c was estimated to 300 kPa, which means that the sample preparation procedure used in their study lead, even for loose sand, to an overconsolidated material in the low stress range (beginning of test).

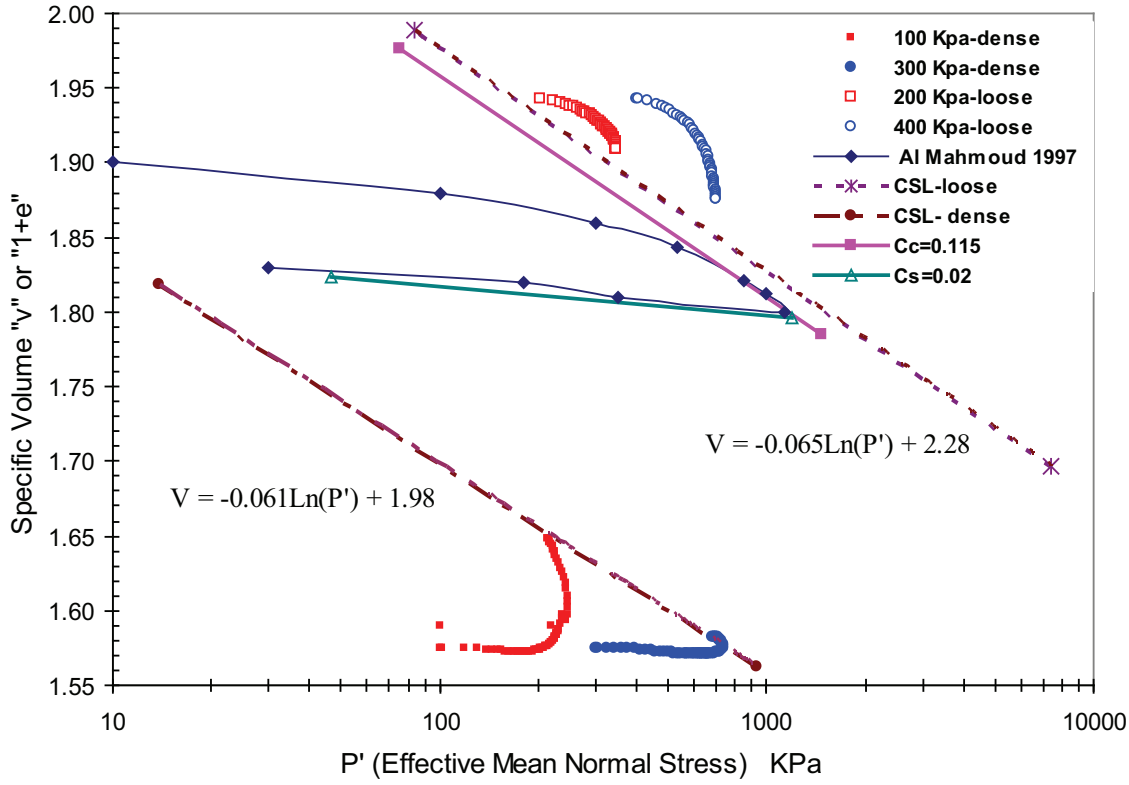

Figure 3.3 *Isotropic compression tests on Silica sand and Hostun RF*

In the tests done on silica sand for this study, no constant volume deformation was observed, although for dense samples an inflexion could be noticed in the variation of the volumetric strain for axial strains corresponding roughly to stress peak, indicating a decrease in the sample dilating rate from this state onwards.

As is shown in Fig.3.3, CSL for different values of density or void ratio of Silica sand can be modeled by the relation $v = \Gamma - \lambda \ln p'$ where Γ lies between 1.98 and 2.28 λ between 0.061 and 0.065.

3.1.4 Failure and Dilatancy Properties

If the dilatancy angle ψ is defined by the relation $\tan\psi = -(\delta\varepsilon_v / \delta\varepsilon_1)$, Fig.3.1c illustrates the variation of the maximum dilatancy angle (ψ_{max}) with cell pressure for several sands. It can be observed that ψ_{max} depends both on initial density and cell pressure. For loose sand, a contracting behavior ($\psi_{max}<0$) is observed for both high and low cell pressures, whereas for dense sand a dilating behavior is observed, the values of ψ_{max} decreasing with increasing cell pressure, the dilation taking place after a small initial compression. The magnitude of the

dilation also depends very strongly on the density of the soil, with denser samples expanding more rapidly.

To express the relationship existing between the angle of friction and the angle of dilation, let's recall that the angle of friction φ' expresses the ratio of a shear stress to a normal stress, and can be defined in terms of principal stresses (Fig. 3.4):

$$\sin\phi' = \frac{\sigma_1' - \sigma_3'}{\sigma_1' + \sigma_3'} \qquad (3.4)$$

In a similar way the angle of dilation ψ expresses the ratio between a volumetric strain rate and a shear strain rate. For the case of plane strain ($\varepsilon_2 = 0$) it can be defined in terms of the principal strain rates (Figure 3.4):

$$\sin\psi = \frac{-(\dot{\varepsilon}_1 + \dot{\varepsilon}_3)}{\dot{\varepsilon}_1 - \dot{\varepsilon}_3} \qquad (3.5)$$

The minus sign in Equation 3.5 is introduced so that the angle of dilation is positive when the soil expands.

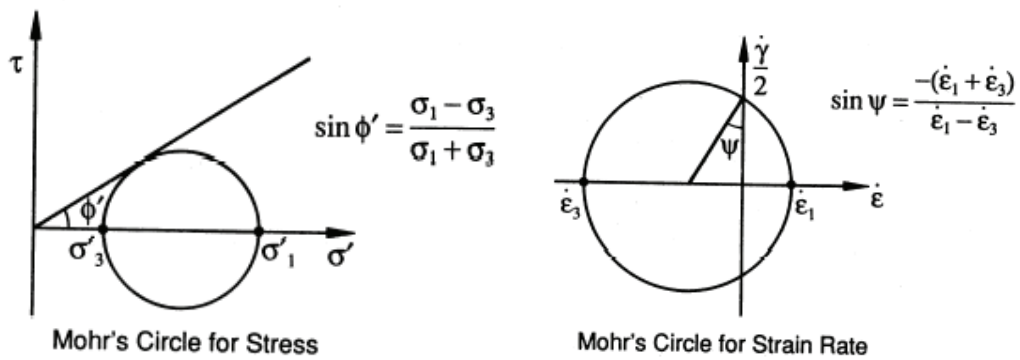

Figure 3.4 *Definitions of the angles of friction and dilation, (Houlsby, 1991)*

Note that Equation (3.5) could be expressed in terms of strain increments δε rather than strain rates $\dot{\varepsilon}$.

According to Rowe (1962) dilatancy can be related to internal friction as follows:

$$\frac{\sigma_1'}{\sigma_3'} = \left(\frac{\sigma_1'}{\sigma_3'}\right)_c \left[1 - \frac{\partial\varepsilon_\upsilon}{\partial\varepsilon_1}\right] \qquad (3.6)$$

In Equation (3.6) the subscript c means critical (effective stress ratio for a zero dilatancy rate).

The relation of stress ratio σ'_1/σ'_3 to axial strain ε_1 and dilatancy in drained triaxial test for silica sand are shown in fig.3.5, and illustrate the fact that the maximum stress ratio for loose sand is 3.23 and for dense sand 5.40. The associated stress–dilatancy relationships for loose and dense silica sand are established in Fig.3.5b, where the dilatancy D is defined as in Rowe's relationships (1962) equal to $1-(\delta\varepsilon_v^p / \delta\varepsilon_1^p)$ where $\delta\varepsilon_v^p$ and $\delta\varepsilon_1^p$ are the increments of the plastic volumetric strain and the plastic axial strain respectively. As seen in fig.3.5b, the maximum value of dilatancy D for loose sand ranges from 0.26 to 0.66 and for dense sand from 1.02 to 1.26.

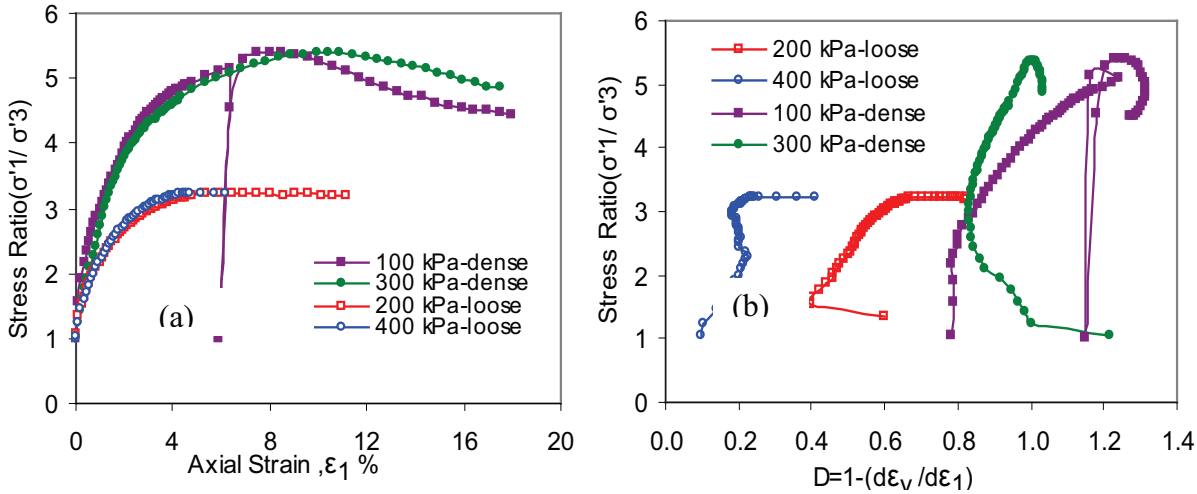

Figure 3.5 *Drained triaxial tests for silica sand for confining pressures of 200 and 400 kPa for loose (open symbols), and 100 and 300 kPa for dense(closed symbols): (a) stress ratio σ'_1/σ'_3 versus axial strain ε_1, (b) stress ratio σ'_1/σ'_3 versus dilatancy D*

The dilatancy behavior can be studied more closely with R–D plots, where $R = \sigma'_1/\sigma'_3$ is the principal stress ratio, and $D = 1 - d\varepsilon_v/d\varepsilon_1$ is referred to as the dilatancy factor. As summarized in Fig.3.6, provided $R > 2.25$, the stress dilatancy behavior follows Rowe's (1962) stress dilatancy equation 3.6, expressed as follows:

$$R = KD \qquad (3.7)$$

The value of K is 2.56 and at failure, where the soil samples were essentially manifesting no dilatancy, $R_{cr} = 4.81$ (where R_{cr} is the principal stress ratio at critical state). This value of R_{cr} implies a critical state friction angle equal 32.2°. For quartz sands, a typical value of 33° is

reported for the critical friction angle (Bolton, 1986). For Hostun RF sand, values between 30 and 32° were reported for $ø'_c$ (Biarez and Ziani 1991, and Konrad *et al.* 1991).

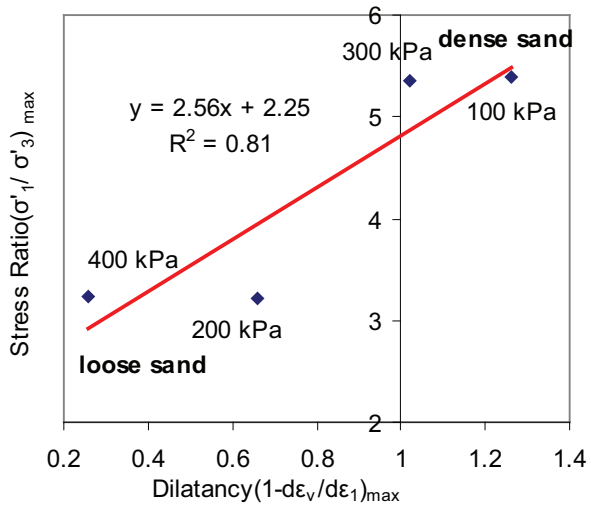

Figure 3.6 *Stress ratio versus dilatancy relationship after Rowe (1962)*

3.2 Permeability of Silica sand and Silica sand-cement

3.2.1 Factors affecting Permeability

Permeability is not a fundamental property of soil, but depends upon a number of factors such as particle size distribution, particle shape, mineralogical composition, void ratio, degree of saturation , soil fabric, nature of percolating fluid , type of flow and temperature.

The smaller the particles, the smaller the voids between them, and therefore the resistance to flow of water increases with decreasing particle size. The 'effective grain size', D_{10} is significant in this respect, and provides the basis of Hazen's formula, whereas Hazen's observations were limited to sands of fairly uniform grain size.

$$k = 0.01\ (D_{10})^2\ \ m/s \qquad (3.8)$$

where D_{10} is expressed in millimeters. Particles with a rough surface texture provide more frictional resistance to flow than do smooth-textured particles. Both effects tend to reduce the rate of flow of water through the soil, i.e. to reduce its permeability. In fine-grained soils the mineralogical composition is an additional factor because different types of minerals hold on to different thicknesses of adsorbed water and consequently the effective pore size vary. Silica

sand ($D_{10}=0.203$) should have a permeability of approximately $k = 4.12*10^{-4}$ m/s according to Hazen's formula.

3.2.2 Permeability Results in Silica Sand-Cement

3.2.2.1 Calculation and data analysis

The pressure gradient is calculated across the specimen as follows:

$$\Delta P = P_{drive} - P_{ambient} \qquad (3.9)$$

Where P_{drive} = Drive pressure, kPa

$P_{ambient}$ = Atmospheric pressure, kPa (Standard 101.325 kPa)

The effluent volumetric flow rate (q) for each reading during the steady-state portion of the test is computed as follows:

$$q\ (\text{ml/s}) = \frac{\Delta V}{\Delta t} \qquad (3.10)$$

Where, ΔV= incremental effluent volume collected, or incremental effluent volume inlet (measured by volume change apparatus),

Δt = time interval during which the volume was collected.

The steady-state volumetric flow rate is taken as the average volumetric flow rate over five or more time intervals. The total volume of fluid collected versus elapsed time for the test schematically is plotted in figure 3.7. When the resulting curve was linear over five or more readings, steady-state flow was obtained.

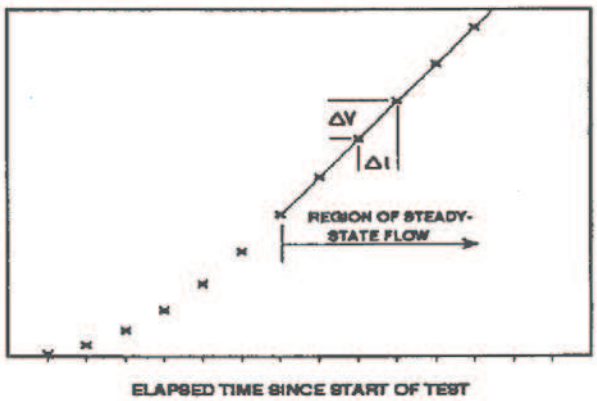

Figure 3.7 *Determination of Steady-State Flow (CRD-C 163-92)*

Linearity of the volume-time curve is determined graphically and is compared for mix design C200L0 and C200L80 for several confining pressure as shown in Fig 3.8.

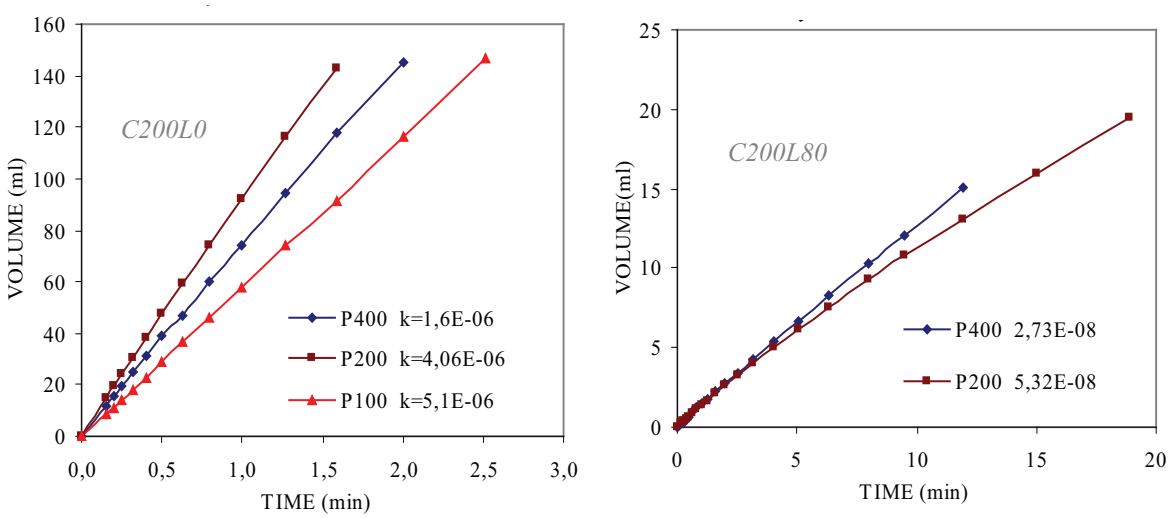

Figure 3.8 *Determination of Steady-State Flow and Permeability for Silica sand- cement, for different confining pressure, mix design C200L0 and C200L80.*

3.3 Tensile Strength of Cemented Silica Sand

Unlike sands, the cemented sands possess some tensile strength. Due to a lack of practical and reliable technique, very few results can be found in the literature on that matter. Clough *et al.* (1980, 1981) reported results for Brazilian tests on cemented sand and stated that the tensile strength is about 10 to 12 percent of the unconfined compressive strength and also that the cohesion intercept is about twice the tensile strength. A parabolic stress-strain variation in the tensile region is usually assumed. Additional data for tensile strength of cemented sands are needed, by adopting similar techniques that provide fairly good data for concrete, rocks and clay in tension (Saxena, 1988).

Brazilian tensile tests (or splitting tension tests) were carried out on cylindrical samples of 11 at180 days specimens, with the test set-up schematically shown in Fig. 3.9. The variables were considered and summarized in Table 3.1.

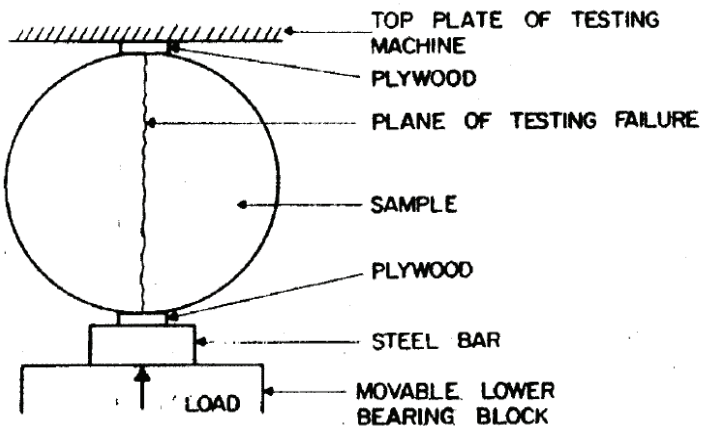

Figure 3.9 *Schematic Diagram of Test Set-up for Brazilian Tests (Saxena, 1988)*

The samples tested were prepared by the method of under compaction in the same way as for static triaxial tests. Circular steel plates with diameter slightly larger than the length of the samples were fixed to the plate of testing machine in such a manner that the load applied is distributed over the entire length of the specimen. Two bearing strips of 2.5 cm wide and 0.5 cm in thickness of smooth plywood of a length equal to length of specimen were used. One of the plywood strips was placed in the center of the lower bearing block. After precise measurement of length and diameter, the specimen was placed on this lower plywood strip. The upper plywood strip was then placed lengthwise on top of the specimen. The movable lower bearing block was raised slowly until the sample and the plywood strips were gripped by the top plate. The samples were loaded vertically on the side until a diagonal crack indicated a tensile mode of failure. The loads at which the first crack appeared and the sample failed were recorded. No measurements for strains were made. The tensile strength of specimen was calculated using the following expression:

$$\sigma_t = \frac{2P}{\pi LD} \qquad (3.11)$$

where σ_t is the tensile strength in kPa, P is the maximum applied load in kN, L is the length of the specimen in cm and D is its diameter in cm.

Table 3.1 *Results of split tensile tests on silica sand- cement*

MIX CODE	Samples Age days	Weight gr	Diameter cm	height cm	Failure force KN	Tensile strengh kPa	Wet density gr/cm^3	Dry Density gr/cm^3
C50L0	180	281.8	5.02	7.93	0.064	10.2	1.796	1.391
C50L20	180	366.6	5.03	10.13	0.156	19.5	1.822	1.420
C50L40	180							1.440
C100L0	180	309.5	4.95	9.00	0.420	60.0	1.788	1.450
C100L40	180	371.5	4.98	10.40	1.301	160.0	1.835	1.500
C100L80	180	377.0	5.00	10.55	2.173	262.4	1.821	1.550
C150L0	180	387.7	5.00	10.25	2.623	326.0	1.927	1.500
C150L60	180	407.0	5.03	10.55	3.666	440.0	1.942	1.580
C150L120	180	406.5	5.02	10.51	5.200	627.8	1.955	1.660
C200L0	180	395.0	5.03	10.50	6.517	786.0	1.894	1.560
C200L80	180	399.7	5.00	10.25	8.400	1044.0	1.987	1.680
C200L160	180	406.6	5.00	10.57	9.400	1132.9	1.960	1.690

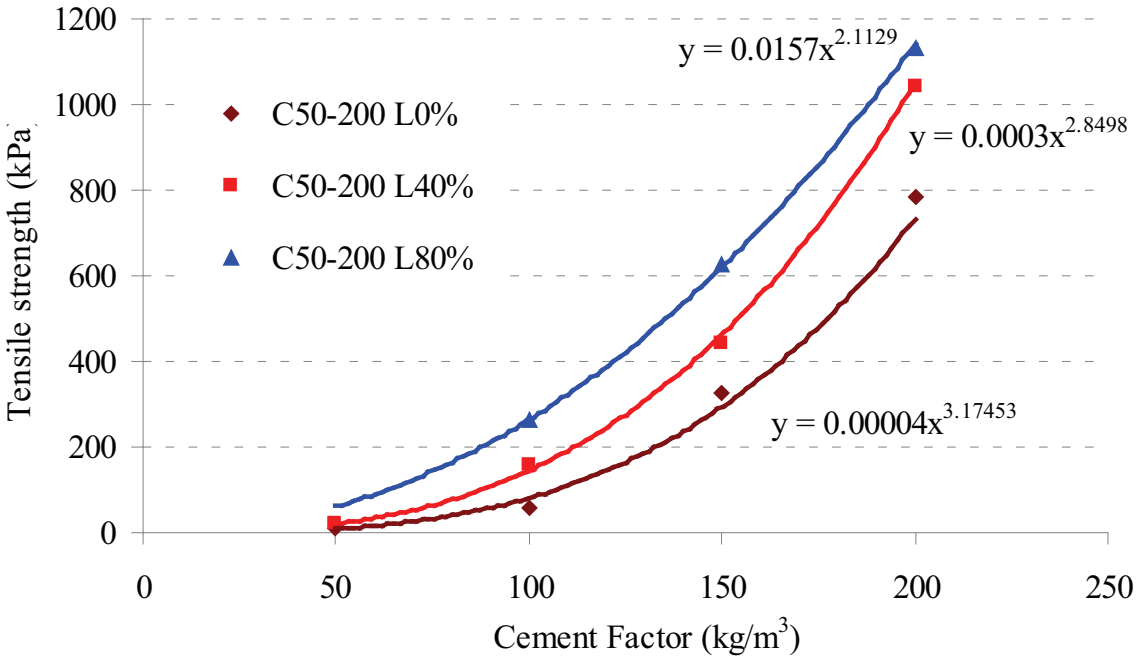

Figure 3.10 *Variation of tensile strength of cemented silica sand with cement content for 0 to 80 % of lime and silica fume (after 180 days of curing)*

Figure 3.10 shows the variation of tensile strength with cement content for different percentage of lime and silica fume agents. Samples with Portland cement including 80% lime and silica fume showed the highest tensile strength.

3.4 Unconfined Compression Strength of Cemented Silica Sand

Unconfined compression tests are routinely performed to assess the strength of the improved sand. The effects of different binders on the increase of strength are appropriately described in terms of general strength levels and rate of increasing strength.

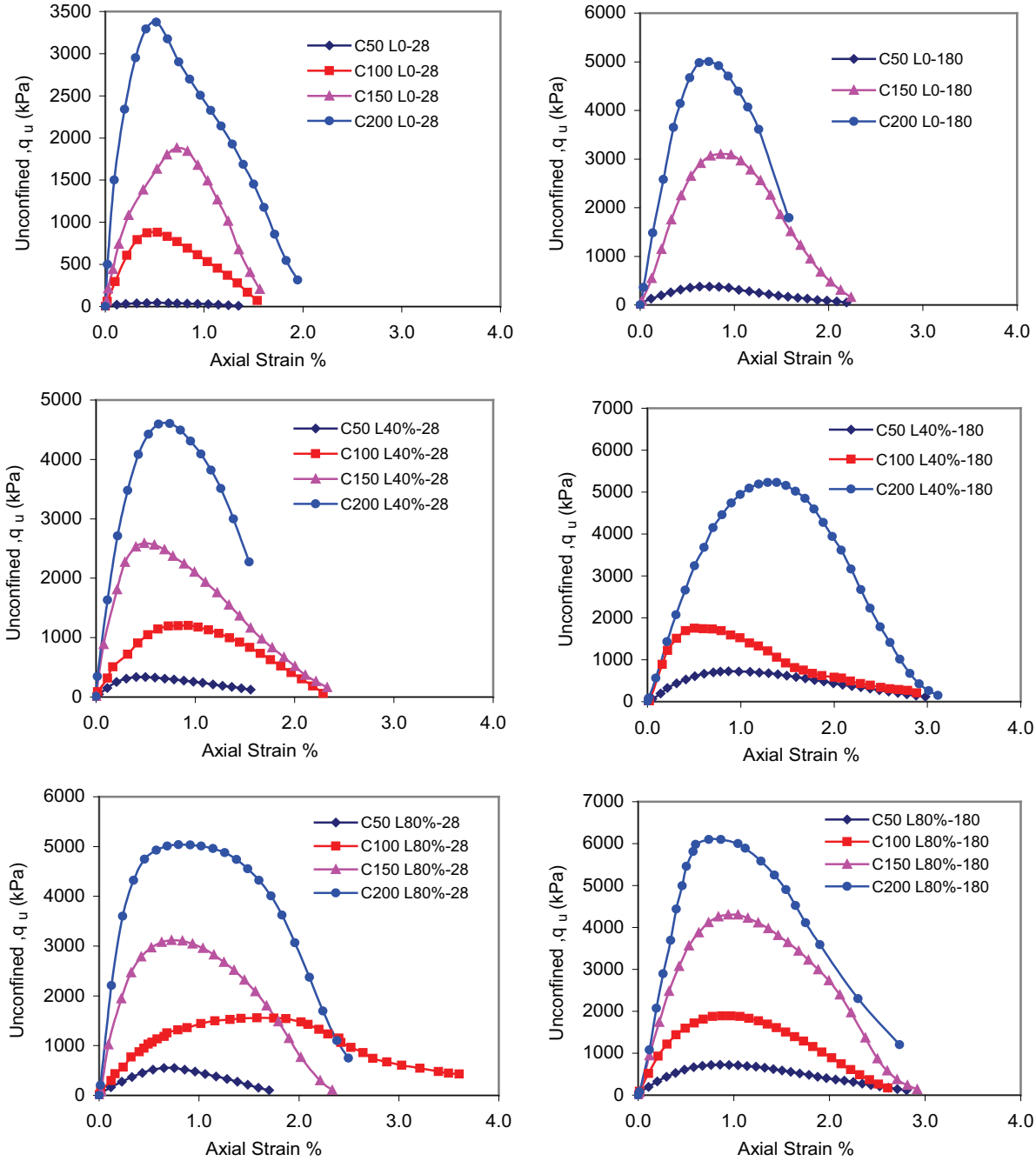

Figure 3.11 *Unconfined compression stress–strain responses of cemented samples for silica soil-cement with 50 to 200 kg/m^3 Portland cement plus 0,40 and 80 % binder (lime+ silica fume), compared after 28 and 180 days curing times.*

Figure 3.11 shows the behavior of silica cemented sand in unconfined compressive strength in a q_u-ε_1 space samples with 50 to 200 kg/m^3 cement and 0 to 80 % lime/cement ratio, for 28 and 180 days curing times. During the first month after mixing, the most rapid strength increase occurs in samples treated with binders containing Portland cement.

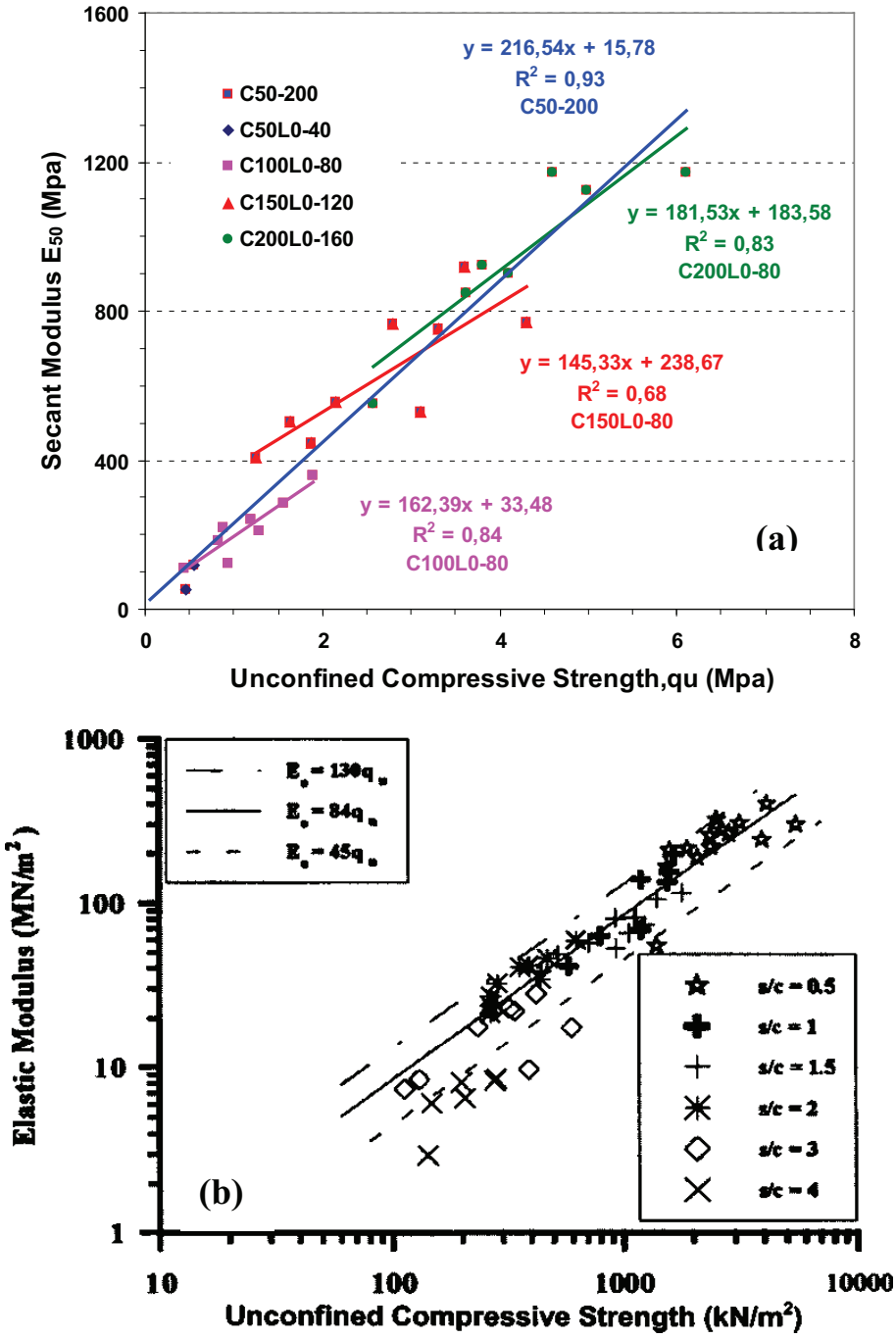

Figure 3.12 *(a) Relationship between E_{50} and unconfined compressive strength of cement –lime treated silica sand (this study), and (b) cement treated clay prepared from dried-pulverized clay, (Lee et al.,2005).*

The secant modulus at a stress level equal to 50% of the unconfined compression strength q_u, E_{50}, was also obtained from these stress-strain curves. Fig.3.12a shows the secant modulus of silica sand treated with cement –lime and silica fume in relation to the unconfined compressive strength obtained in the present study, as compared to previously published studies (Fig.3.12b) on deep mixing for dried-pulverized and slurry clay mixes (Lee *et al.*, 2005). As can be seen, E_{50} / q_u for treated Silica sand lies between 100 and 300 and, in comparison with previous studies for clayey soil-cement (fig.3.12b), is more than two times of the fitted value. Asano *et al.* (1996) and Saitoh *et al.* (1996) also measured E_{50}. Both studies seem to suggest that E_{50} / q_u lies between 100 and 700.

3.5 Mechanical Behavior of Cemented Silica Sand in the Triaxial Test

3.5.1 Stress–Strain Behavior and Volumetric Response

Fig. 3.13 to 3.15 show the results of drained triaxial compression tests on silica sand cemented with different binder mixtures following Table 2.1, under confining pressures of 100, 200 and 400 kPa, after 28 days curing. They illustrate the underlying mechanisms of the strength enhancement and volumetric dilation due to cementation effects. Other data for several curing times are collected and summarized in Table 3.2., where unconfined compression tests are also recalled. All results indicate an increase in strength due to increasing confining pressure and curing time. Data for ultimate strength (critical state) are summarized in Table 3.3. They show that the rate of mobilization of the deviator stress increases with effective confining stress.

Fig. 3.13 to 3.15 show a general trend of an increase in the axial strain at failure ε_{1f} with an increasing effective confining pressure for samples with low cement content. A comparison of the behavior of the uncemented sand sample with similar void ratios (Fig. 3.1) also reveals that the cementation completely alters the volumetric response from contraction to dilation. This dilation is due to densification and cementation effects.

Figs 3.16 to 3.18 show the q - ε_1 coupled with q – p' plots, for silica soil-cement with 50 to 200 kg/m^3 Portland cement plus 0,40 and 80% binder (lime + silica fume) for different effective confining pressures (0 to 400 kPa) at 28 days curing for all the drained compression

tests. Curves for principal stress ratio versus axial strain $\sigma'_1/\sigma'_3 - \varepsilon_1$ for silica cemented sand in the same conditions are plotted in Figs 3.19 and 3.20. Fig. 3.21 in turn shows volume strain versus effective mean normal stress $\varepsilon_v - p'$.

Table 3.2 *Peak Strength versus confining pressure, for different mix designs for cemented silica sand: 50-200 kg/m³ cement and 0, 40 and 80% binder (lime+silica fume)*

MIX CODE	12 DAYS Curing				28 DAYS Curing				180 DAYS Curing			
	(σ'1-σ'3)p (Mpa)				(σ'1-σ'3)p (Mpa)				(σ'1-σ'3)p (Mpa)			
	σ'3 =0.0 (MPa)	σ'3 =0.1 (MPa)	σ'3 =0.2 (MPa)	σ'3 =0.4 (MPa)	σ'3 =0.0 (MPa)	σ'3 =0.1 (MPa)	σ'3 =0.2 (MPa)	σ'3 =0.4 (MPa)	σ'3 =0.0 (MPa)	σ'3 =0.1 (MPa)	σ'3 =0.2 (MPa)	σ'3 =0.4 (MPa)
C50-L0	0.050	0.280	0.500		0.170	0.471	0.690		0.360	0.630	0.860	1.390
C100-L0	0.613	0.918	1.246	1.750	0.880	1.258	1.540	2.152	1.290	1.726	2.090	2.760
C150-L0	1.250	1.530	1.955		1.880	2.242	2.670		3.100	3.640	4.140	4.930
C200-L0	2.570	3.056	3.440	4.112	3.810	4.340	4.920	5.870	4.980	5.852	6.530	7.520
C50-L20	0.150	0.430	0.705	1.268	0.280	0.648	1.014	1.654	0.455	0.813	1.160	1.795
C100-L40	0.820	1.172	1.560	2.160	1.200	1.670	2.035	2.807	1.750	2.217	2.650	3.450
C150-L60	1.630	2.010	2.400	3.090	2.790	3.430	3.940	4.846	3.600	4.160	4.730	5.580
C200-L80	3.620	4.297	4.820	5.680	4.600	5.360	6.060	6.831	5.230	6.070	6.860	7.820
C50-L40	0.417	0.762	1.110	1.775	0.550	0.903	1.280	1.960	0.717	1.130	1.450	2.270
C100-L80	0.932	1.356	1.691	2.420	1.560	2.010	2.450	3.227	1.891	2.463	2.950	3.790
C150-L120	2.150	2.693	3.130	4.040	3.314	4.205	4.700	5.600	4.300	5.070	5.670	6.670
C200-L160	4.100	4.640	5.330	6.400	5.040	5.880	6.740	7.970	6.100	7.029	7.680	8.980

Table 3.3 *Ultimate Strength versus confining pressure, for different mix designs for cemented silica sand: 50-200 kg/m³ cement and 0, 40 and 80% binder (lime+silica fume)*

MIX CODE	12 DAYS Curing				28 DAYS Curing				180 DAYS Curing			
	(σ'1-σ'3)cr (Mpa)				(σ'1-σ'3)cr (Mpa)				(σ'1-σ'3)cr (Mpa)			
	σ'3 =0.0 (MPa)	σ'3 =0.1 (MPa)	σ'3 =0.2 (MPa)	σ'3 =0.4 (MPa)	σ'3 =0.0 (MPa)	σ'3 =0.1 (MPa)	σ'3 =0.2 (MPa)	σ'3 =0.4 (MPa)	σ'3 =0.0 (MPa)	σ'3 =0.1 (MPa)	σ'3 =0.2 (MPa)	σ'3 =0.4 (MPa)
C50-L0		0.185	0.390			0.290	0.550			0.255	0.515	1.020
C100-L0		0.406	0.660	1.350		0.400	0.820	1.420		0.484	0.872	1.520
C150-L0		0.520	0.930			0.630	1.040	1.840		0.658	1.200	2.112
C200-L0		0.860	1.590	2.434		0.790	1.565	2.720		0.980	1.770	3.180
C50-L20		0.264	0.500	1.000		0.120	0.772	1.470		0.356	0.653	1.320
C100-L40		0.560	0.850	1.600		0.460	0.930	1.780		0.560	1.056	1.900
C150-L60		0.680	1.090	2.100		1.040	1.150	2.200		0.946	1.566	2.600
C200-L80		1.170	1.830	3.100		1.380	1.660	3.050		1.150	2.040	3.600
C50-L40		0.364	0.726	1.461		0.220	0.920	1.650		0.400	0.852	1.612
C100-L80		0.480	1.010	1.840		0.540	1.120	1.970		0.640	1.228	2.345
C150-L120		0.730	1.380	2.400		0.975	1.580	2.727		0.980	1.800	3.350
C200-L160		1.200	1.980	3.300		1.220	2.230	3.510		1.400	2.470	4.320

These results allow the effect of the cement content of the binders to be examined. In all figures the low cement content samples appear to have flatter compression curves than their high cement counterparts, giving smaller reductions in void ratio. Clearly, the initial void ratio would have an effect on the compression behavior of the soil-cement. A similar behavior pattern can be identified from the volumetric strain response presented as $\varepsilon_v - \varepsilon_1$ plots in Fig.

3.13 to 3.15. The effect of the cementing agent on the volumetric response depends on the confining stress. For tests conducted at high confining pressure, the responses were dominantly compressive, although the behavior may have become slightly dilatant at high axial strain. Tests conducted at lower confining stress showed strongly dilatant behavior and the small volumetric compression occurred only during the initial stage of shearing. The behavior pattern of both the q–ε_1 and ε_v– ε_1 curves is similar to that of artificially bonded sand presented by Leroueil and Vaughan (1990) and Wardani (2002). This provides strong support to the hypothesis that cemented soil can be interpreted within the framework of a structured soil.

3.5.2 Secant Modulus and Elastic parameters

The elastic parameters of silica sand-cement are summarized in Tables 3.4 and 3.5.

Table 3.4 *Elastic Modulu, E_{50} (Mpa) for different mix designs for cemented silica sand: 50-200 kg/m^3 cement and 0, 40 and 80% lime+silica fume*

MIX CODE	12 DAYS Curing				28 DAYS Curing				180 DAYS Curing			
	Elstic Modulus, E_{50} (Mpa)				Elstic Modulus, E_{50} (Mpa)				Elstic Modulus, E_{50} (Mpa)			
	σ'_3 =0.0 (MPa)	σ'_3 =0.1 (MPa)	σ'_3 =0.2 (MPa)	σ'_3 =0.4 (MPa)	σ'_3 =0.0 (MPa)	σ'_3 =0.1 (MPa)	σ'_3 =0.2 (MPa)	σ'_3 =0.4 (MPa)	σ'_3 =0.0 (MPa)	σ'_3 =0.1 (MPa)	σ'_3 =0.2 (MPa)	σ'_3 =0.4 (MPa)
C50-L0	52.0	47.6	62.2		42.1	41.9	41.9		99.1	73.5	69.3	159.5
C100-L0	87.1	171.7	129.5	122.9	230.6	184.7	204.4	161.3	260.0	266.0	205.7	240.9
C150-L0	197.0	324.3	229.2		436.5	361.0	359.4	336.2	493.0	309.6	422.6	617.2
C200-L0	370.0	427.5	333.4	412.0	707.0	649.0	705.0	585.9	973.0	692.4	644.3	972.7
C50-L20	60.0	37.5	46.6	51.7	80.0	46.4	50.2	61.0	94.0	73.3	71.5	68.9
C100-L40	250.0	144.4	158.9	209.0	350.0	270.1	213.4	226.9	350.0	259.6	311.7	361.8
C150-L60	448.0	361.5	298.5	373.7	600.0	501.6	542.4	544.0	675.0	495.4	553.0	696.5
C200-L80	715.0	547.2	484.5	679.7	929.0	839.1	892.1	865.7	958.0	700.7	768.5	1038.5
C50-L40	160.2	61.3	81.2	70.1	171.0	94.5	74.6	101.1	172.0	174.5	139.5	131.7
C100-L80	300.0	156.8	168.1	205.6	400.0	304.9	277.3	293.0	447.0	402.8	387.1	552.0
C150-L120	522.0	380.2	393.1	477.3	820.0	610.7	581.6	592.6	766.0	723.6	642.2	797.6
C200-L160	771.0	626.9	590.4	779.0	1000.0	985.4	994.9	953.4	1049.0	968.9	1091.1	1240.1

For uncemented sands, the secant modulus E_{50} increases linearly with the effective stress σ_3'. The dependency of the secant modulus on the effective stress is less pronounced for cemented sands, especially for high cement contents. The secant modulus for cemented silica sand is

here improved by a ratio of 0.5 to 20, depending on the mean stress value and on the nature and cement content of the grout, as compared to the secant modulus for uncemented sands.

Table 3.5 *Poisson's ratio υ for different mix designs of cemented silica sand: 50-200 kg/m³ cement and 0, 40 and 80% lime+silica fume*

MIX CODE	12 DAYS Curing			28 DAYS Curing			180 DAYS Curing		
	Poisson's Ratio (ν)= $\left[\frac{1}{2}(1-\frac{\varepsilon_v}{\varepsilon_1})\right]$			Poisson's Ratio (ν)			Poisson's Ratio (ν)		
	σ'3 =0.1 (MPa)	σ'3 =0.2 (MPa)	σ'3 =0.4 (MPa)	σ'3 =0.1 (MPa)	σ'3 =0.2 (MPa)	σ'3 =0.4 (MPa)	σ'3 =0.1 (MPa)	σ'3 =0.2 (MPa)	σ'3 =0.4 (MPa)
C50-L0	0.282	0.255		0.306	0.307		0.455	0.408	0.377
C100-L0		0.243	0.272	0.210	0.208	0.212	0.321	0.287	
C150-L0	0.256	0.204		0.204		0.195	0.271	0.170	
C200-L0	0.231	0.183	0.229	0.168	0.151	0.182	0.149	0.222	0.100
C50-L20		0.290		0.312	0.323	0.289	0.406	0.449	0.447
C100-L40				0.233	0.266	0.240	0.312	0.303	0.259
C150-L60	0.247		0.218	0.205	0.237	0.219	0.280	0.263	0.228
C200-L80	0.224	0.207	0.207	0.191	0.203	0.181	0.251	0.219	0.215
C50-L40	0.307	0.250	0.280	0.312	0.283	0.285	0.341	0.348	0.353
C100-L80	0.261		0.242	0.279	0.270	0.259	0.317	0.257	0.340
C150-L120	0.262	0.248	0.206		0.227	0.217	0.272	0.225	0.265
C200-L160	0.237		0.206	0.214	0.174	0.186	0.252	0.197	0.206

The change of stiffness with shearing can be studied more closely by plotting the tangential stiffness modulus E versus ε_1 in logarithmic scale, where E is defined by $E = dq/d\varepsilon_1$. In the example curves shown in Fig. 3.22, a sharp bend can be detected for all the tests. The tangential stiffness prior to reaching this bend remains approximately constant with shearing, but reduces rapidly after passing it. Hence this point defines the occurrence of first yield. It is usually occurring at an axial strain of *0.1–0.2%*. The rate of reduction in E increases with higher values of σ'_3.

3.5.3 Mode of failure (brittleness) of cemented silica sand

In this section the effect of cementation on brittleness and the dilative behavior of soils is examined. The cemented soil brittleness depends on the cement content and cement type. Consoli *et al.* (1998) defined the brittleness index using the following equation:

$$I_B = (q_{peak} / q_{ult}) - 1 \qquad (3.12)$$

Where I_B is the brittleness index, q_{peak} is the shear strength and q_{ult} is the ultimate strength.

Table 3.6 shows the brittleness index (I_B) calculated in drained conditions for cemented silica sand (50-200 kg/m^3 cement and 0 to 80% lime+silica fume).

Table 3.6 *Brittleness Index I_B in drained conditions for different mix design of cemented silica sand: 50-200 kg/m^3 cement and 0, 40 and 80% lime+silica fume*

MIX CODE	12 DAYS Curing Brittleness Index (I_B)			28 DAYS Curing Brittleness Index (I_B)			180 DAYS Curing Brittleness Index (I_B)		
	σ'_3 =0.1 (MPa)	σ'_3 =0.2 (MPa)	σ'_3 =0.4 (MPa)	σ'_3 =0.1 (MPa)	σ'_3 =0.2 (MPa)	σ'_3 =0.4 (MPa)	σ'_3 =0.1 (MPa)	σ'_3 =0.2 (MPa)	σ'_3 =0.4 (MPa)
C50-L0	0.33	0.19		0.46	0.14		1.06	0.48	0.26
C100-L0	1.01	0.68	0.23	1.72	0.71	0.43	2.13	1.14	0.56
C150-L0	1.67	0.84		3.26	1.31	0.70	3.93	2.10	1.12
C200-L0	2.29	1.03	0.59	3.99	1.61	1.00	4.51	2.42	1.21
C50-L20	0.46	0.29	0.19	0.46	0.25	0.06	1.00	0.59	0.28
C100-L40	0.93	0.68	0.28	2.16	0.98	0.62	2.51	1.27	0.61
C150-L60	1.71	1.02	0.34	3.33	2.07	1.19	3.07	1.79	1.02
C200-L80	2.46	1.47	0.74	4.10	2.37	1.40	3.94	2.15	1.25
C50-L40	0.86	0.41	0.17	0.82	0.32	0.15	1.46	0.57	0.33
C100-L80	1.51	0.56	0.26	2.30	1.01	0.59	2.46	1.21	0.53
C150-L120	2.37	1.11	0.61	3.00	1.75	0.92	3.79	1.94	0.83
C200-L160	2.65	1.54	0.99	3.53	1.86	1.14	3.75	1.95	0.99

Figure 3.23 shows the variation of the brittleness index I_B for different effective confining pressures and curing times of 12, 28 and180 days. It is shown that I_B increases with increasing cement content and curing time, but decreases with increasing confining pressure.

3.5.4 Strength Parameters and Critical State

The values obtained for the cohesion and friction angle at peak (c'_p , φ'_p) and ultimate/critical state (c'_{cr} , φ'_{cr}) are summarized in Table (3.7).

Table 3.7 *Angle of shearing resistance and cohesion for peak and residual states for different mixtures of cemented silica sand*

MIX CODE	12 DAYS Curing				28 DAYS Curing				180 DAYS Curing				Dry Density gr/cm^3
	Peak strength		ultimate strength		Peak strength		ultimate strength		Peak strength		ultimate strength		
	Ø'p (°)	C'p (Mpa)	Ø'cr (°)	C'cr (Mpa)	Ø'p (°)	C'p (Mpa)	Ø'cr (°)	C'cr (Mpa)	Ø'p (°)	C'p (Mpa)	Ø'cr (°)	C'cr (Mpa)	
C50-L0	31.9	0.016	29.7	0	32.5	0.066	36.4	0.004	34.1	0.098	34.6	0	1.391
C100-L0	35.3	0.173	36.9	0.037	36.8	0.239	38.0	0.032	39	0.334	41.7	0.02	1.450
C150-L0	38.2	0.315	43.9	0.045	39.9	0.460	43.9	0.018	42.8	0.704	45	0.04	1.500
C200-L0	41.0	0.591	46.4	0.080	44.0	0.880	49.7	0.048	46.9	1.046	51.1	0.06	1.560
C50-L20	35.0	0.046	33.7	0.001	37.5	0.094	41.2	0.004	38.2	0.123	37.6	0.02	1.420
C100-L40	37.7	0.217	37.2	0.020	40.2	0.300	39.8	0.037	42.1	0.403	44.7	0.03	1.500
C150-L60	40.2	0.388	46.7	0.017	43.5	0.630	44.8	0.030	44.5	0.788	46.7	0.11	1.580
C200-L80	44.0	0.801	49.1	0.105	46.3	0.987	46.9	0.127	47.9	1.092	51.1	0.11	1.680
C50-L40	38.7	0.103	40.0	0.002	39.6	0.134	42.1	0.013	41.1	0.175	33.8	0	1.440
C100-L80	39.8	0.236	42.2	0.044	41.8	0.368	43.9	0.018	43.5	0.445	47.2	0.03	1.550
C150-L120	43.2	0.510	46.2	0.048	45.0	0.740	50.0	0.030	46.4	0.899	46.1	0.02	1.660
C200-L160	45.8	0.898	49.4	0.063	48.5	1.060	53.0	0.080	49.8	1.189	51.6	0.07	1.690

Peak-state and ultimate/critical state parameters are also shown in Figs. 3.24 to 3.26. It is shown that both C_p' and φ_p' increase with increasing cement content. Moreover, the cementation enhances the friction angle at the ultimate/critical state φ'_{cr}, where the influence of strain localization is not considered. The enhancement of φ'_{cr} follows a general trend: it increases with increasing cement content but is suppressed by increasing confinement. Two hypotheses are suggested to account for the increase in φ'_{cr}. First, the cementing particles may still be connected to the sand particles and this may increase the roughness of the particle interfaces. Second, there still exist various sizes of bonded clusters at this ultimate state, which provide stronger force-chain networks to lead to higher strength. Wang and Leung (2008), based on the findings in Mitchell and Soga (2005), Skinner (1969) and Thornton (2000), suggested that the interparticle friction angle is of secondary importance to the associated macroscopic friction angle when compared with the normal contact forces in the strong force-chain networks. This is because the deviator stress q is mainly supported by the normal contact forces in these networks and not by the tangential forces that are directly related to the interparticle friction angle. In this context, the second hypothesis, i.e. the presence of bonded clusters and associated stronger force chain networks, is relevant in the cause of the increase in φ'_{cr}.

In Figure 3.27 all the peak and critical-state strength points have been grouped based on mean effective stresses. A well defined linear band can be seen for all tests that are grouped in different confining pressures. The amount of cement and addition of lime and silica fume does not appear to have an effect on the critical state line of cemented silica sand in q-p' space. According to Figure 3.27, the average value of M_{cr} is 2.14 for different cement contents, which corresponds to a value of φ'_{cr} ranging from 48° to 50°.

3.5.5 Stress – Dilatancy Behavior and Relationships

The stress–dilatancy behavior associated to the rate of dilation $d\varepsilon_v/d\,\varepsilon_s$ and their relationships for 28 days curing samples are shown in Figs 3.28 and 3.29. In Fig.3.28 the stress is presented in terms of the stress ratio q/p', where q and p'= deviatoric and volumetric stress, respectively.

The dilatancy d is defined as ($-\delta\varepsilon_v^p / \delta\varepsilon_s^p$), where $\delta\varepsilon_v^p$ and $\delta\varepsilon_s^p$ are the increments of the plastic volumetric strain and the plastic triaxial shear strain, respectively. Similar to the observation by Cuccovillo and Coop (1999), it is found in this study that cementation hinders the dilatancy prior to yielding. The yield points in figures 3.28 and 3.29 are determined as the starting points of the transition from a stiff to a less-stiff response. As shown, the increase in dilatancy accelerates afterwards and the maximum dilatancy appears after peak stress ratio. However, with agreement from the finding by Wang (2008), the peak strength (or the peak–stress ratio) and the maximum dilatancy do not occur at the same axial strain, as can be seen in Fig. 3.30. It shows deviator stress and volume strain versus axial strain in space (q-ε_1-ε_V) of silica cemented sand (50-200 kg/m^3 cement plus 10% silica fume) in drained condition at 180 days curing time. Unloading-reloading cycles are shown for 150 and 200 kg/m^3 cement content samples.

3.5.6 Stress Dilatancy and Bond Breakage

Cuccovillo and Coop (1999) suggested that the total work done by the stresses at the boundary of a specimen (ΔW) can be simply considered to be dissipated by frictional loss (ΔW_{fric}) and breakage of the cementing bond (ΔW_{bond}), i.e. (Wang, 2008):

$$\Delta W = \Delta W_{\text{fric}} + \Delta W_{\text{bond}} \qquad (3.13)$$

By applying the stress–dilatancy theory in an axisymmetric condition, and considering a unit volume, Eq. (3.13) can be written as:

$$q\,\delta\varepsilon_s^p + p'\,\delta\varepsilon_v^p = MP'\,\delta\varepsilon_s^p + \Delta W_{bond} \qquad (3.14)$$

Or:

$$\frac{q}{p'} = M - \frac{\delta\varepsilon_v^p}{\delta\varepsilon_s^p} + \frac{\Delta W_{bond}}{p'\,\delta\varepsilon_s^p} \qquad (3.15)$$

Hence, the stress ratio q/p' is determined by three components. They are the critical-state stress ratio M (*i.e.* friction at the critical state), the dilatancy d defined as ($-\delta\varepsilon_v^p / \delta\varepsilon_s^p$), and the energy used in the bond breakage or destructuration, which is related to the mobilized cohesion component. The bond breakage initially is not intensive and occurs randomly. The

bonding network at this stage can still redistribute the carried load and an elastic response is maintained. The bond breakage then accelerates, eventually leading to yielding, for an axial strain level depending on confining pressure, cement content or kind of binders (see Fig. 3.13 to 3.15 and Fig.3.30). As shown in Figure 3.28 and 3.29, the stress ratio rapidly increases prior to yielding, however the bonding network hinders the plastic response and the associated dilatancy. It means that the applied energy is mainly used to break bonds rather than to dilate the specimen. After yielding, the increase in the stress ratio gradually slowers but the augmentation of dilatancy speeds up. The peak strength is attained for $\varepsilon_v = 0$ in $\varepsilon_v - \varepsilon_1$ space (Figs. 3.13 and 3.30). The bond-breakage leads to a decrease in strength, but at the same time, produces clusters and decemented particles. These clusters and particles are released from the bonding network and can contribute to the volumetric dilation, which in turn increases the dilatancy d and strength (Wang and Leung, 2008). The applied energy at the peak state therefore is used for bond breakage, dilatancy and friction.

This explains why the measured peak strength parameters c_p' and φ'_p are influenced by the cement content as shown in Figs. 3.24 to 3.26. After the peak strength, bond breakages are numerous and concentrated within the shear band. The strength reduction owing to decementation at this stage gradually overwhelms the strength compensation due to the dilatancy. This is why, as shown in Figs. 3.28 to 3.30, the strength for maximum dilatancy is lower than the peak deviator stress, although the associated dilatancy is maximized.

Lambe (1960) identified cohesion, dilatancy, and friction as the three strength components to describe the strength behavior in clayey soils, each component considered to be mobilized and prevail at different strain levels. The same attempt is made here for cemented silica sand as shown in Figs. 3.28 and 3.30. The friction and dilatancy components are simply estimated according to the stress–dilatancy relationship of the original Cam Clay model (Roscoe and Schofield 1963):

$$q = p'M - P'\frac{\delta\varepsilon_V^P}{\delta\varepsilon_S^P} \qquad (3.16)$$

The value of M is derived based on the associated ultimate-state friction angle. Eq. 3.15 indicates that cementation serves as the third component of q or q/p', *i.e.* the mobilized

cohesion. Thus, the predictions from the stress-dilatancy relationship without considering cohesion are expected to underestimate the value of *q* or *q*/*p*' (Mántaras and Schnaid 2002, Lo *et al.* 2003).

Fig. 3.31 presents the stress ratio *q*/*p*' against the dilatancy *d* at the state of peak strength in space q_p/p'_p - $d\varepsilon_V/d\varepsilon_s$ for cemented silica sand (50-200 kg/m^3 cement with addition of 0 ,40 and 80% lime+silica fume) at 28 days curing. The stress–dilatancy relationships of the original Cam Clay (Roscoe and Schofield, 1963) is indicated in Fig. 3.31 and Rowe's equation (Rowe 1962) is also plotted in space $R=\sigma'_1/\sigma'_3$ – $D=1-d\varepsilon_V/d\varepsilon_1$ as a comparison in Fig.3.32. The results shown in Figs. 3.31 and 3.32 also explain why the measured peak-state strength parameters are related to the cement content. The dilatancy at the peak state increases with increasing cement content and decreasing confining pressure, so that the peak friction angle φ'_P follows the same trend.

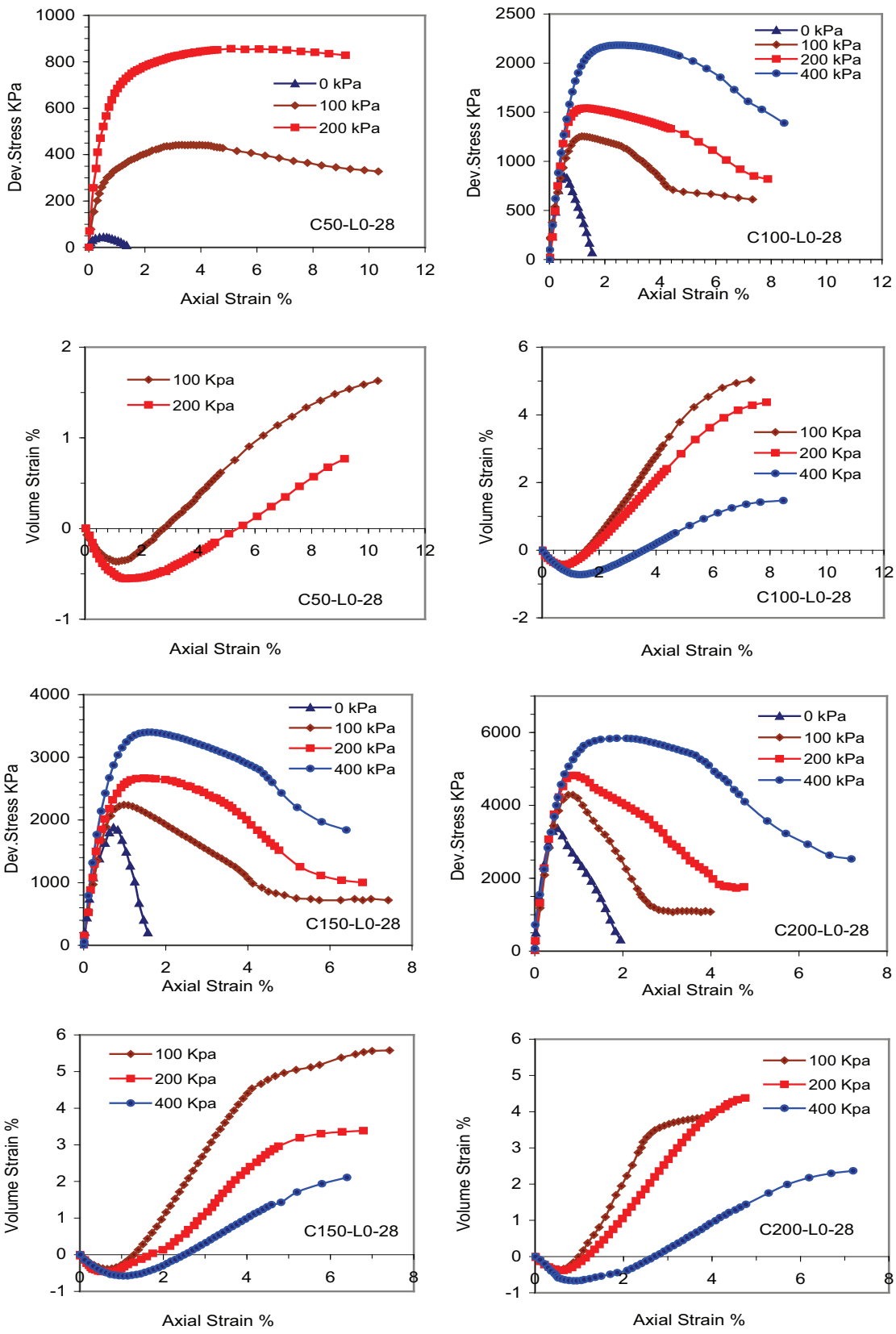

Figure 3.13 *Stress–strain behavior of cemented sand for silica soil-cement with 50 to 200 kg/m^3 Portland cement plus 10 % silica fume, for different effective confining pressures (0 to 400 kPa) at 28 days curing time*

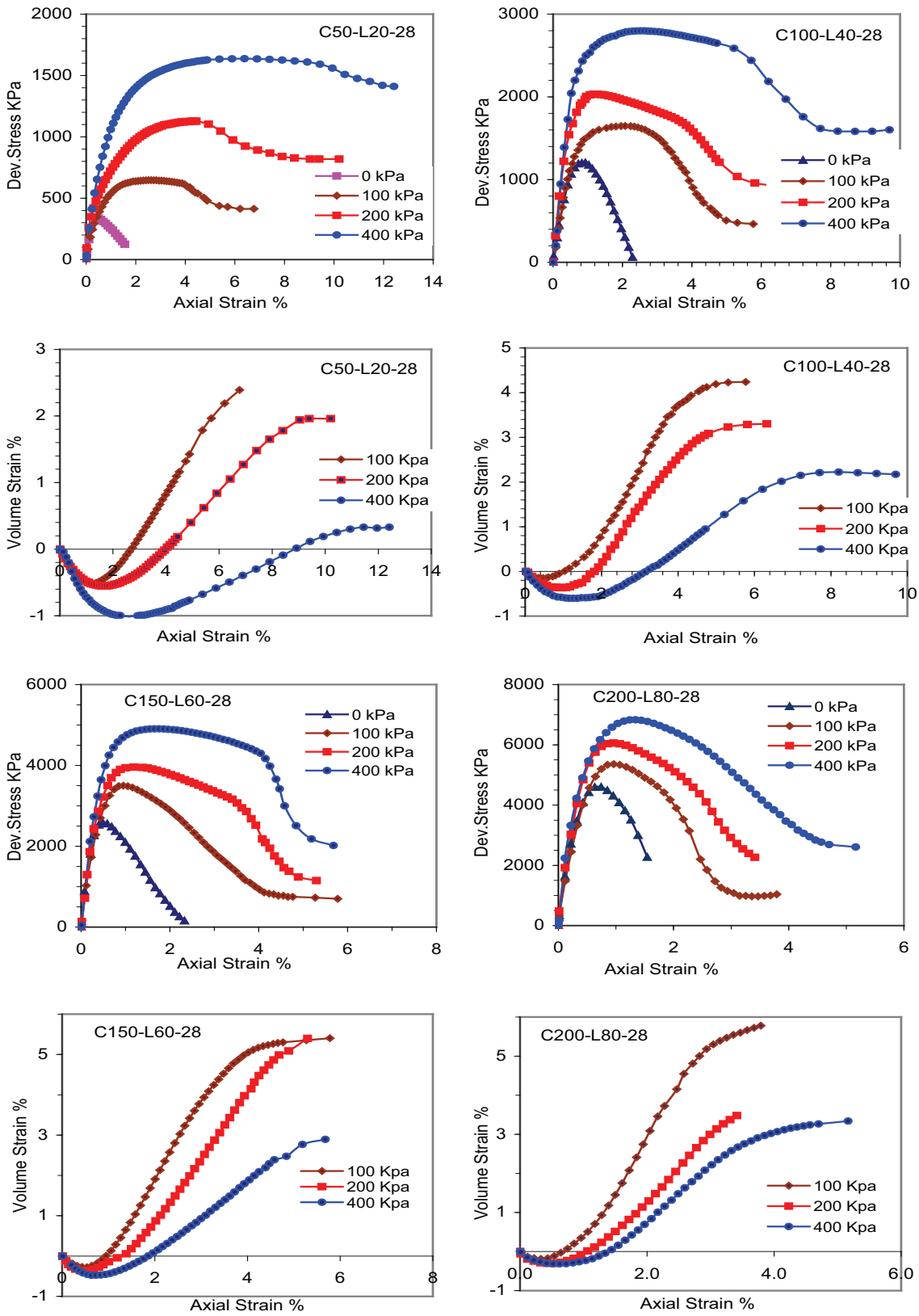

Figure 3.14 *Stress–strain behavior of cemented sand for silica soil-cement with 50 to 200 kg/m^3 Portland cement plus 40 % lime+silica fume, for different effective confining pressures (0 to 400 kPa) at 28 days curing time*

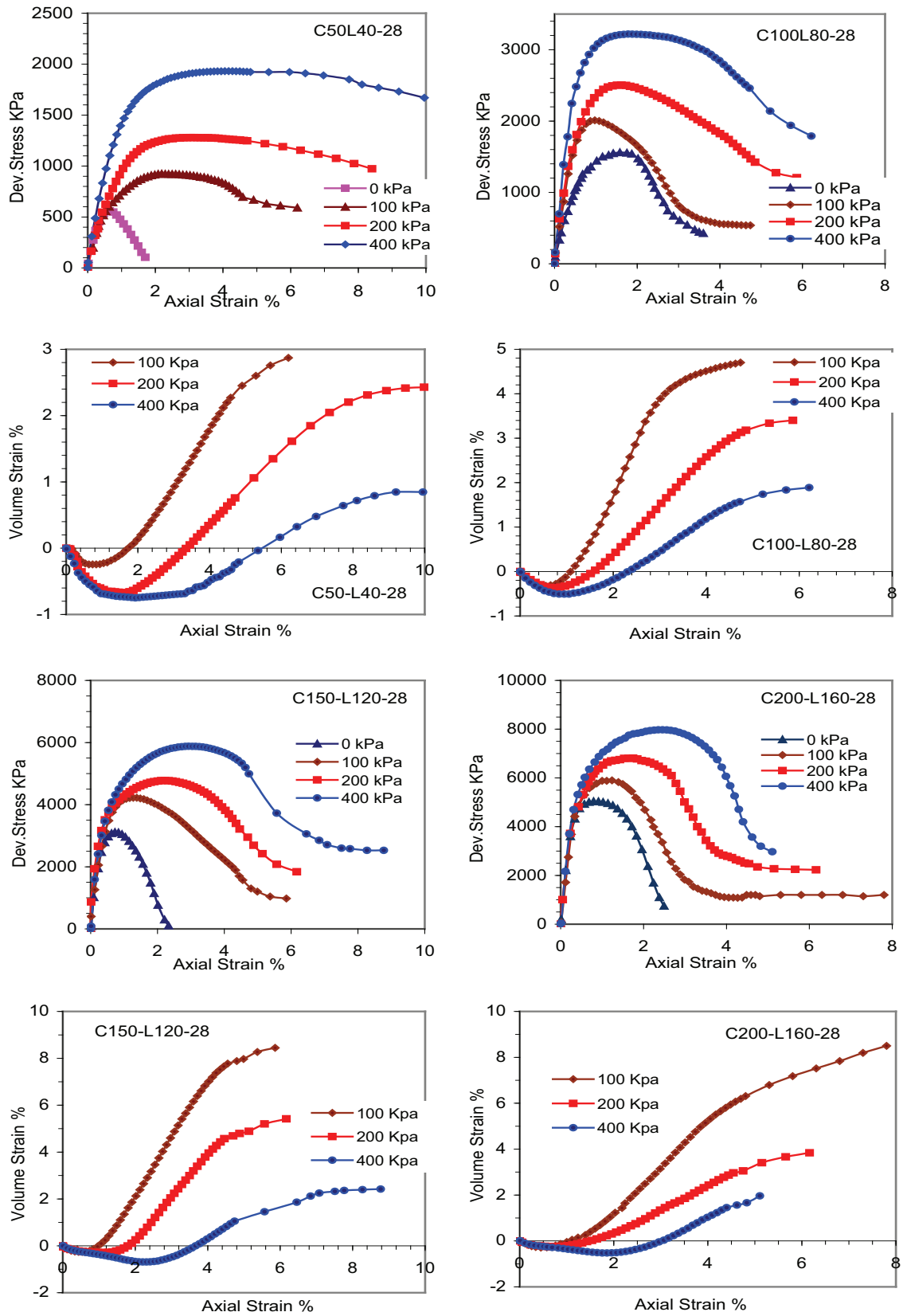

Figure 3.15 *Stress–strain behavior of cemented sand for silica soil-cement with 50 to 200 kg/m^3 Portland cement plus 80 %lime+silica fume, for different effective confining pressures (0 to 400 kPa) at 28 days curing time*

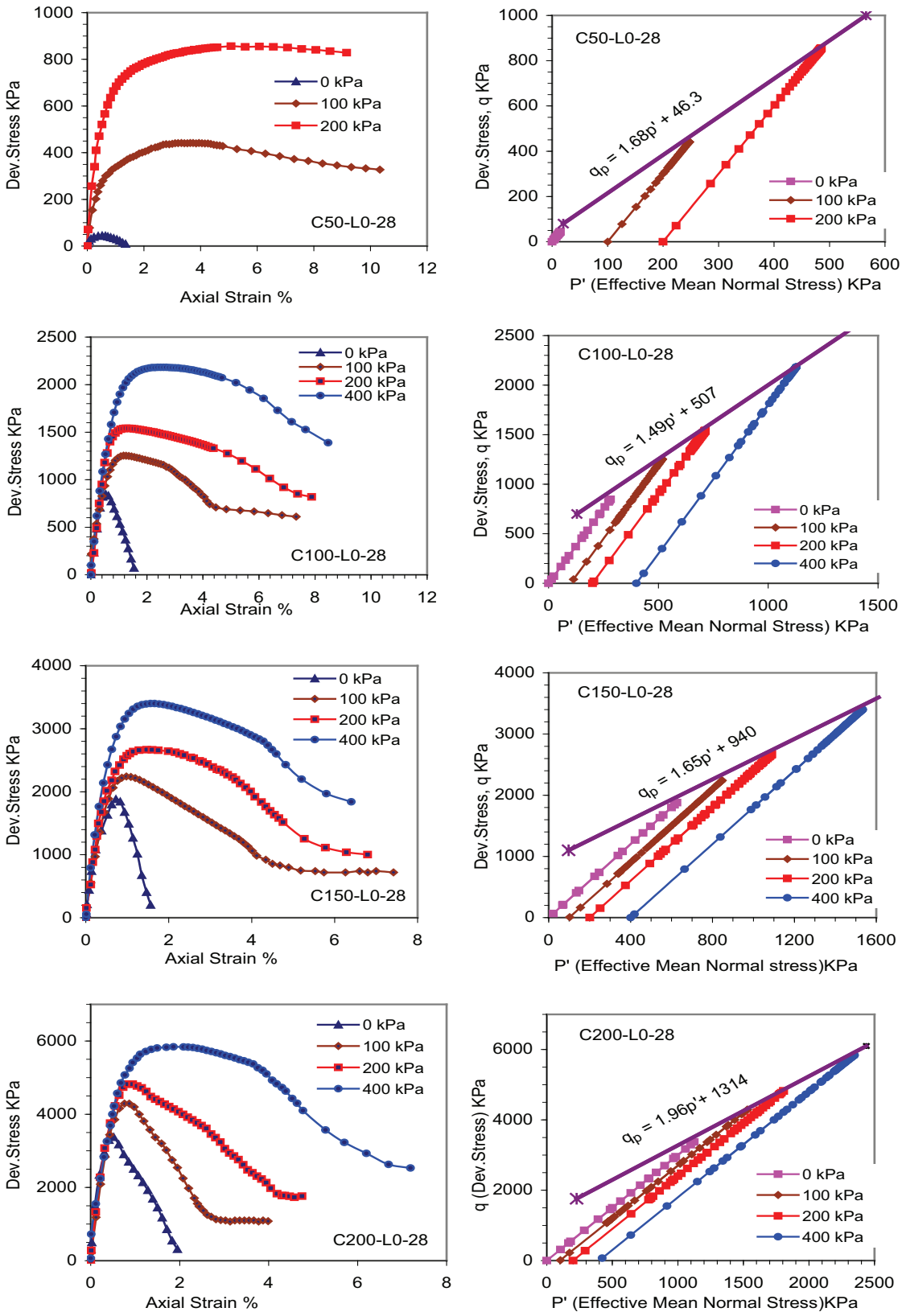

Figure 3.16 *Stress-strain and failure data for silica soil-cement with 50 to 200 kg/m^3 Portland cement plus 10 % silica fume, for effective confining pressures 0 to 400 kPa at 28 days curing*

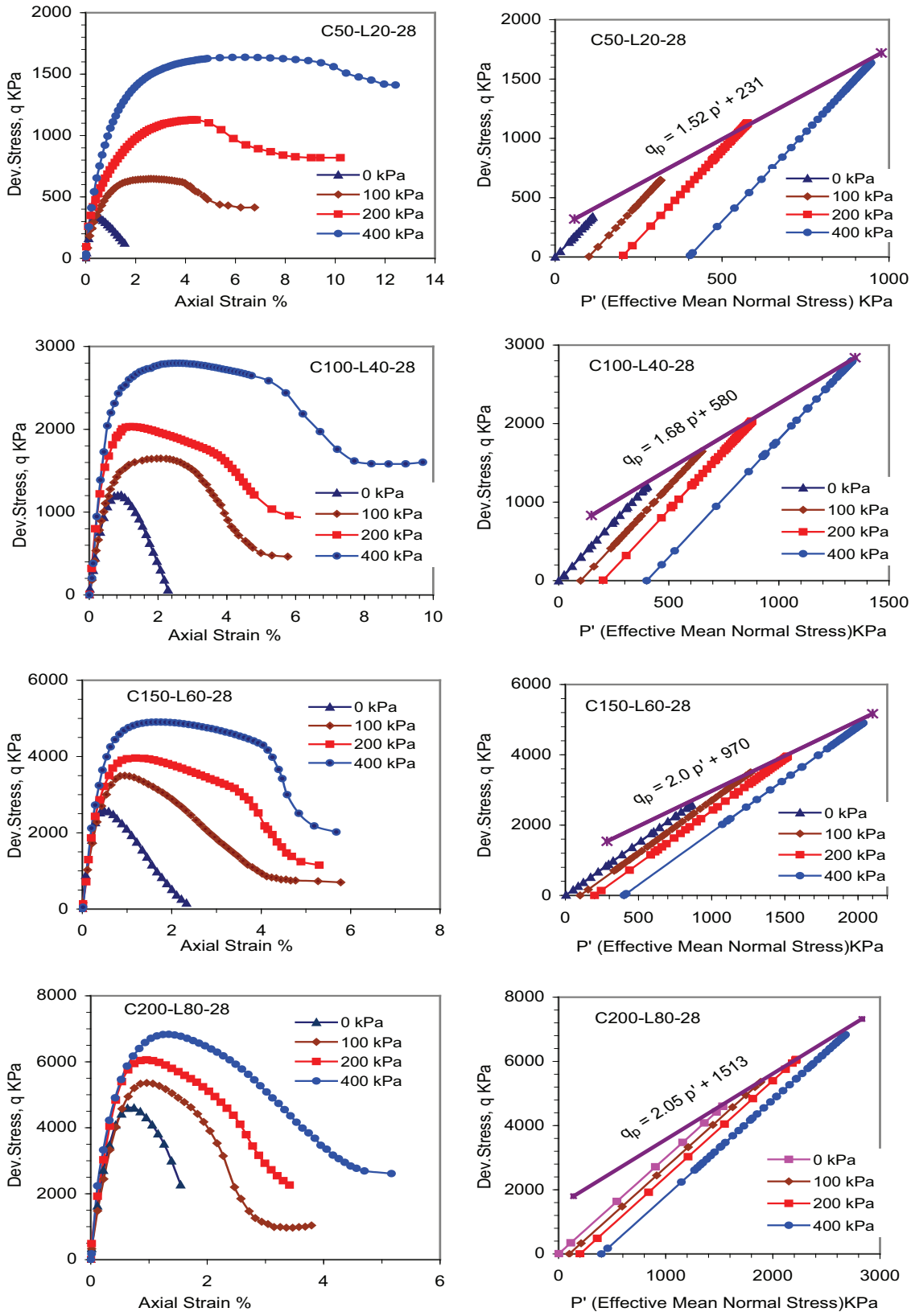

Figure 3.17 *Stress-strain and failure data for silica soil-cement with 50 to 200 kg/m^3 Portland cement plus 40 % lime+silica fume, for effective confining pressures 0 to 400 kPa at 28 days curing*

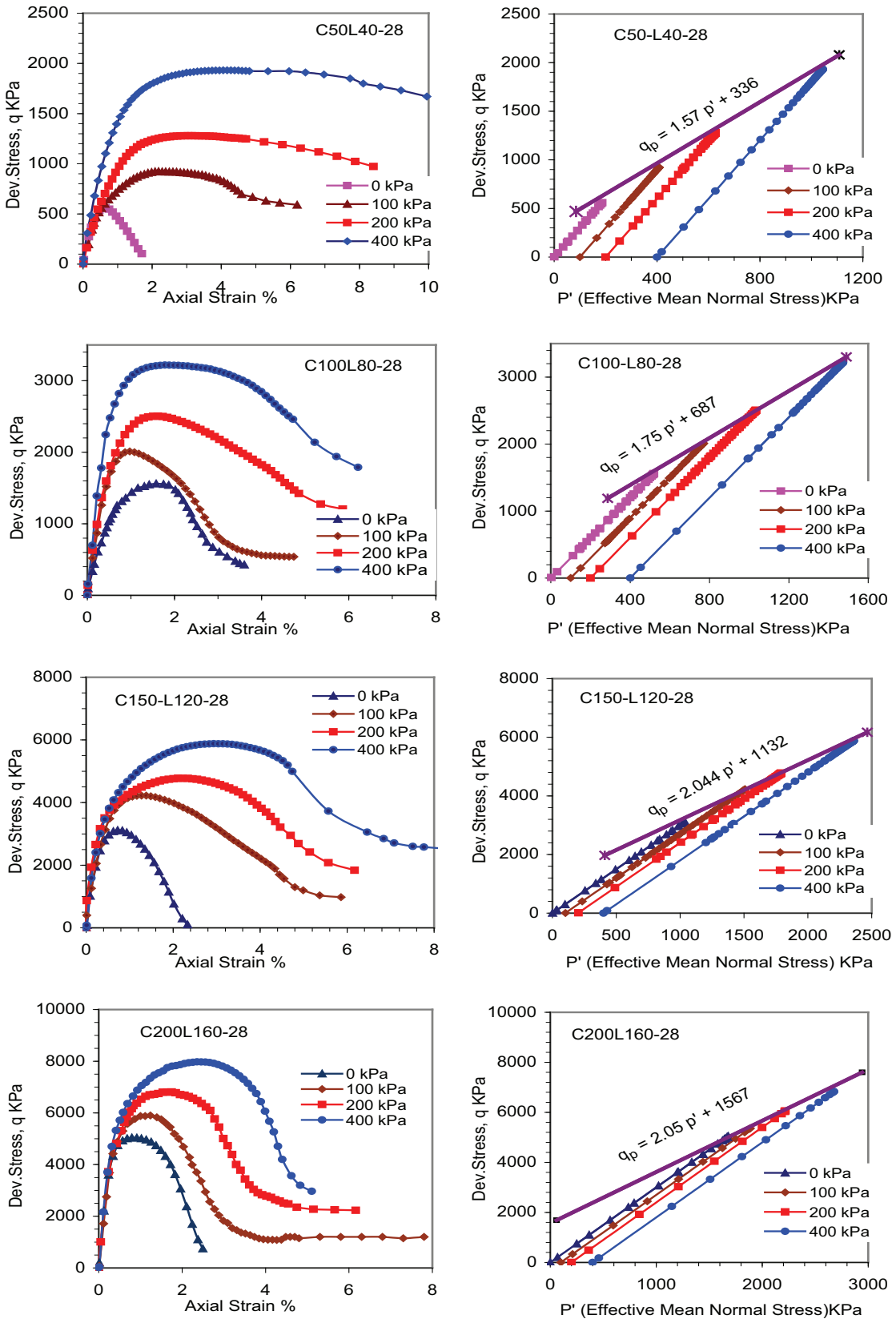

Figure 3.18 *Stress-strain and failure data for silica soil-cement with 50 to 200 kg/m^3 Portland cement plus 80 % lime+silica fume, for effective confining pressures 0 to 400 kPa at 28 days curing*

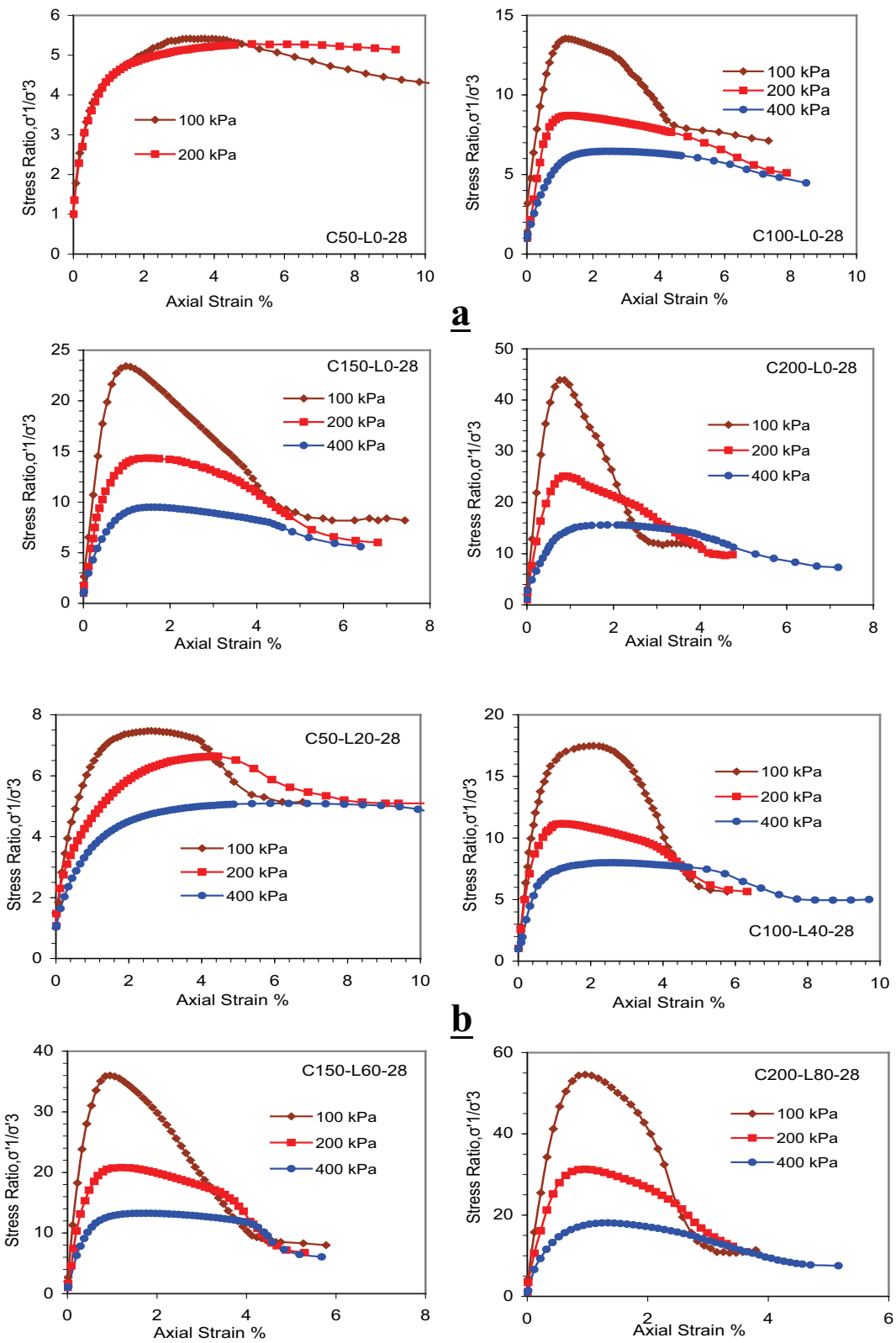

Figure 3.19 *Principal stress ratio versus axial strain,$\sigma'_1/\sigma'_3 - \varepsilon_1$ for: (a) Silica sand cemented with 50 to 200 kg/m^3 Portland cement plus 10% silica fume, compared with (b)samples cemented with 50 to 200 (kg/m^3) Portland cement plus 40% (lime+ silica fume) for effective confining pressures 0 to 400 kPa at 28 days curing.*

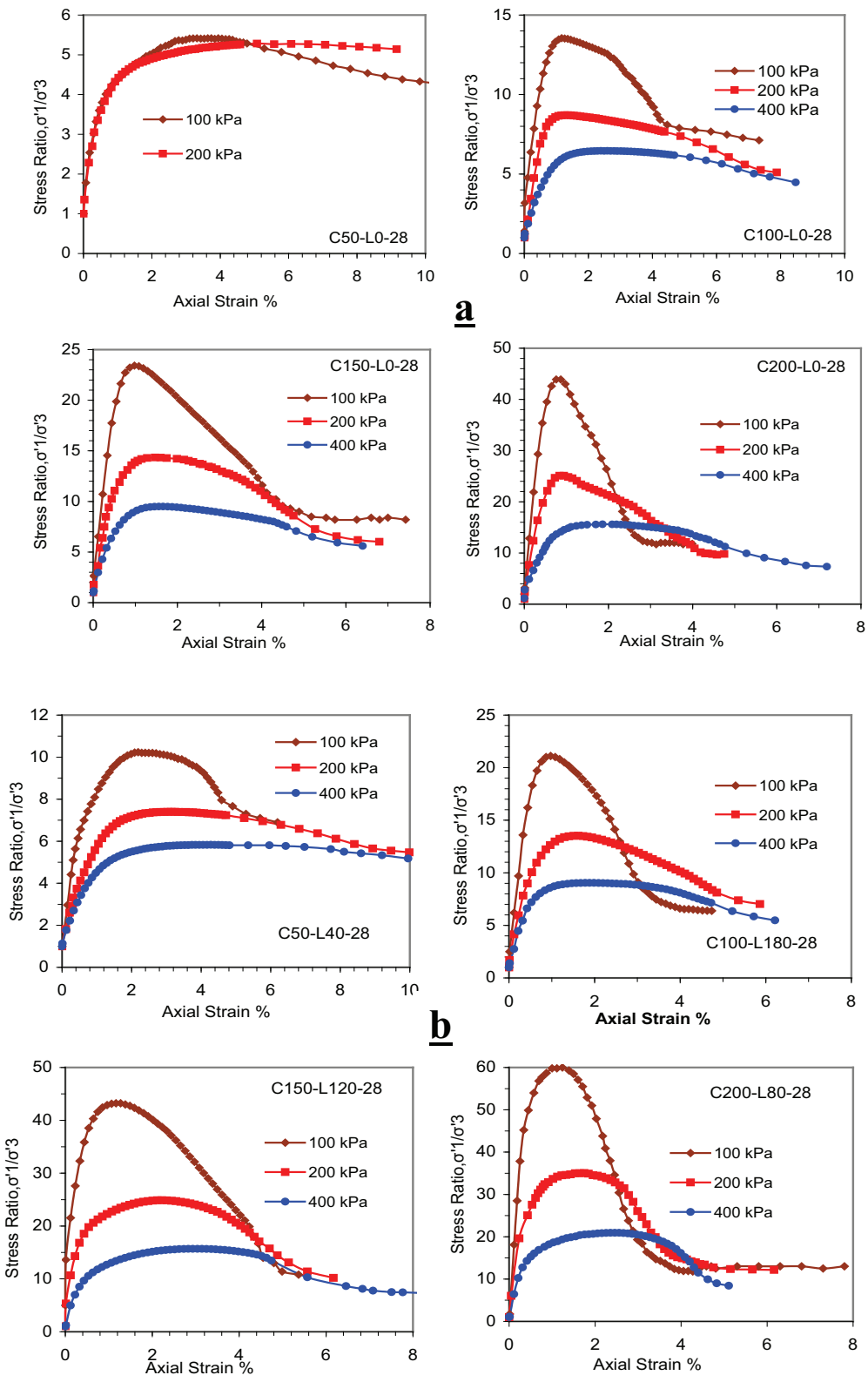

Figure 3.20 *Principal stress ratio versus axial strain,$\sigma'_1/\sigma'_3 - \varepsilon_1$ for: (a) Silica sand cemented with 50 to 200 kg/m^3 Portland cement plus 10% silica fume, compared with (b)samples cemented with 50 to 200 (kg/m^3) Portland cement plus 80% (lime+ silica fume) for effective confining pressures 0 to 400 kPa at 28 days curing.*

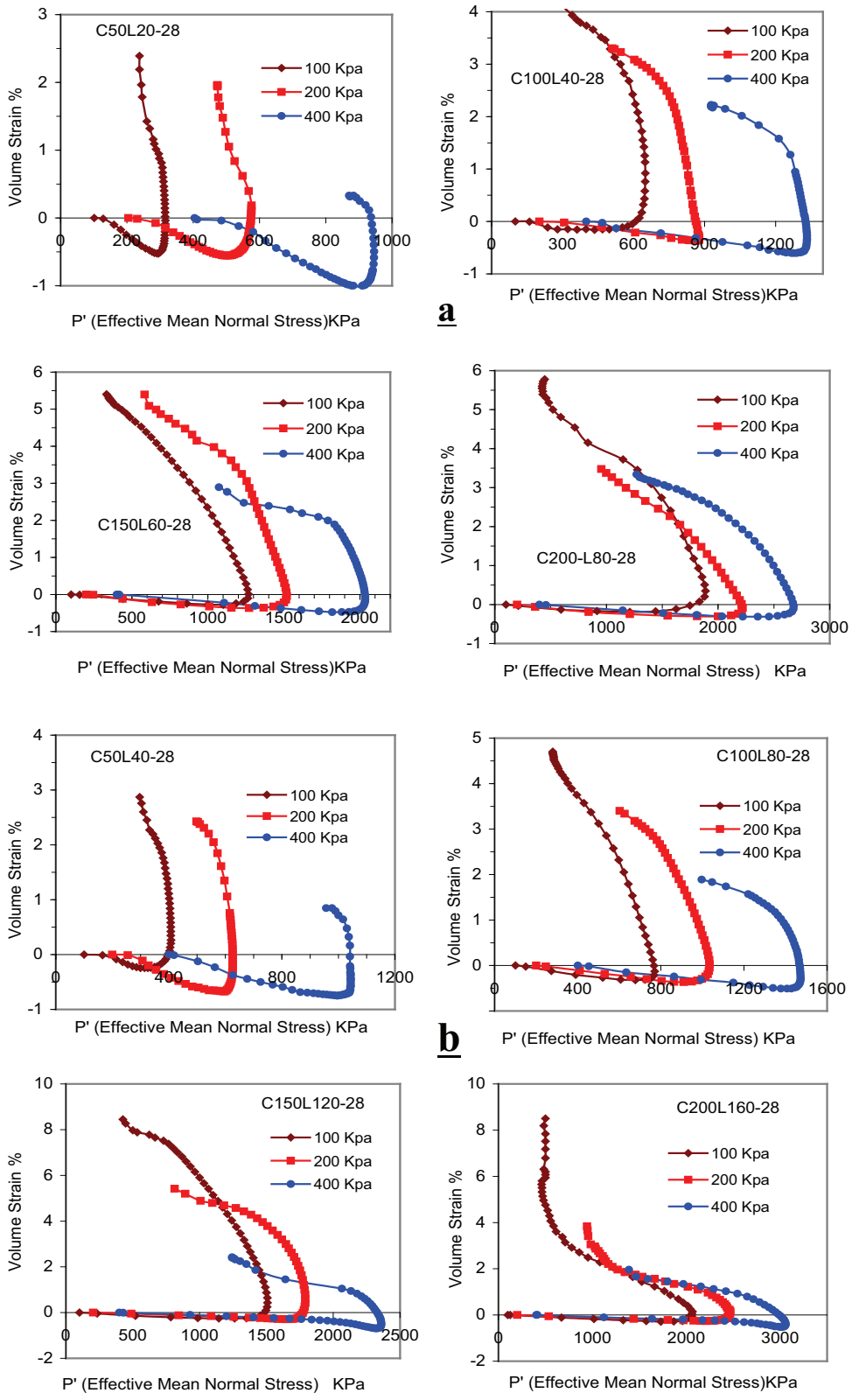

Figure 3.21 *Volume Strain versus effective mean normal stress, $\varepsilon_v - p'$, for: (a) Silica sand cemented with 50 to 200 kg/m^3 Portland cement plus 10% silica fume, compared with (b) samples cemented with 50 to 200 kg/m^3 Portland cement plus 40% (lime+ silica fume) for effective confining pressures 0 to 400 kPa at 28 days curing.*

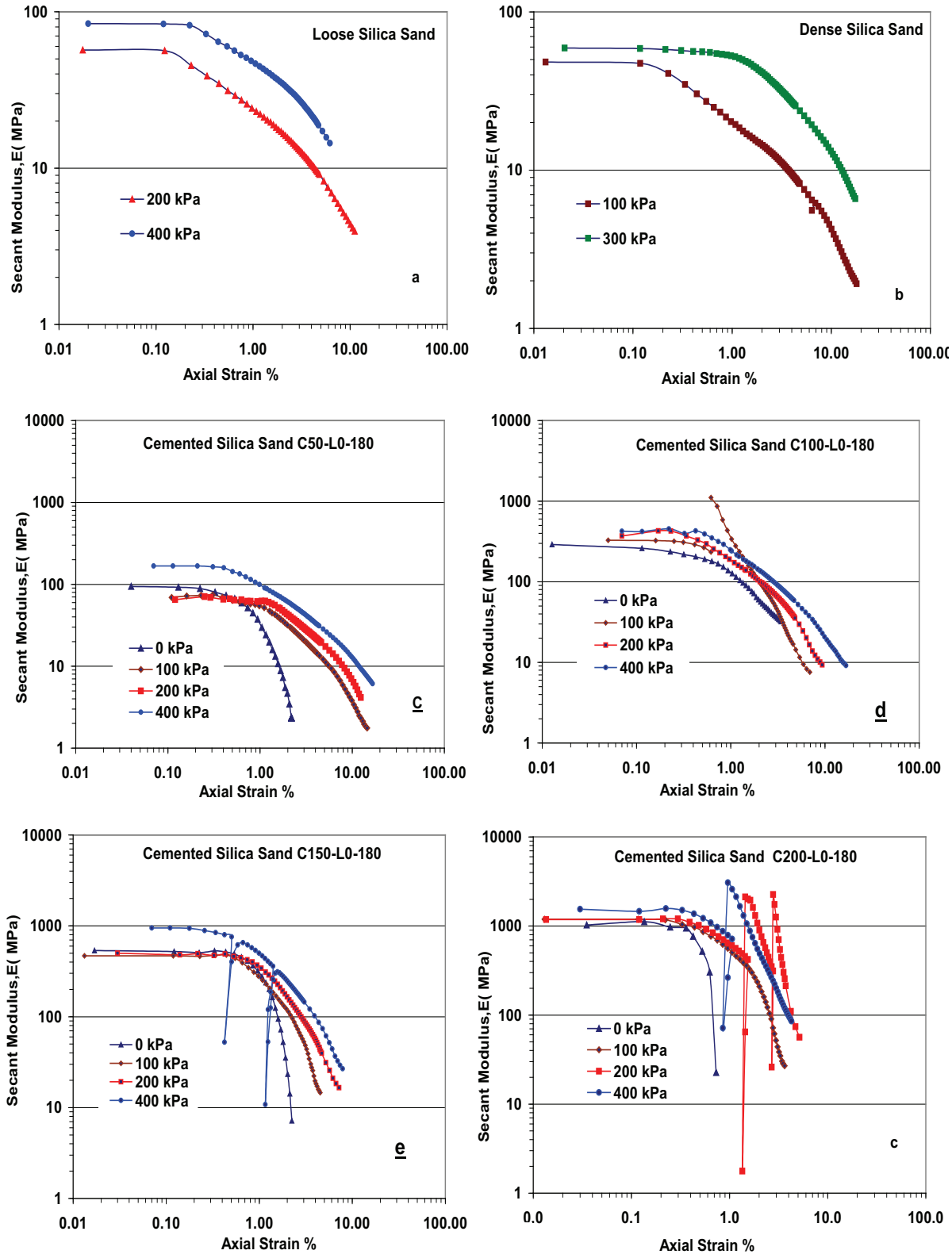

Figure 3.22 *Secant modulus versus axial strain E- ε_1 in a logarithmic scale for: (a) Loose Silica sand (b) Dense Silica sand and (c,d,e,f) cemented silica sand with 50 to 200 kg/m^3 Portland cement, for effective confining pressures 0 to 400 kPa at 180 days curing.*

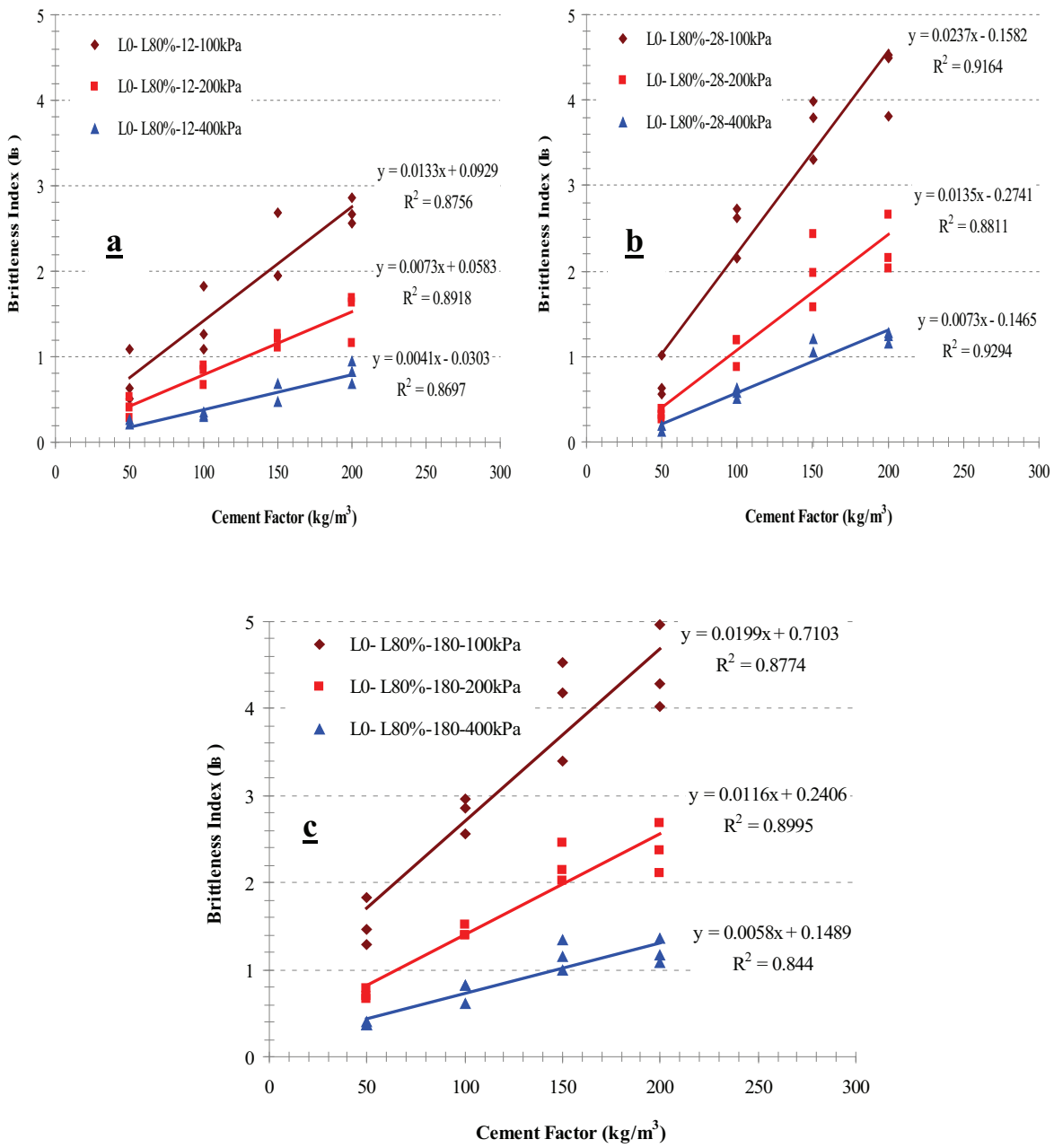

Figure 3.23 *Variation of the brittleness index I_B in drained conditions for different mix designs of cemented silica sand (50-200 kg/m^3 cement and 0 to 80% lime+silica fume): (a) 12 days curing, (b) 28 days curing, (c) 180 days curing*

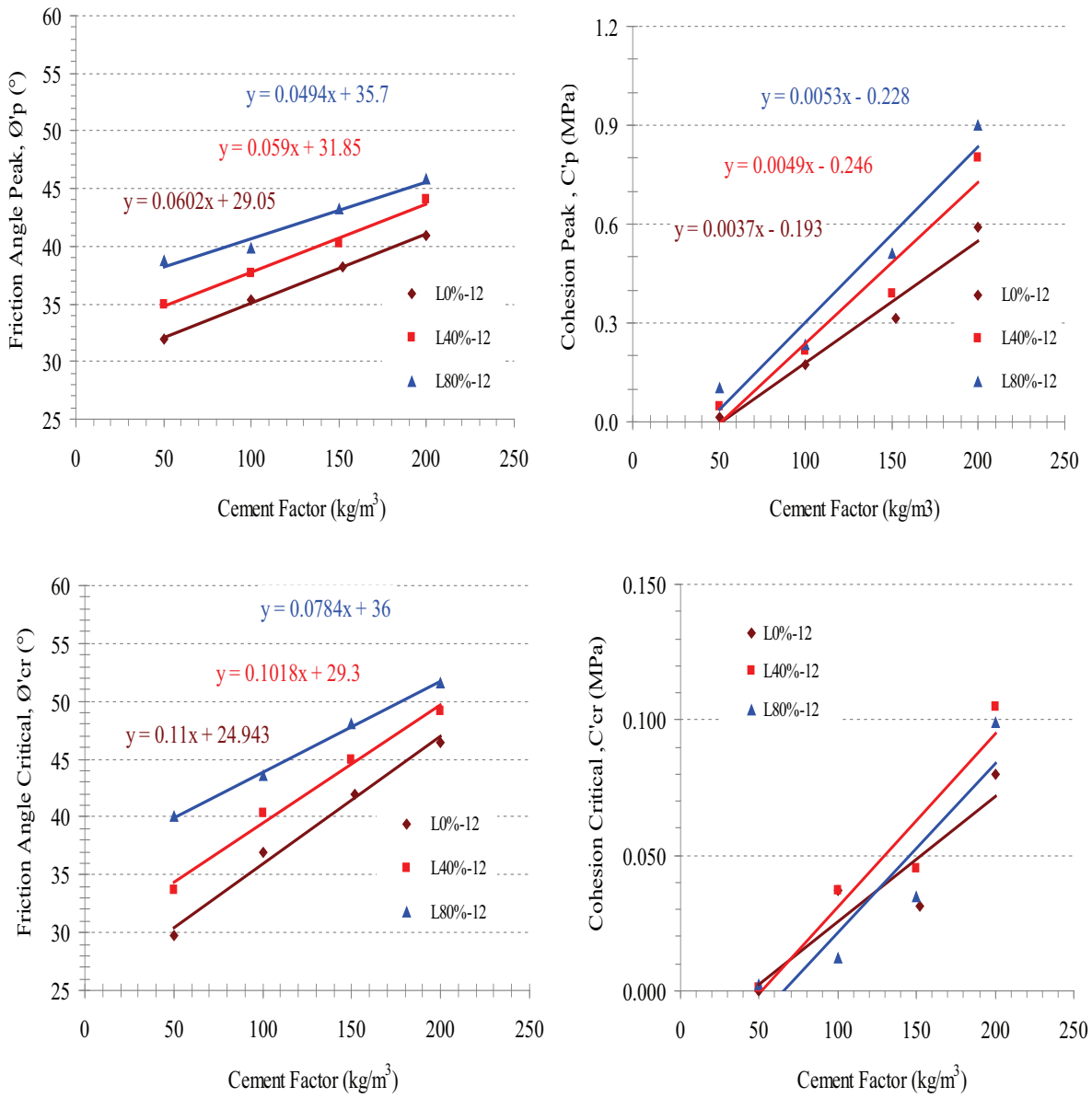

Figure 3.24 *Peak-state strength parameters C'_p , $Ø'_p$ and ultimate /critical-state strength parameters,(C'cr , Ø'cr) of cemented silica sand: 50-200 kg/m^3 cement and 0 ,40 and 80% lime+silica fume at 12 days curing*

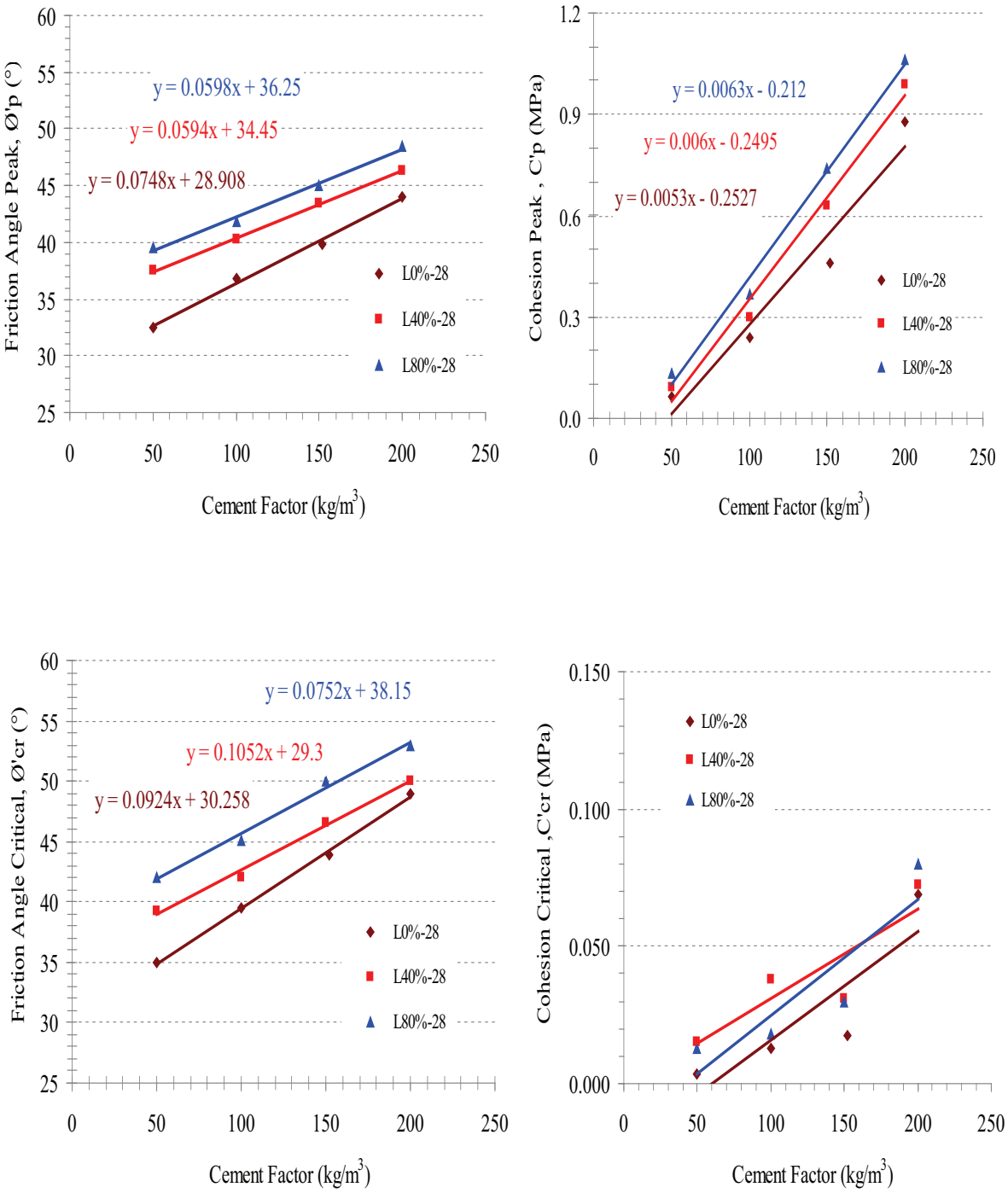

Figure 3.25 *Peak-state strength parameters C'_p , $Ø'_p$ and ultimate /critical-state strength parameters,(C'cr , Ø'cr) of cemented silica sand: 50-200 kg/m^3 cement and 0 ,40 and 80% lime+silica fume at 28 days curing*

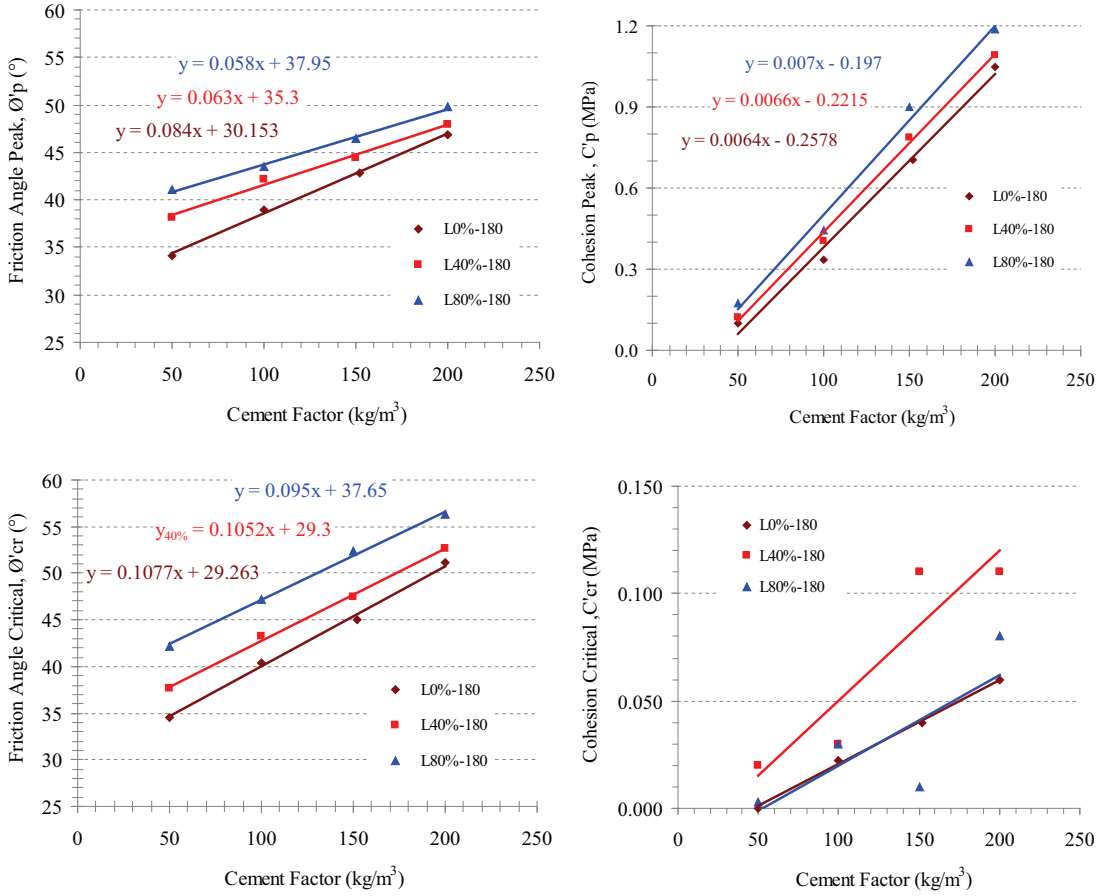

Figure 3.26 *Peak-state strength parameters C'_p , $Ø'_p$ and ultimate /critical-state strength parameters,(C'cr , Ø'cr) of cemented silica sand: 50-200 kg/m^3 cement and 0 ,40 and 80% lime+silica fume at 180 days curing*

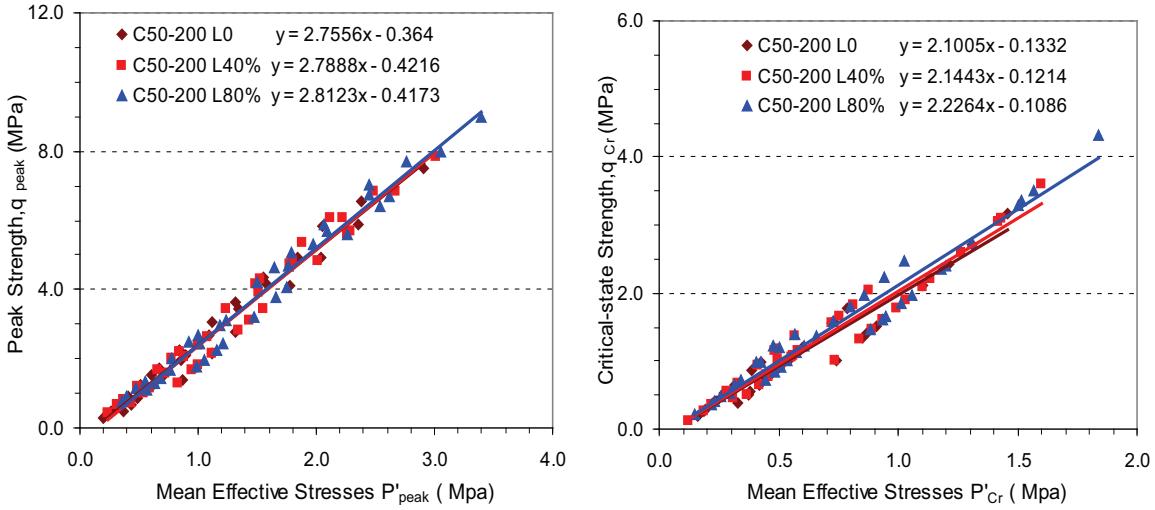

Figure 3.27 *Peak-state strength and ultimate /critical-state strength versus mean effective stress q_p, p'_p of cemented silica sand: 50-200 kg/m^3 cement and 0 ,40 and 80% lime+silica fume in drained condition at 12 to180 days curing*

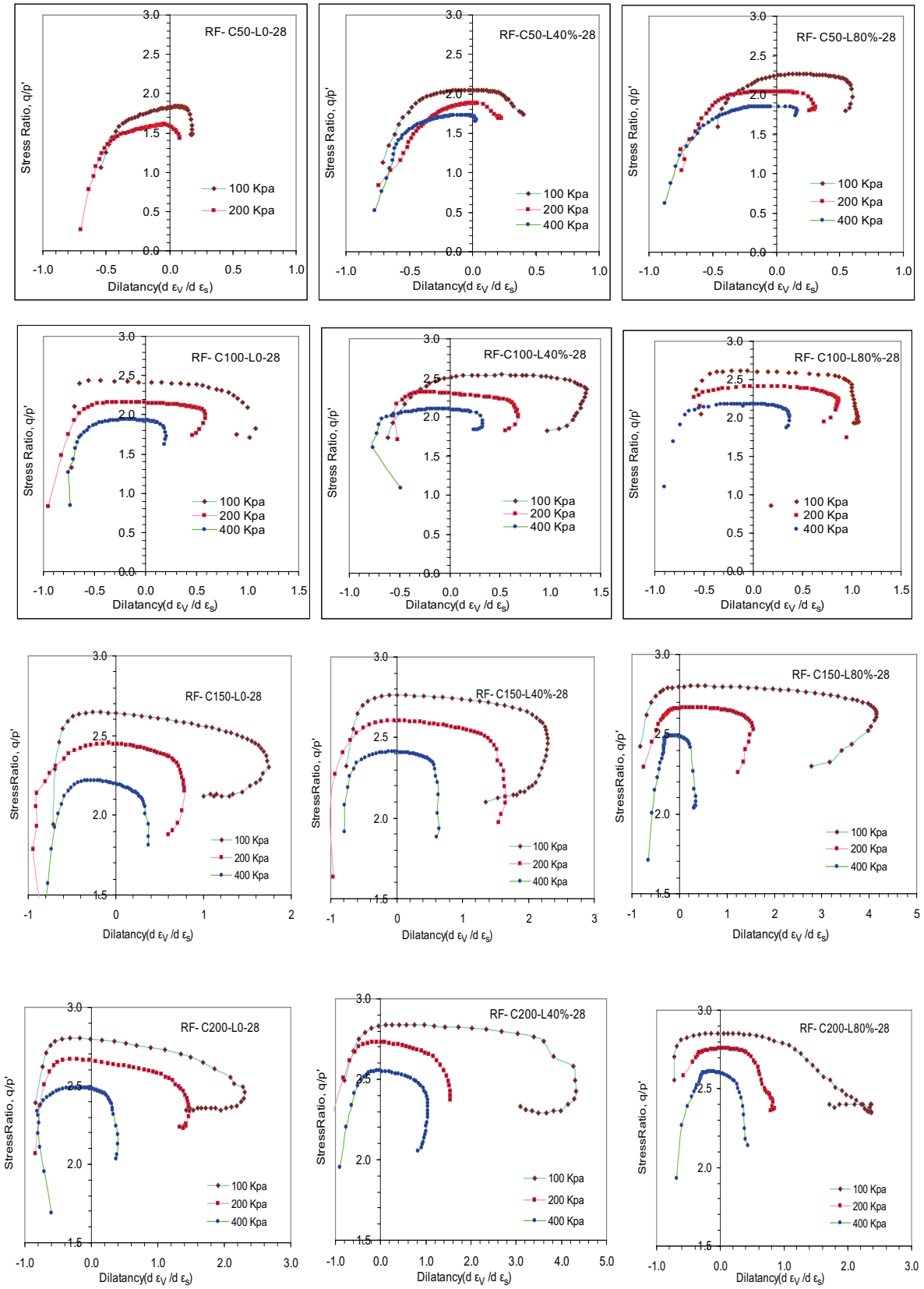

Figure 3.28 *Stress ratio versus dilatancy in space (q_p/ p'_p - d ε_V /d ε_s) of cemented silica sand: 50-200 kg/m^3 cement and 0 ,40 and 80% lime+silica fume in drained conditions at 28 days curing*

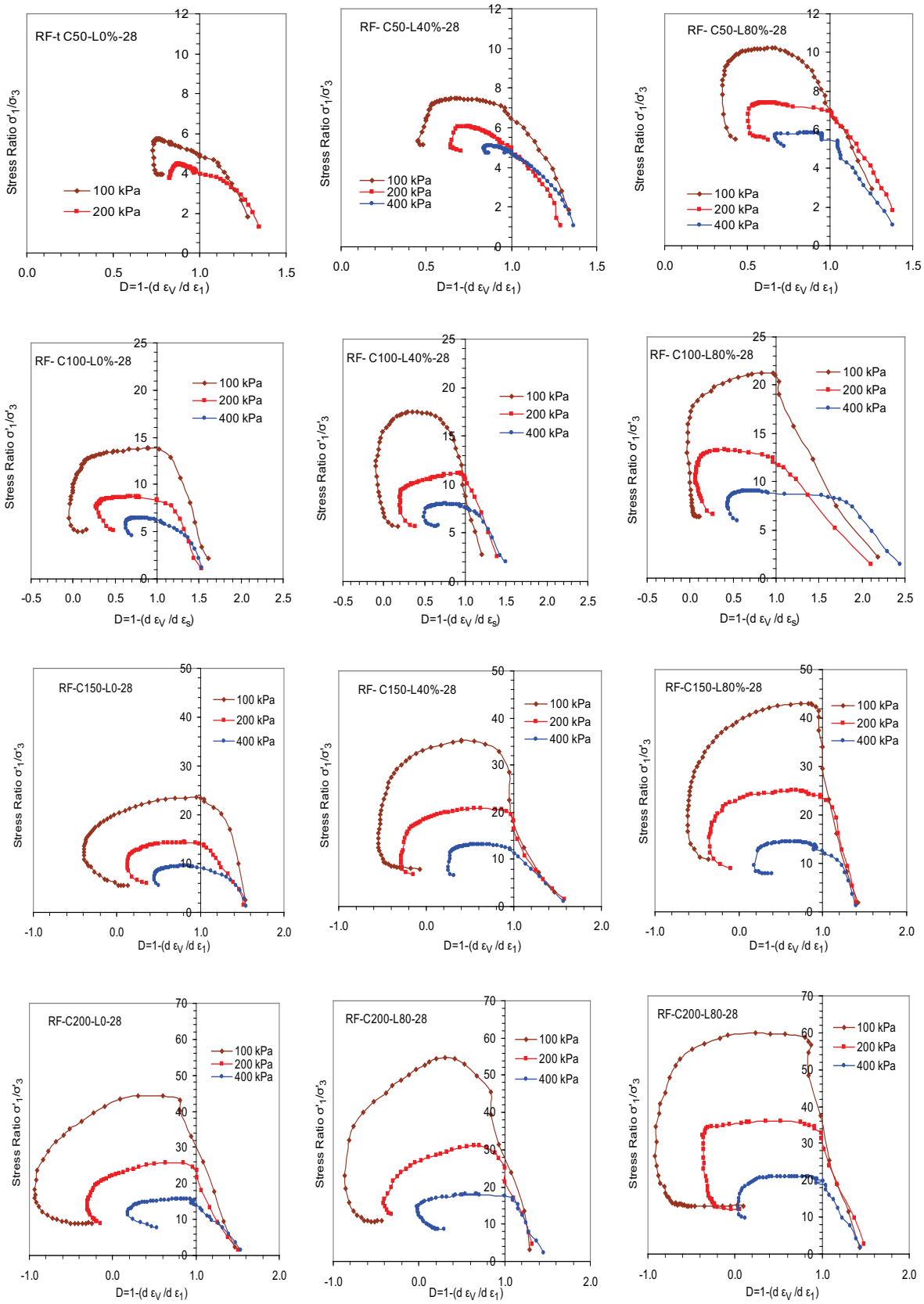

Figure 3.29 *Stress ratio versus dilatancy in space (σ'_1/σ'_3 - $d\,\varepsilon_V/d\,\varepsilon_1$) of cemented silica sand: 50-200 kg/m^3 cement and 0, 40 and 80% lime+silica fume in drained conditions at 28 days curing*

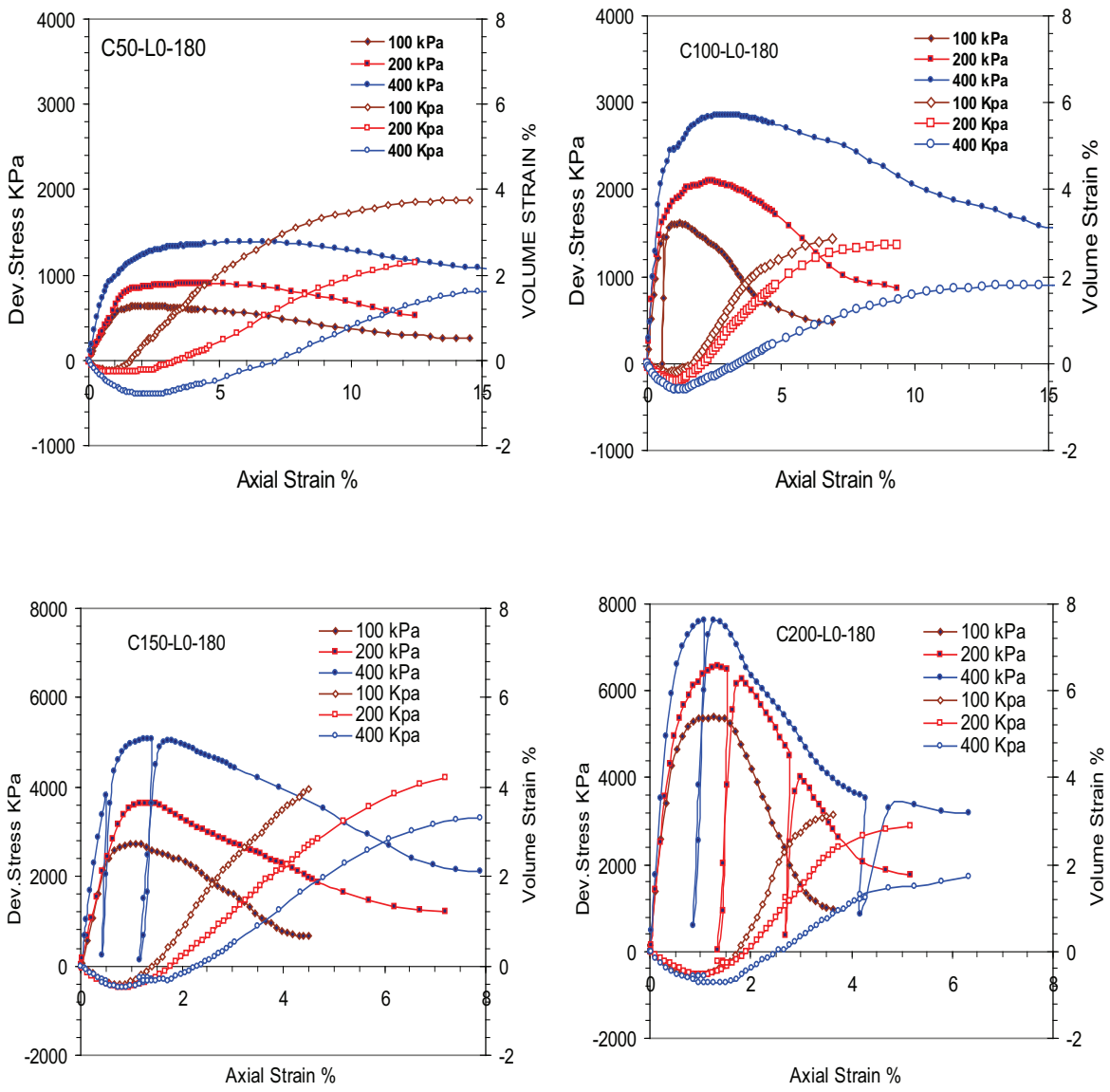

Figure 3.30 *Deviator stress and volumetric strain versus dilatancy in space (q-ε_1-ε_V) of cemented silica sand: 50-200 kg/m^3 cement plus10% silica fume in drained conditions at 180 days curing. Unloading- reloading cycles were carried out for 150 and 200 kg/m^3 cement content*

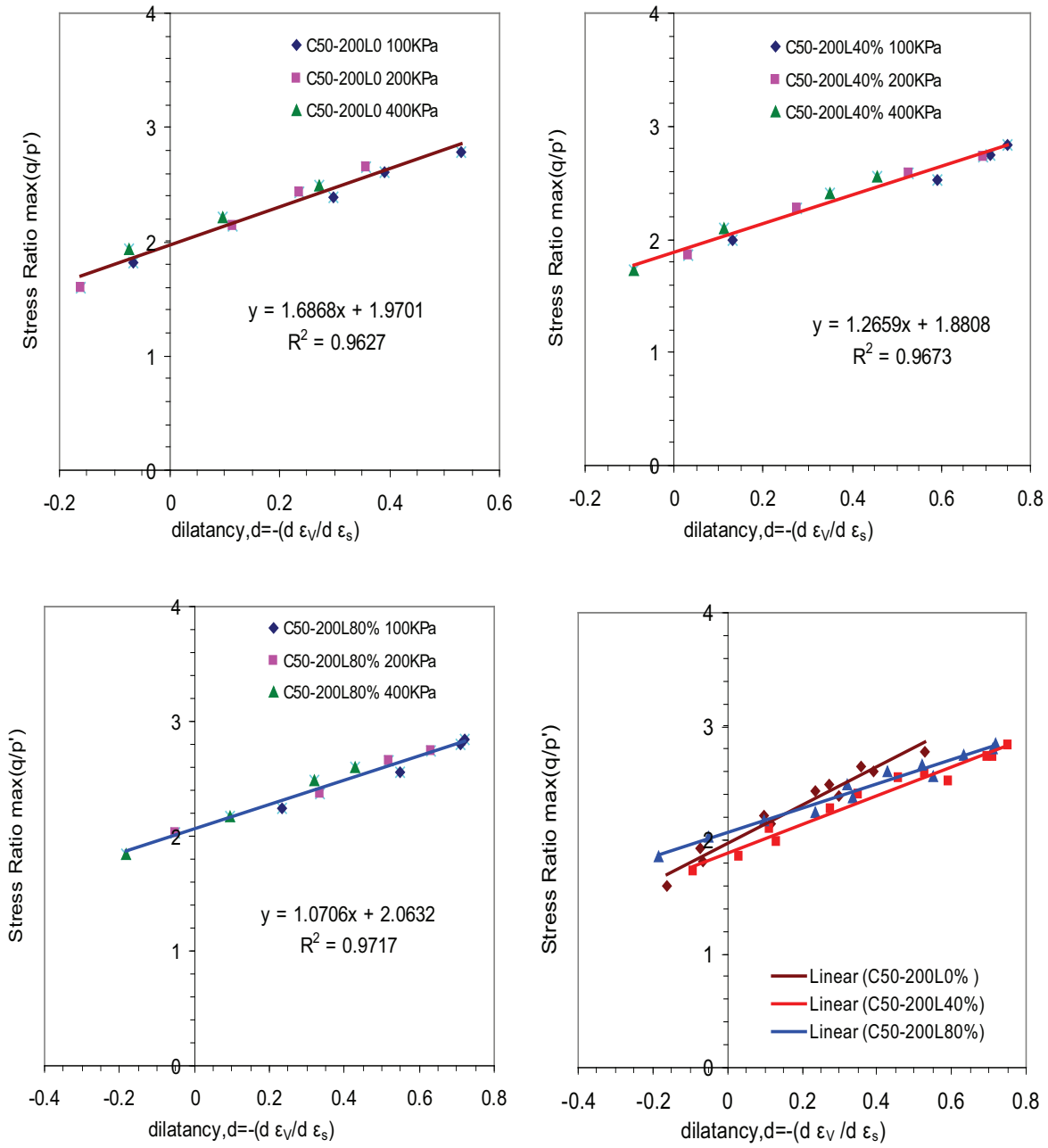

Figure 3.31 *Stress ratio versus dilatancy in space (q_p / p'_p - d ε_V /d ε_s) of cemented silica sand: 50-200 kg/m^3 cement with addition of 0 ,40 and 80% lime+silica fume at 28 days curing*

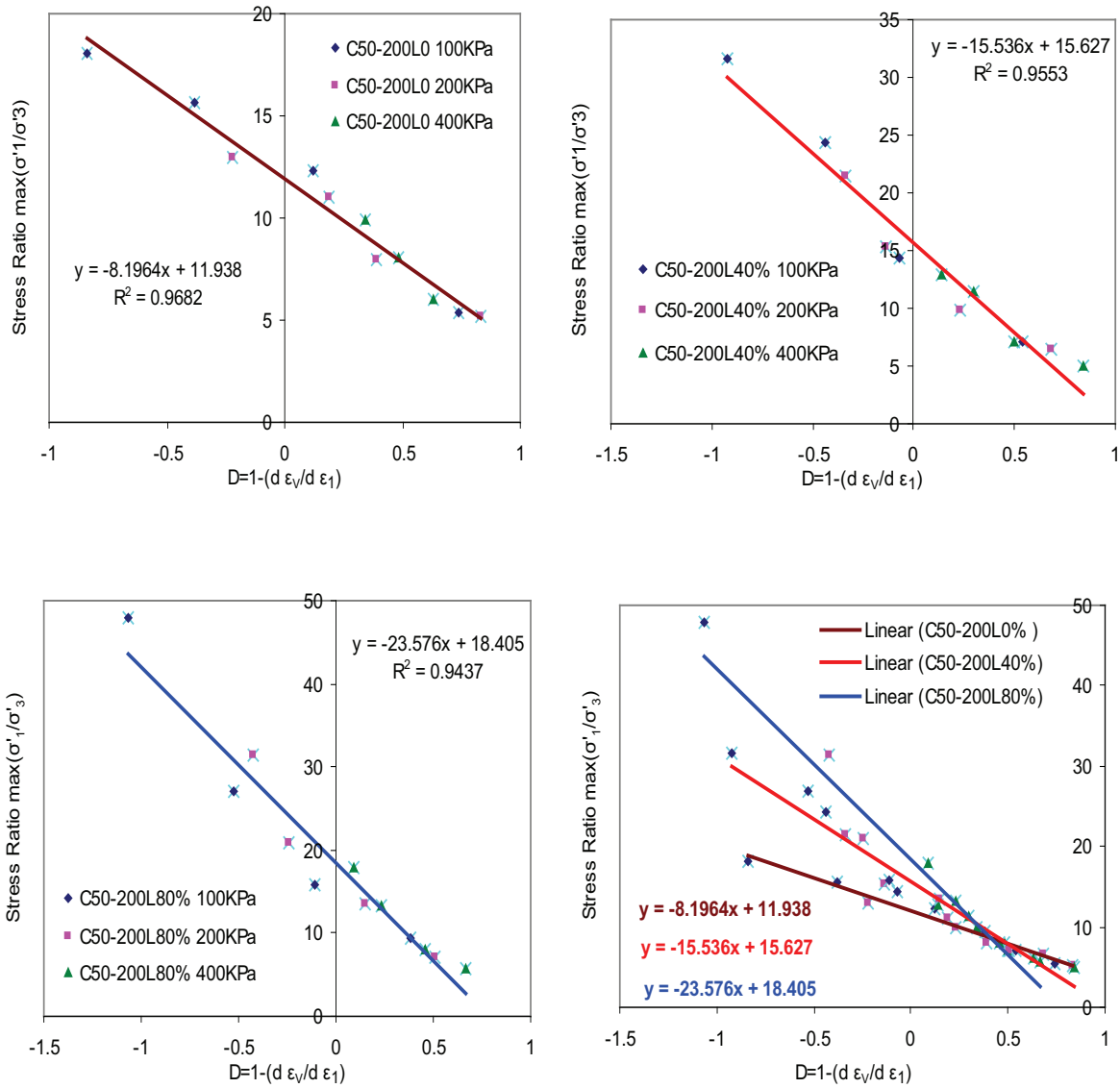

Figure 3.32 *Stress ratio versus dilatancy in space R – D where R= σ'_1/σ'_3 and D=1- ($d\,\varepsilon_V/d\,\varepsilon_1$), for cemented silica sand: 50-200 kg/m^3 cement with addition of 0, 40 and 80% lime+silica fume at 28 days curing*

3.6 Mechanical Behavior of Cemented Silica Sand by Direct Shear Tests

3.6.1 Shearing Procedure and Coulomb Envelope

For each specimen in mix design Table 2.1, the shear stress and vertical strain at peak and residual failure τ_f, τ_r are plotted against horizontal strain ε_1 (Fig. 3.33). The shear strength decreases rapidly from the peak value at first, but eventually reaches a steady state (ultimate) value which is maintained as the displacement increases. In this condition there is no expansion or contraction due to shear and the void ratio remains constant at the critical value. The shear strength ultimately reached is known as the 'residual strength', which is often lower than the 'peak strength'. The shear stress versus the corresponding normal stress, $\sigma_n^{'}$ for set of shear box tests on cemented silica sand for cement factors 50-200 kg/m^3 after180 days curing are shown in Fig 3.34. Coulomb envelopes, the best fit lines through the three points, are drawn for peak and residual stress, according to Equ. 3.17 and 3.18:

$$\tau_f = c' + \sigma' \tan\varphi' \qquad (3.17)$$

$$\tau_r = c_r' + \sigma' \tan\varphi_r' \qquad (3.18)$$

The obtained angle of friction φ and cohesion intercept *C* is summarized in Table 3.8.

Table 3.8 *Angle of shearing resistance and cohesion for peak and residual states for different mixtures of cemented silica sand in direct shear tests*

MIX CODE	180 DAYS Curing			
	Peak strength		ultimate strength	
	Øp (°)	Cp (Kpa)	Øcr (°)	Ccr (Kpa)
C50-L0	33	53	31.4	14
C100-L0	41.8	141	36.4	9
C150-L0	46	199	39	21.4
C200-L0	49.3	229	41.4	22
C50-L20	33.9	67	31	26
C100-L40	43.2	148	35.9	14
C150-L60	47.6	220	39.7	20
C200-L80	49.2	307	42	30
C50-L40	34.5	90	31.4	21
C100-L80	45.6	181	34.7	25.5
C150-L120	50	239	40.5	23
C200-L160	51	352	40.7	20

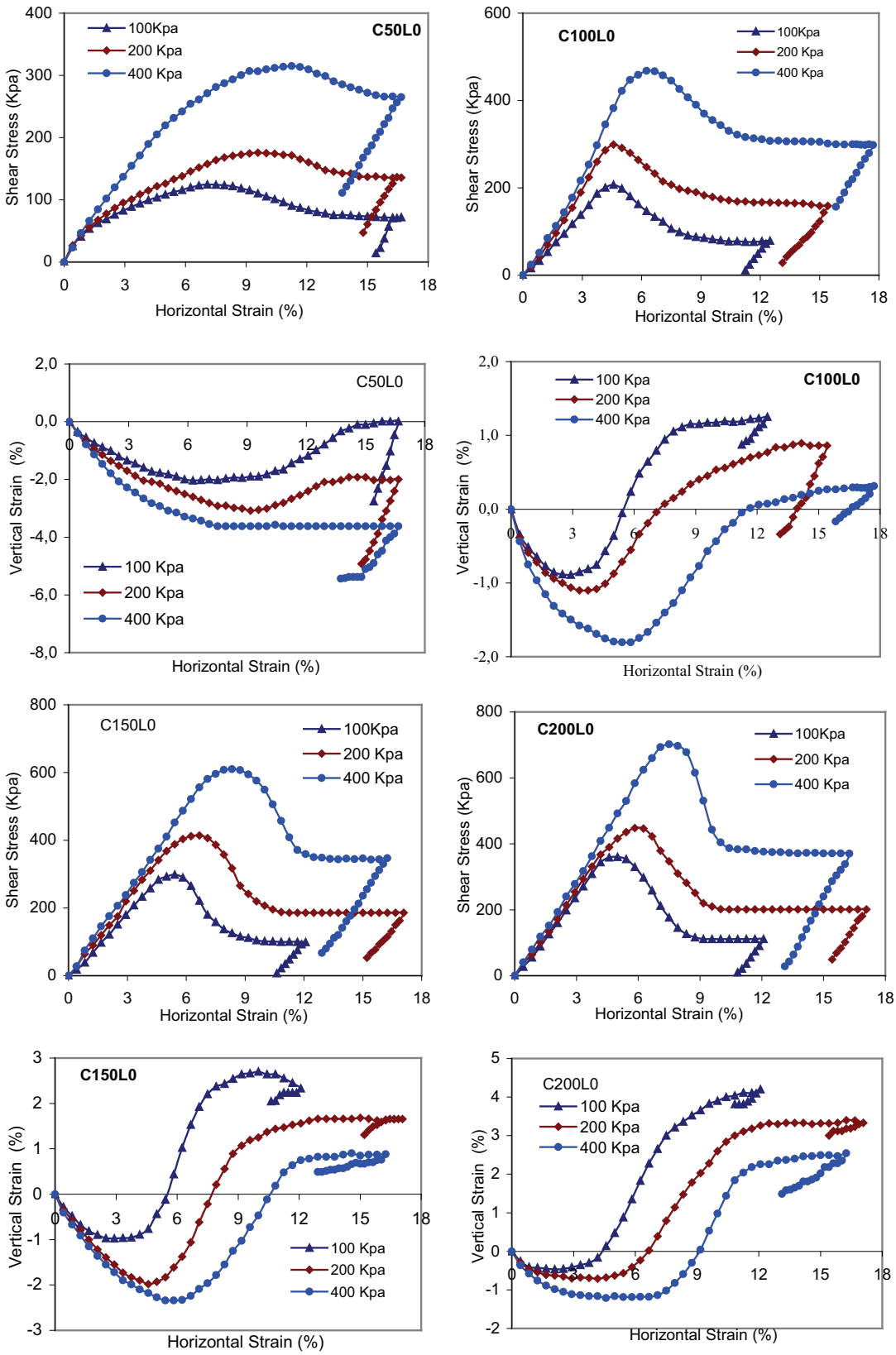

Figure 3.33 *Peak and residual shear strength and vertical strain versus horizontal strain from shear box tests on cemented silica sand (cement factors 50-200 kg/m^3 after180 days curing)*

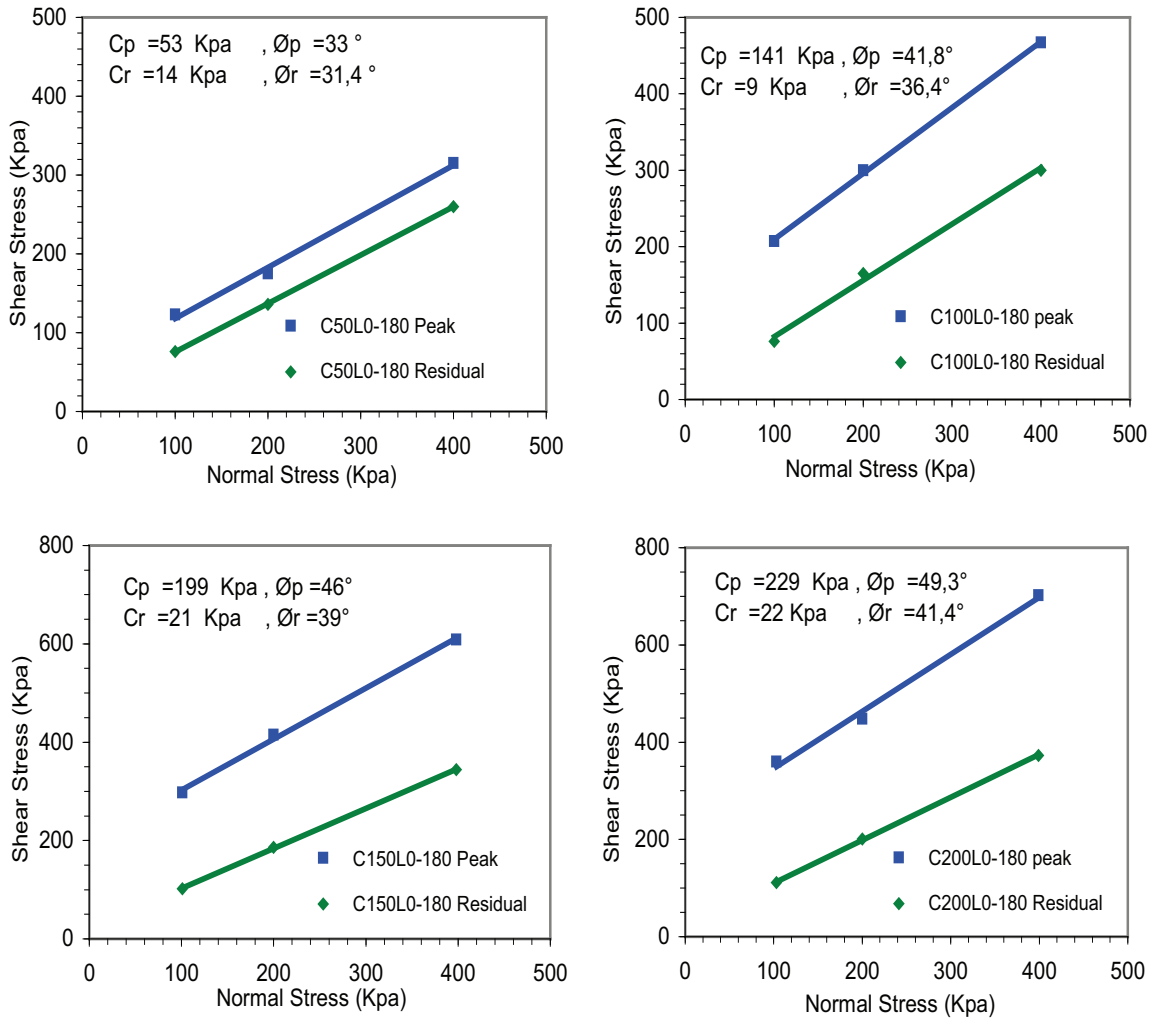

Figure 3.34 *Coulomb envelopes for peak and residual conditions in shear box tests on cemented silica sand (mix design cement factors 50-200 kg/m^3 after180 days curing)*

3.6.2 Shear modulus of cemented silica sand

Shear strain is the angular γ deformation resulting from the application of a shear stress τ.

Fig 3.35 shows the relation of shear stress versus shear strain and Fig 3.36 shows the relation of stress ratio versus shear strain in direct shear tests for cemented silica sand (cement factors 50-200 kg/m^3 after180 days curing). The shear modulus G is defined as $G = \Delta\tau / \Delta\gamma$ and is summarized in Table 3.9. Fig.3.37 shows the correlation of shear modulus versus cement contend at 180 days curing.

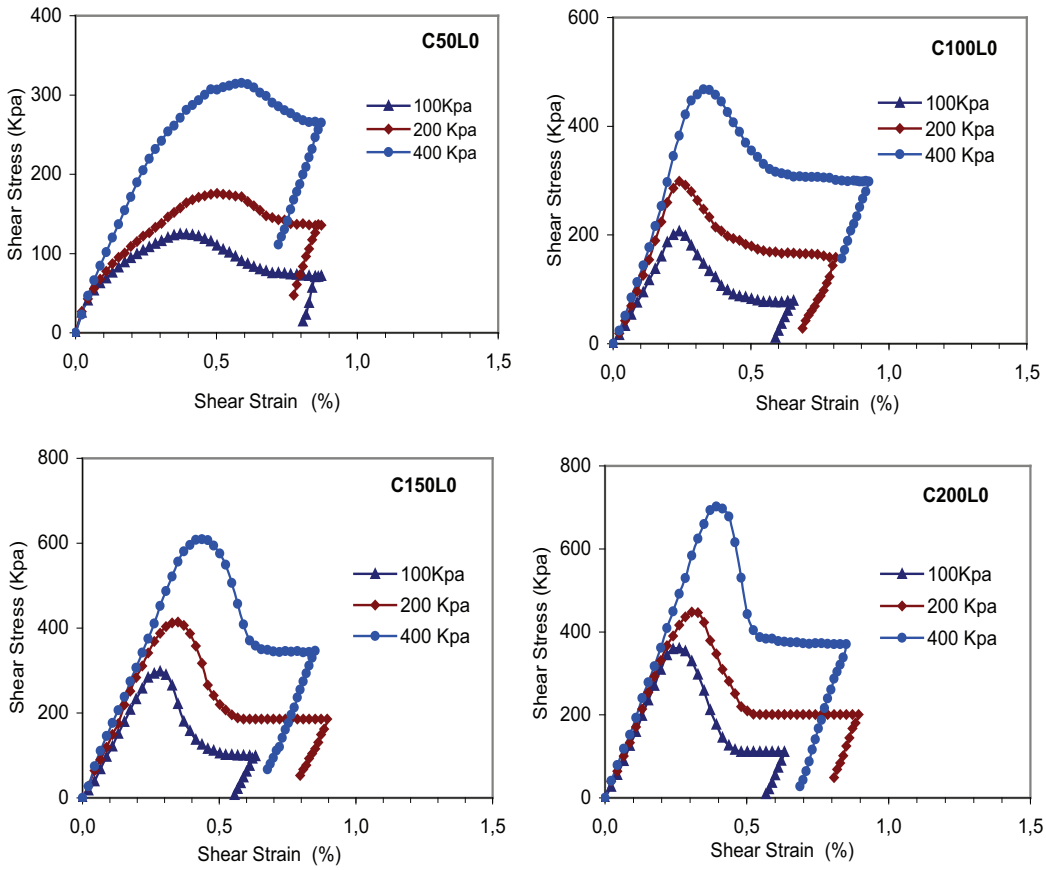

Figure 3.35 *Shear stress versus shear strain for shear box tests on cemented silica sand (cement factors 50-200 kg/m^3 after180 days curing)*

Table 3.9 *Shear modulus G_0 for shear box tests on cemented silica sand- (cement factors 50-200 kg/m^3 and 0, 40 and 80% lime+silica fume) at 180 days curing*

MIX CODE	180 DAYS Curing		
	Shear Modulus, G_0 (Mpa)		
	σ_n =0.1 (MPa)	σ_n =0.2 (MPa)	σ_n =0.4 (MPa)
C50-L0	73.7	86.8	95.4
C100-L0	86.4	108.3	125.8
C150-L0	115.7	138.0	158.7
C200-L0	140.9	158.0	185.0
C50-L20	81.4	96.1	109.0
C100-L40	102.0	123.5	145.7
C150-L60	124.5	148.9	173.0
C200-L80	154.5	176.6	203.6
C50-L40	93.0	108.1	124.5
C100-L80	126.3	144.2	161.7
C150-L120	137.6	157.4	190.0
C200-L160	172.0	188.0	221.0

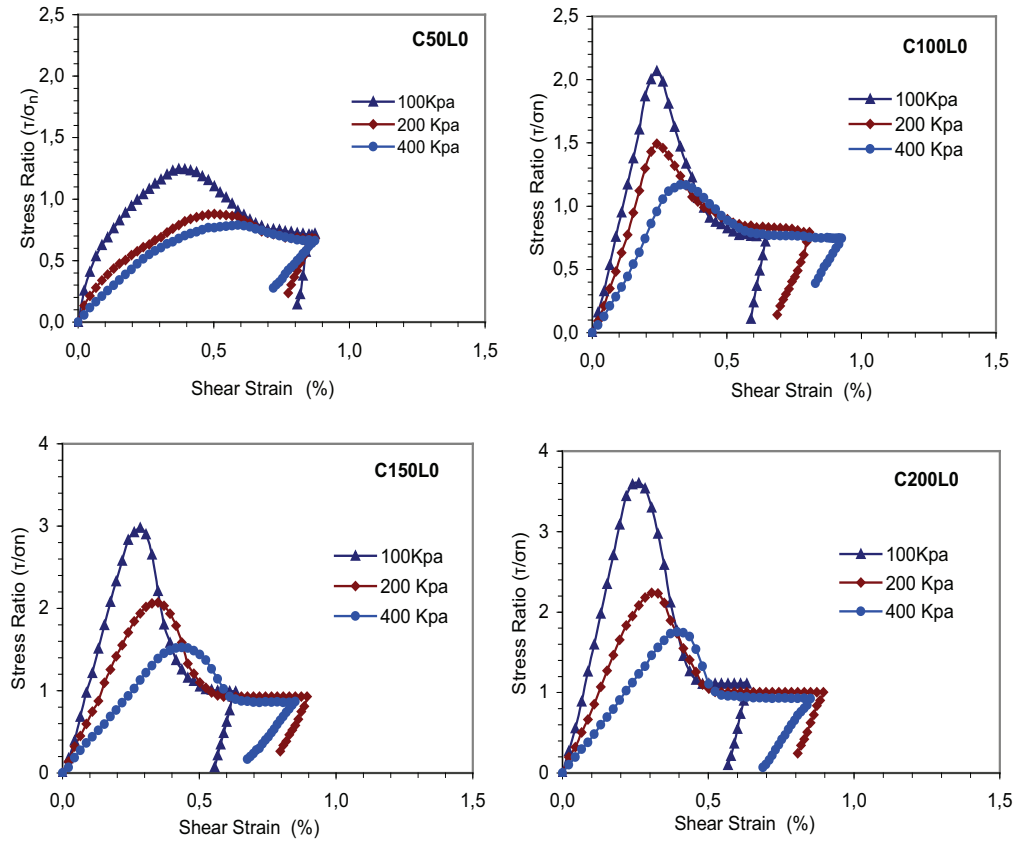

Figure 3.36 *Stress ratio versus shear strain for shear box tests on cemented silica sand (cement factors 50-200 kg/m^3 after180 days curing)*

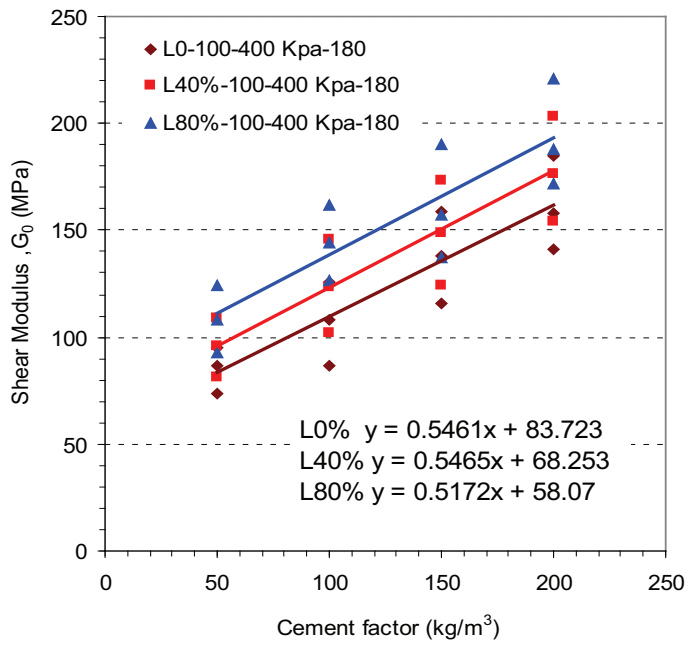

Figure 3.37 *Shear modulus G_0 versus cement factor for shear box tests on cemented silica sand (cement factors 50-200 kg/m^3 plus 0 to 80 % lime and silica fume) at 180 days curing*

Chapter 4: DISCUSSION

Effect of Binders,
Confining stress and curing
On silica sand-cement properties

4 Effect of Binders, Confining Stress and Curing on Silica Soil-Cement Properties

4.1 General Effects

Mixing binders into a soil will affect the fundamental properties of the natural, unimproved soil to varying extents. The strength and deformation properties are typically those of main interest when designing the extent of improvement required for ground modification. However, in assessing strength and deformation parameters from various tests, it is also important to consider the changes in other properties and their possible influence on the behavior of the improved soil.

Furthermore, a basic understanding of the types of chemical reaction that take place and the compounds formed when using different binders is essential in analyzing the rate and type of changes in properties that may develop. This also applies to the durability of improved soils. However, chemical durability aspects have not been included in this work.

A number of properties of the improved soil are thus addressed, with focus on the strength properties.

4.2 Binders Reactions

The chemical reactions involved in the hydration of different types of cement or lime have been described and discussed thoroughly in many papers and textbooks (*e.g.* Taylor 1997, Boynton 1980). The various chemical processes involved in soil improvement using a variety of binders have also been described in the literature (*e.g.* Chew *et al.* 2004, Janz and Johansson 2001, Saitoh *et al.* 1985, Ingles and Metcalf 1972, Ruff and Ho 1966), mainly for the two most common binders, cement and lime.

The reactions generated when mixing various binders with soil vary by process, intensity and duration, but in general exhibit many similar characteristics. As the binder is mixed into the soil, hydration takes place; silica fume being an activator for lime to start this process. Some reactions involve cementation directly, while others may lead to further reactions with the soil and its minerals.

The reaction products formed are of different types. When using lime, which contains large amounts of calcium oxide (denoted C), hydration will occur as the lime comes into contact with the pore water in the soil, resulting in the formation of calcium hydroxide (denoted CH). Some of this calcium hydroxide will be adsorbed onto the soil particles. Ion exchange will take place and react with the silica fume (denoted SF). These reactions, called pozzolanic, will result in the formation of calcium silicate hydroxide (CSH) (e.g. TRB, 1987). When using cement, primarily CSH is produced and the silica fume added to the soil acts mainly as a pozzolanic material, reacting with the free calcium hydroxide generated by cement hydration and regenerate calcium silicate hydroxide (CSH). However, pozzolanic reactions are normally relatively slow, due to the restricted accessibility of the silica fume added in the soil. The reactions forming CSH upon hydration of cement involve minerals contained in the binder itself and are thus more rapid than pozzolanic reactions with the other additives.

4.3 Changes in Basic Geotechnical Properties

The behavior of cemented sand is found to be influenced by factors such as strain level, type of cement, cement content, density, time, effective consolidation pressure, grain size distribution, structure, method of sample preparation, water content, degree of saturation, *etc.* (Saxena, 1988). A certain increase in bulk density and decrease in water content can be expected when binders are mixed with loose sand. These changes normally lead to an increase in strength, as well as a decrease in compressibility and also a decrease in permeability. Tables 3.1 and 4.1 summarize the physical properties of different samples used in triaxial and other compression tests. The average void ratio for the high binder content silica sand was 0.675 whereas for the low binder content silica sand it was 0.79, as can be calculated from Table 4.1.

When using dry binders, the density can be expected to be slightly higher than that of the natural, unimproved soil. The addition of binder at quantities 100 to 360 kg/m^3 in the loose silica sand, studied here was found to increase the density by 4 to 28%, as shown in Fig.4.1.

Table 4.1 *Physical properties of cemented silica sand*

Code Mix Design	Dry Density gr/cm^3	Void Ratio e_0	Dr I_D	W_S gr	V_S $W_S/(e_o+1)*\gamma_s$ cm^3
C50L0	1.391	0.879	0.17	294.2	112.6
C100L0	1.450	0.816	0.35	305.8	116.1
C150L0	1.500	0.757	0.51	317.4	120.4
C200L0	1.560	0.702	0.65	329.0	123.9
C50L20	1.420	0.841	0.28	299.6	114.6
C100L40	1.500	0.745	0.54	316.9	121.1
C150L60	1.580	0.660	0.77	333.8	127.3
C200L80	1.680	0.582	0.98	355.2	133.6
C50L40	1.440	0.804	0.38	305.1	117.4
C100L80	1.550	0.680	0.71	327.8	125.9
C150L120	1.660	0.572	1.01	350.4	134.3
C200L160	1.690	0.540	1.10	358.2	137.6

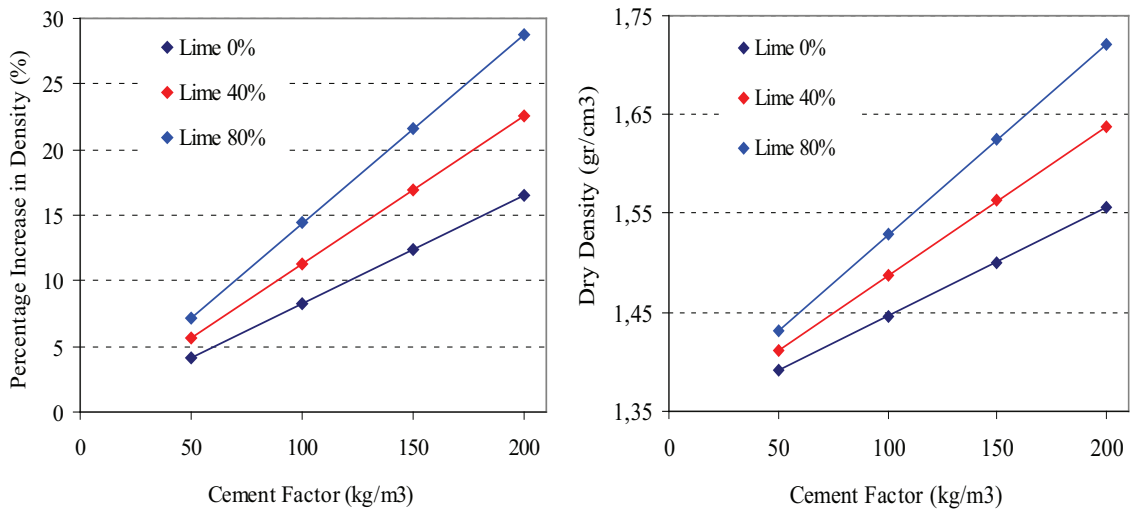

Figure 4.1 *Alteration of dry density and its percentage increase versus cement factor and lime content, for treated silica sand*

4.4 Influence on tensile and unconfined compressive strength

Results of tensile and unconfined compression tests were made on 12 specimens of different mix designs for 180 days curing time, and the results are summarized in Table 4.2. The

unconfined samples were prepared by the method of under compaction described earlier and then tested without membranes in triaxial cell.

A statistical analysis on the available experimental data with cemented silica sand (Table 4.2) provided the following correlations between unconfined compressive strength q_u and shear strength parameter c':

- For low cementation: (C50-L0-80%) $q_u = 3.5 \text{ to } 4.0\ c'$ (4.1)
- For high cementation: (C200-L0-80%) $q_u = 4.75 \text{ to } 5.13\ c'$ (4.2)

Similar investigation with Brazilian test results and unconfined compression test results resulted with the following correlation:

- For low cementation: (C50-L0-80%) $\sigma_t = (2.8 \text{ to } 5.0)\ \%\ q_u$ (4.3)
- For high cementation: (C200-L0-80%) $\sigma_t = (15.8 \text{ to } 20.0)\ \%\ q_u$ (4.4)

This relation has been found valid at all cementation levels and leads to the following discussion about the applicability of Griffith's theory of failure (1920) for cemented sand. Indeed, according to Griffith's theory, the failure envelope is expressed as:

$$(\sigma_1 - \sigma_3)^2 = -8\sigma_t(\sigma_1 + \sigma_3) \qquad (4.5)$$

For uniaxial compression conditions ($\sigma_3 = 0$, $\sigma_1 = q_u$):

$$q_u = -8\,\sigma_t \qquad (4.6)$$

This expression is to compare to the following, derived from Eq. 4.3 and 4.4 above:

$$q_u = -(11 \text{ to } 13)\,\sigma_t \qquad (4.7)$$

$$q_u = -(9 \text{ to } 10)\,\sigma_t \qquad (4.8)$$

Marclintock and Walsh (1962) and Brace (1963) suggested modifications to Griffith's theory and derived the following expression:

$$\frac{q_u}{\sigma_t} = \frac{4}{(1+\mu^2)^{1/2} - \mu} \qquad (4.1)$$

In which μ is the coefficient of friction for the crack surface. Considering an average angle of shearing resistance of 41.5° for cemented silica sands (Table 4.2), and assuming $\mu = \tan \varphi$, the above expression reduces to Eq.4.6.

Fig. 4.2 shows the variation of unconfined compressi ve strength of samples versus different Portland cement factors, with 10 percent silica fume alone or in addition with 40 to 80 % lime, after 12 to 180 days curing times. The unconfined compression strength of cemented silica sand with Portland cement alone varies from 0.17 to 4.95 MPa, whereas with addition of 40 to 80% of lime and silica fume, the unconfined strength increases of 0.44 to 0.66 MPa respectively.

Fig. 4.2 shows the measured variation in unconfined compressive strength, for different categories and quantity of binders. Cement plus silica fume alone or together with a percentage of 0 to 80 % lime, gave the higher short term strength and clearly decreased rates of strength gain in long term. Cement alone or in combination with lime gave 12-day strengths of 0.76 times that at 28 days, and six- month strengths of 1.44 times that at 28 days. After one month, the strength of the samples is seen to level off to an almost constant value, or shows a decreased rate of strength gain. Samples containing cement plus lime and silica fume exhibit a pronounced long-term increase in strength, although this considerably varies with the percentage of lime, as illustrated in Fig. 4.3. The increase in unconfined compressive strength for the cement- lime improved silica sand, which was cured 12 to 180 days, can be approximately described by the expression:

$$q'_t / f'_{C\,28} = 0.25\, Ln\,(t) + 0.18 \qquad (4.2)$$

where t is time (days), and q_t and f'_{C28} are the unconfined compressive strengths after t days and 28 days respectively. Equation (4.10) is similar to relationships reported previously for cement-stabilized soils (*e.g.* Nagaraj *et al.* 1996, Porbaha *et al.* 2000, Horpibulsuk *et al.* 2003, Ahnberg *et al.* 2006), see Fig. 4.4.

Table 4.2 *Cemented silica sand results for unconfined compression, split tensile tests and Griffith*

MIX CODE	Curing days	$q_{u\text{-}180}$ (Mpa)	$\sigma_{t\text{-}180}$ (Mpa)	Fσ' (Mpa)	Peak Strength Ø'p (°)	Peak Strength C'p (Mpa)	Ultimate Strength Ø'cr (°)	Ultimate Strength C'cr (Mpa)	σ_t/q_u %	q_u/c'_p	σ_t^{**}/q_u (%)
C50-L0	180	0.36	0.010	0.317	34.1	0.098	34.6	0	2.8	3.67	13.3
C100-L0	180	1.29	0.060	1.004	39	0.334	41.7	0.02	4.7	3.86	11.9
C150-L0	180	3.10	0.326	1.993	42.8	0.704	45	0.04	10.5	4.40	10.9
C200-L0	180	4.98	0.786	3.077	46.9	1.046	51.1	0.06	15.8	4.76	9.9
C50-L20	180	0.46	0.020	0.369	38.2	0.123	37.6	0.02	4.3	3.70	12.1
C100-L40	180	1.75	0.160	1.171	42.1	0.403	44.7	0.03	9.1	4.34	11.1
C150-L60	180	3.60	0.440	2.161	44.5	0.788	46.7	0.11	12.2	4.57	10.5
C200-L80	180	5.23	1.044	3.064	47.9	1.092	51.1	0.11	20.0	4.79	9.6
C50-L40	180	0.72		0.510	41.1	0.175	33.8	0		4.10	11.4
C100-L80	180	1.89	0.262	1.244	43.5	0.445	47.2	0.03	13.9	4.25	10.7
C150-L120	180	4.30	0.628	2.414	46.4	0.899	46.1	0.02	14.6	4.78	10.0
C200-L160	180	6.10	1.133	3.886	49.8	1.189	51.6	0.07	18.6	5.13	9.1

$\frac{\sigma_t^{**}}{q_u}$ = modified Griffith's theory, see Eq.4.9.

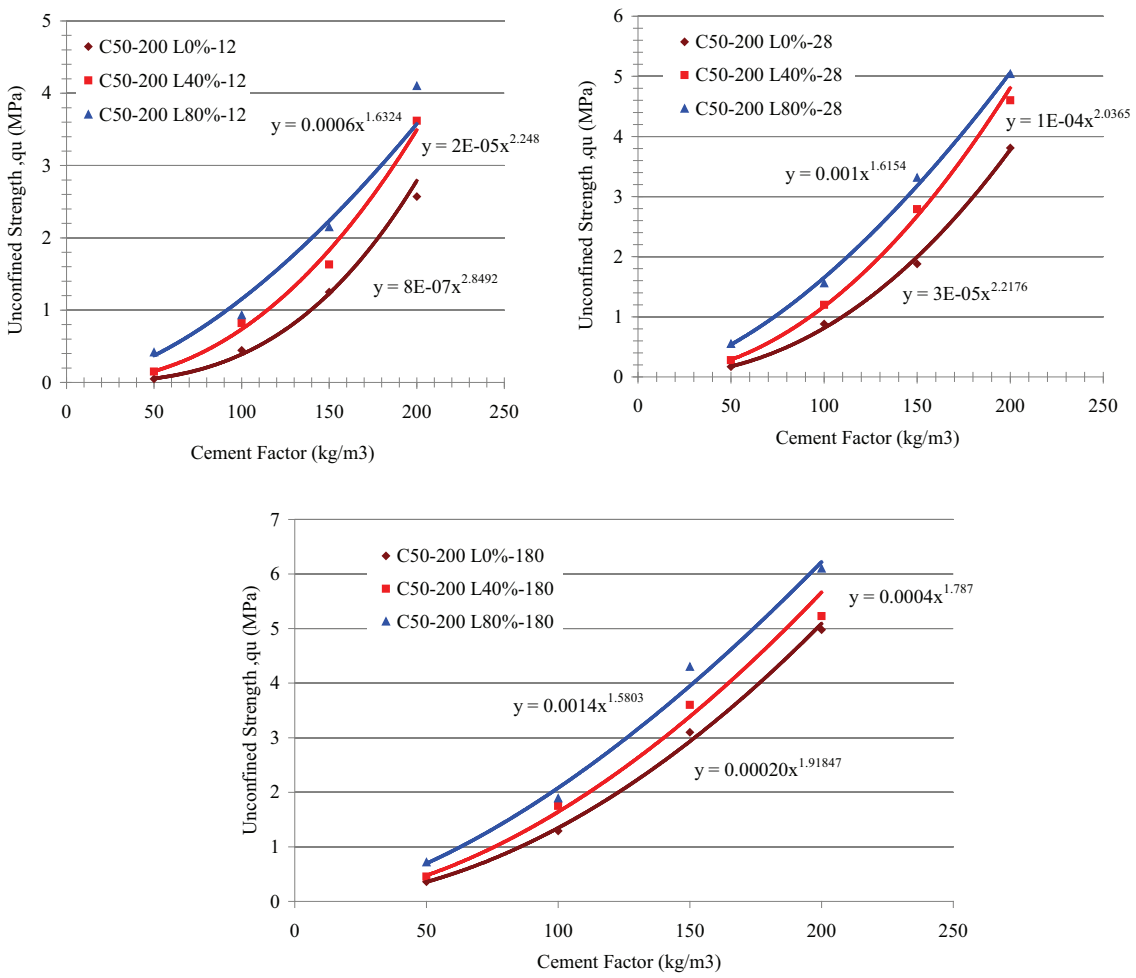

Figure 4.2 *Variation of unconfined compression strength with cement content for different percentage of lime and silica fume after 12 to 180 days curing*

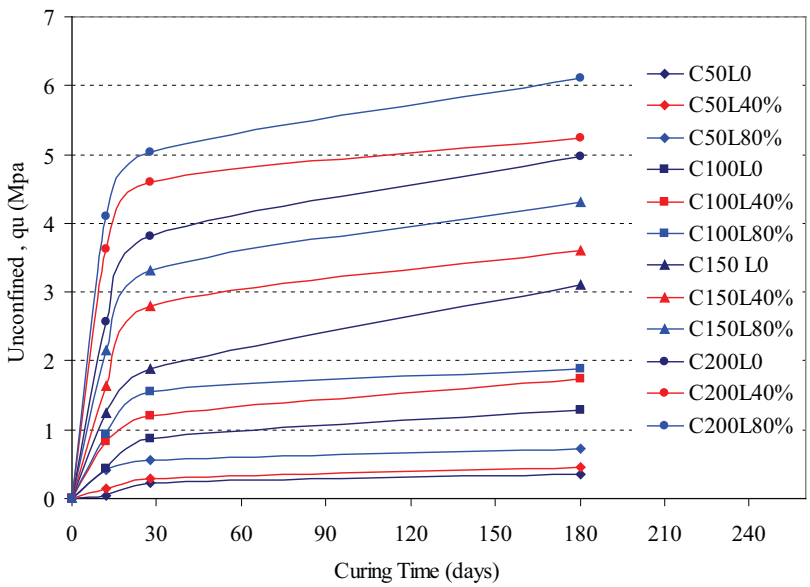

Figure 4.3 *Unconfined compression strength versus curing time after mixing for silica sand with cement and lime (C = cement, L = lime), cement 50 to200 kg/m^3 and lime/cement ratio 0 to 80 %.*

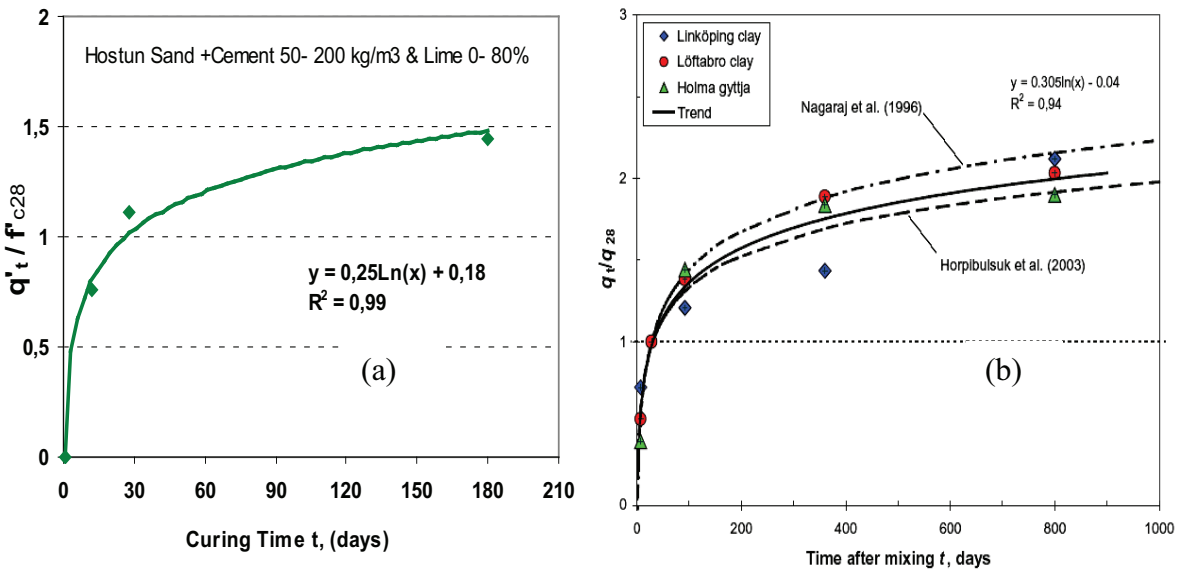

Figure 4.4 *Relative increase in unconfined compressive strength with time for, (a) cement-lime silica fume improved Silica sand and, (b) previously reported for cement-stabilized soils (Ahnberg et al., 2006)*

The relationship between unconfined compression strength and binder/sand ratio is shown in Fig 4.5B, C and D. The influence of binder/sand ratio on optimum moisture content is shown in Fig. 4.5A.

Fig. 4.6a shows the sand–cement and water-cement ratios of silica sand treated with cement–lime and silica fume, as compared to a number of deep mixing studies for projects involving soft, fine-grained soils. As shown in Fig. 4.6b, deep mixing involving soft, fine-grained soils is characterized by higher water-cement ratios than treated silica sand. It should be noted that soft, fine-grained soils in deep mixing is conducted at much higher water contents than sandy soils and water-cement ratio is often higher because of the higher optimum water content.

Fig. 4.7a shows the variation of unconfined compressive strength with the water-binder ratio of treated silica sand as compared in Fig 4.7b with some deep mixing and jet grouting studies (Gallavresi 1992, Kauschinger *et al.* 1992b, Asano *et al.* 1996, Nagaraj *et al.* 1996, Matsuo *et al.* 1996, Uddin *et al.* 1997). Nagaraj *et al.*'s results (1996) suggest that the soil-cement ratio may also affect the strength of soil-cement mix. Gallavresi (1992) proposed that, for a given type of cement mixed with a given type of cohesive soil, the unconfined compressive strength q_u may be correlated to water-cement ratio by the relationship:

$$q_u = q_0 / (w/c)^n \qquad (4.3)$$

where q_0 and n are experimentally fitted values.

In the current study, this type of relation could be used for the correlation between unconfined compressive strength q_u and water-binder ratio. Gallavresi (1992) suggested that for fine-grained cohesive soil, n may range from 1.5 to 3 and q_o typically lies between 5,000 to 10,000 kN/m^2, whereas the fitted value of n suggested for the Singapore marine clay is 1.87 (Lee *et al.*, 2005). As shown in Fig. 4.7, the scatter of the data points around the fitted curve is high, especially at low water-cement or water-binder ratio. The data plotted separately according to soil-binder (S/B) ratios in Fig.4.7 show that for a given water-binder ratio, the unconfined compressive strength of the cement-treated soils increases with a decrease in soil-binder ratio.

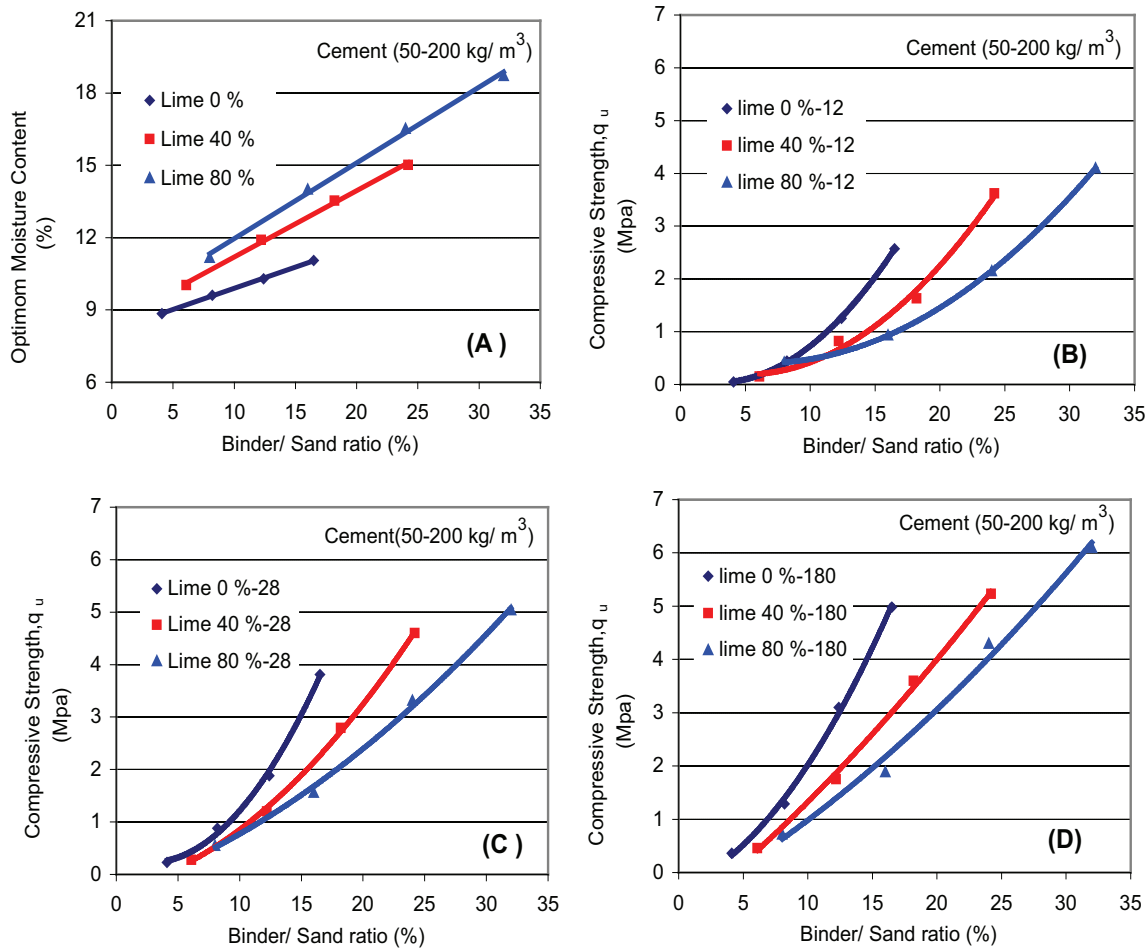

Figure 4.5 *Relationship between optimum moisture content and binder/sand ratio (%),Fig (A), compressive strength q_u versus binder/sand ratio of treated silica sand, in 12 to180 days curing period, Fig (B), (C) and (D).*

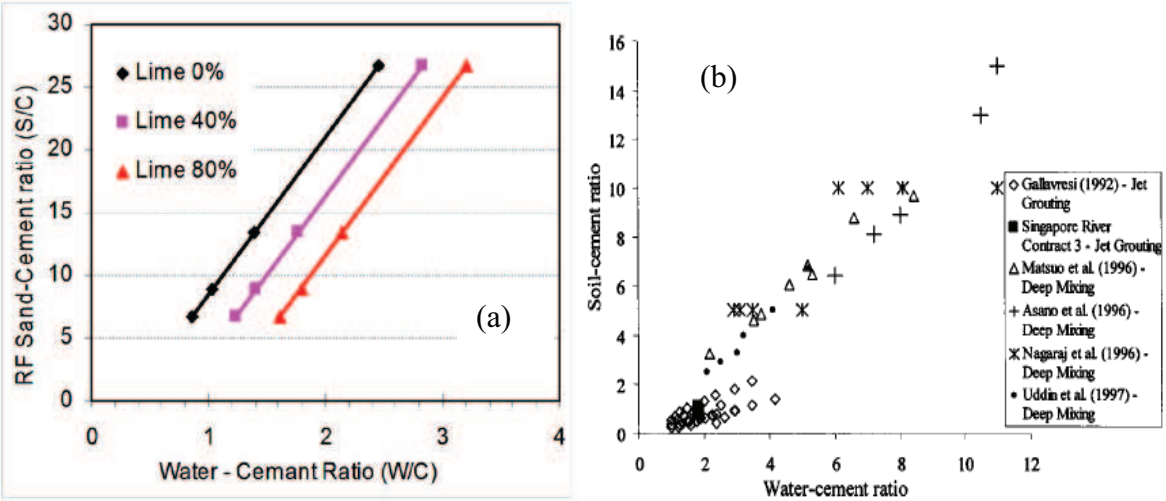

Figure 4.6 *(a) Relation between sand–cement and water-cement ratios of silica sand treated with cement, lime and silica fume, and (b) Soil-cement and water-cement ratios for some previous studies on deep mixing (Lee et al,.2005)*

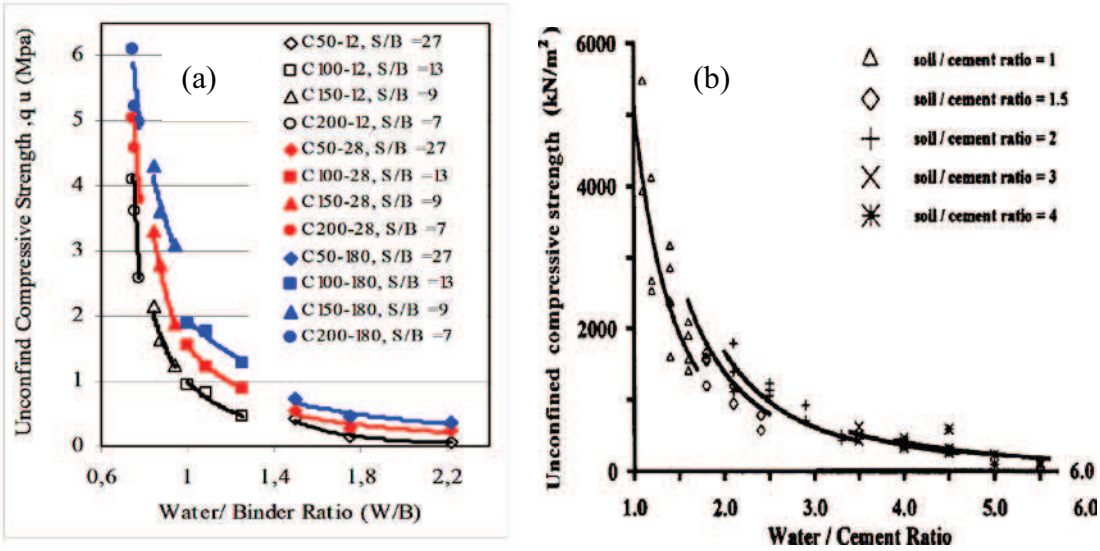

Figure 4.7 *(a) Relation between unconfined compressive strength and water-binder ratio for silica sand treated with cement–lime and silica fume, and (b) 28-day strength of cement treated clay prepared from dried pulverized clay (Lee et al.2005)*

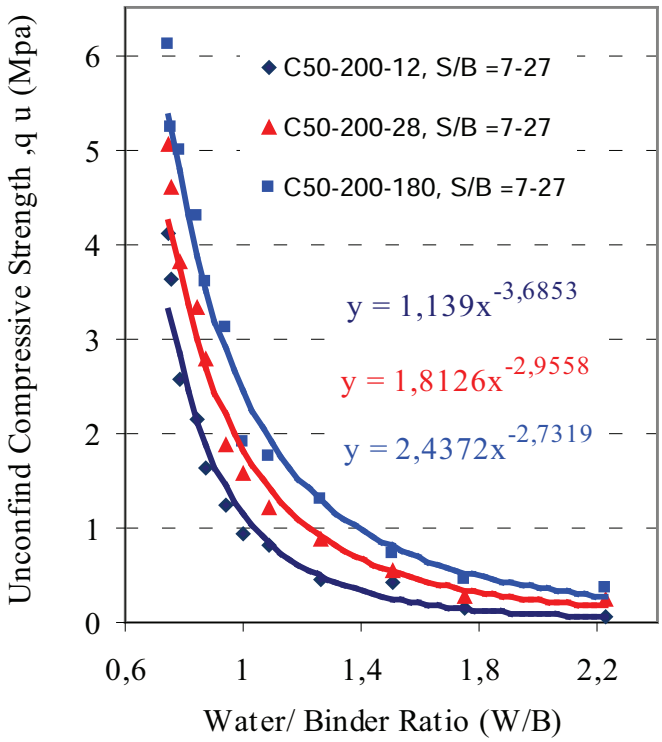

Figure 4.8 *Unconfined compressive strength versus water-binder ratio for silica sand after 12, 28 and 180-day curing times*

Fig. 4.8 shows the results of the 12, 28 and180-day unconfined compressive strength of silica sand treated with cement–lime and silica fume. For cemented silica sand, the best fit to Eq. (4.12) was obtained with n = 2.96 and q_0 =1.81 MPa for 28-day curing time. q_o typically lies

between 1.14 to 2.44 MPa in Eq. (4.13), when *n* may range from 2.7 to 3.7 in Eq. (4.14), as a function of curing time t:

$$q_u = q_0 / (W/B)^n \qquad (4.4)$$

$$q_0 = 0.46\,Ln\,(t) + 0.12 \qquad (4.5)$$

$$n = 4.28 - 0.314\,Ln\,(t) \qquad (4.6)$$

4.5 Influence on Strength Ratio

The increase in strength with time after improvement is governed by a number of factors. The type of binder will normally have a significant impact on the results, although the effect may vary considerably depending on the type of soil. Other factors affecting the increase in strength are the amount of binder, the mixing effort, the temperature and the stresses during curing (*e.g.* Babasaki *et al.*, 1996).

Fig. 4.9 shows the variations of the strength ratio, defined as the ratio of cemented peak strength to uncemented peak strength ($q_{Peak\ cemented}$ /$q_{Peak\ uncemented}$) in drained conditions for different mix designs of cemented silica sand (50 to 200 kg/m^3 cement and 0 to 80% lime-silica fume) at 12, 28 and 180 days curing times. It can be observed that the strength ratio decreases when effective confining stress increases and cement content decreases.

4.6 Pozzolanic Reaction index

The optimal binder to be used for improvement of a soil will vary depending on the desired strength in the short-term as well as the long-term perspective, for both drained and undrained conditions. Robustness and good durability are also important factors in case of varying soil conditions or risks of the improved soil being subjected to aggressive ground water with high mobility. It is observed from Figs. 4.10 to 4.12 that addition of lime plus 30 % silica fume has increased the shear strength of the cemented mixes due to the increase in availability of lime and silica fume for pozzolanic reaction. The rate of gain in shear strength is high for 100-150 kg/m^3 lime and silica fume content (Fig. 4.10).

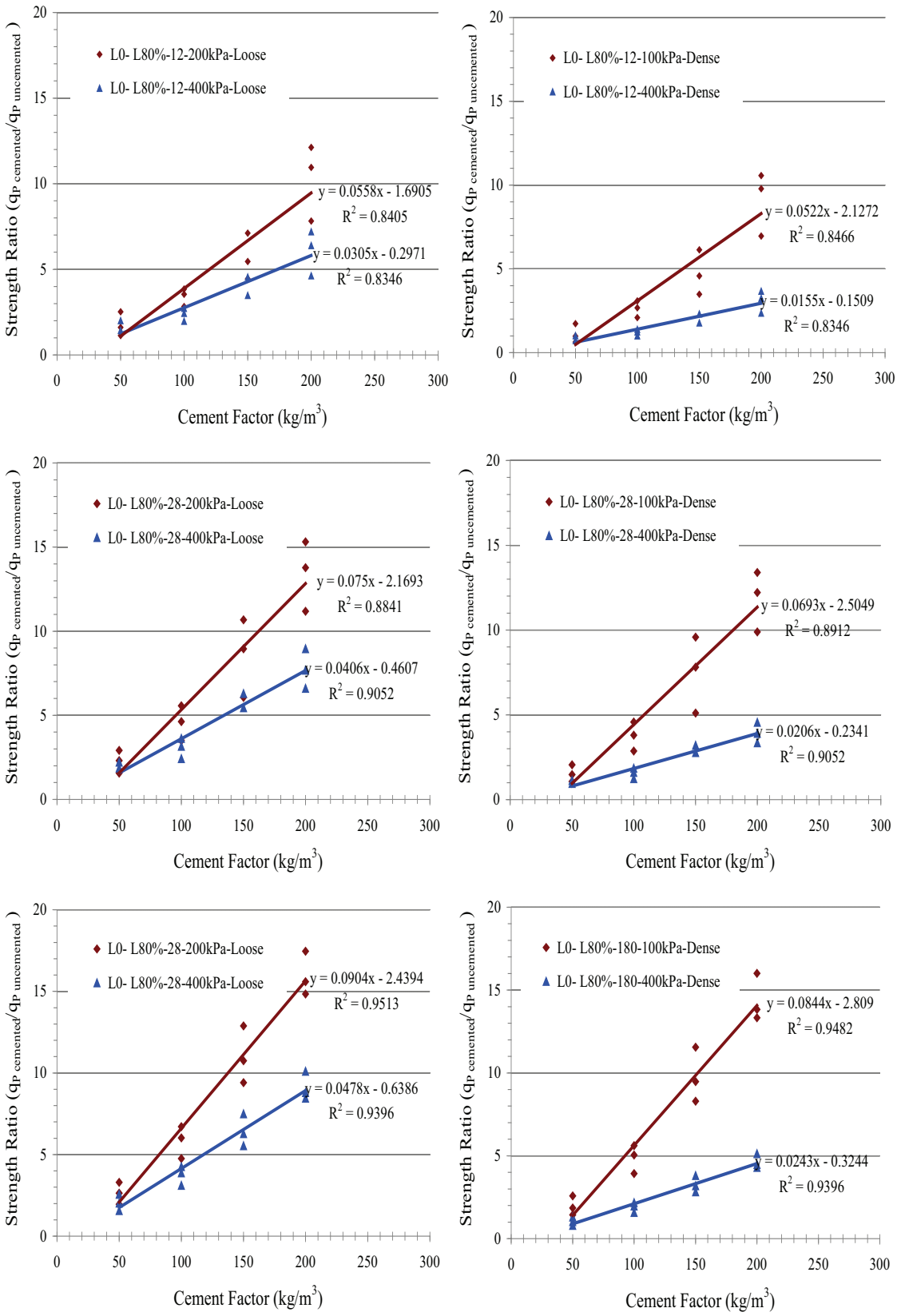

Figure 4.9 *Variations of the strength ratio ($q_{Peak\ cemented}$ /$q_{Peak\ uncemented}$) in drained conditions for different mix designs of cemented silica sand: 50-200 kg/m^3 cement and 0 to 80% lime-silica fume, at 12, 28 and 180 days curing*

Cemented sand without lime, but with 10% silica fume attains 40 to 60% pozzolanic reaction after 180 days curing at different confining pressure (Fig.4.10a), whereas the optimum values are 20 to 30% for mixes with 40% lime and silica fume in 100 kg/m^3 cement content, (Fig.4.10b) and 16 to 30% for mixes with 80% lime and silica fume in 150 kg/m^3 cement content (Fig.4.10c).

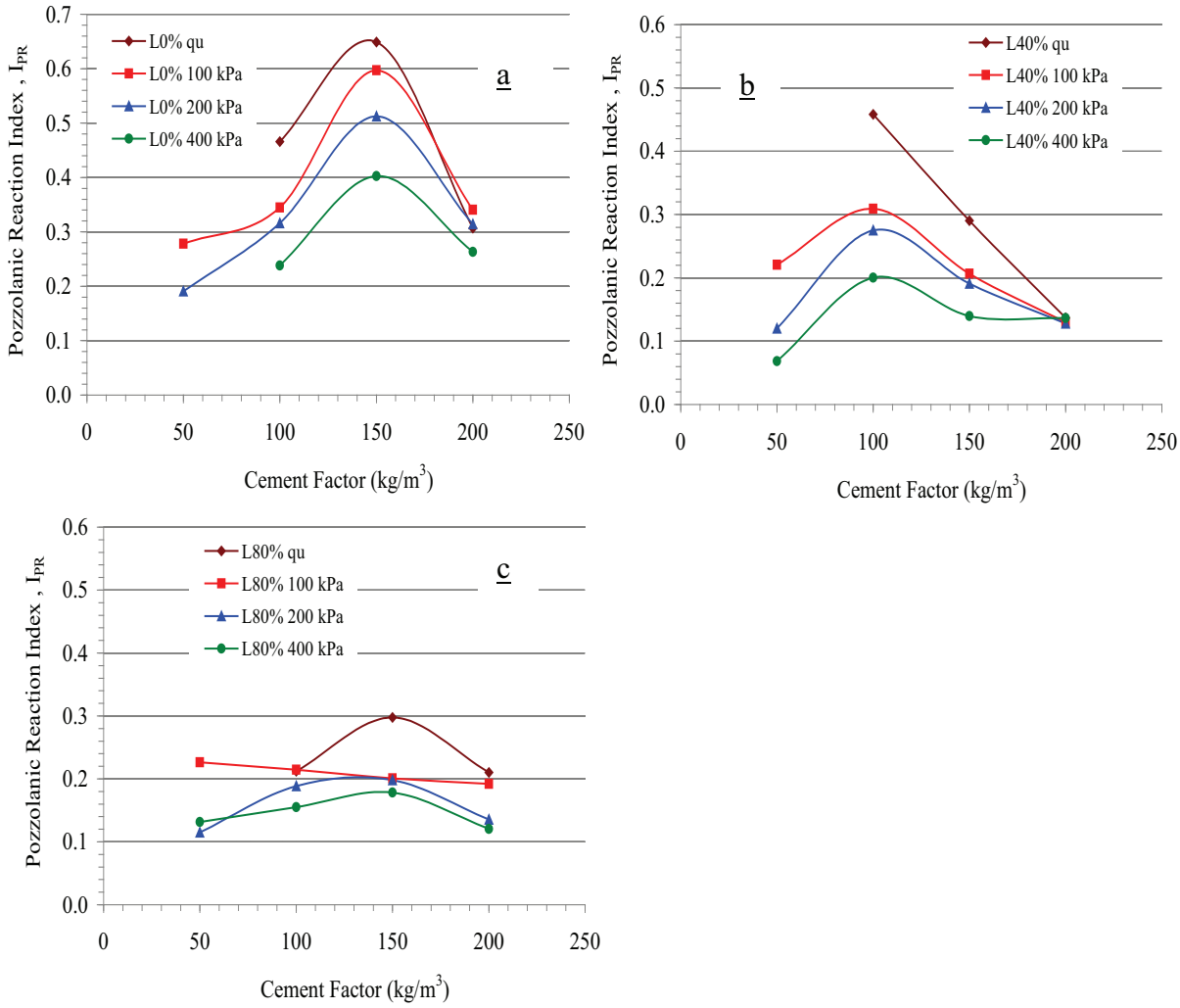

Figure 4.10 *Variation of the pozzolanic reaction index $I_{PR} = (q_{p180} / q_{p28})-1$, as a function of the binder content and confining stress σ'_3, for different mixtures of cemented silica sand (50-200 kg/m^3 cement and 0 to 80% lime-silica fume)*

Table 4.3 and Fig. 4.10 show the values of the pozzolanic reaction index I_{PR} in drained triaxial compressive strength of cemented silica sand, where I_{PR} is calculated from Eq. 4.15:

$$I_{PR} = \frac{q_{p180}}{q_{p28}} - 1 \qquad (4.15)$$

where q_{p180} *is* defined as peak strength of samples at 180 days curing and q_{p28} is defined as peak strength of samples at 28 days curing.

Also shown in Table 4.3 and Fig. 4.11 is the pozzolanic reaction plus density affection index I_{PR+De} defined as:

$$I_{PR+De} = \frac{q_{p180+Lime}}{q_{p180-Lime}} - 1 \qquad (4.16)$$

where $q_{p180+Lime}$ is defined as peak strength of samples with lime and silica fume at 180 days curing, and $q_{p180-Lime}$ is defined as peak strength of samples without lime at 180 days curing.

Table 4.3 *Pozzolanic reaction index of cemented silica sand due to addition of 0, 40 and 80% lime and silica fume at 28 to180 days curing period*

MIX CODE	Pozzolanic Reaction index $I_{PR}=(q_{P180}/q_{P28})-1$				Pozzolanic Reaction +Density $I_{PR+De}=(q_{P180+Lime}/q_{P180-Lime})-1$				Density Affection index $I_{De}=(q_{P28+Lime}/q_{P28-Lime})-1$			
	σ'3 =0.0 (MPa)	σ'3 =0.1 (MPa)	σ'3 =0.2 (MPa)	σ'3 =0.4 (MPa)	σ'3 =0.0 (MPa)	σ'3 =0.1 (MPa)	σ'3 =0.2 (MPa)	σ'3 =0.4 (MPa)	σ'3 =0.0 (MPa)	σ'3 =0.1 (MPa)	σ'3 =0.2 (MPa)	σ'3 =0.4 (MPa)
C50-L0		0.278	0.191									
C100-L0	0.466	0.345	0.316	0.238								
C150-L0	0.649	0.597	0.512	0.403								
C200-L0	0.307	0.341	0.314	0.263								
C50-L20		0.221	0.120	0.069	0.264	0.251	0.283	0.226		0.310	0.364	
C100-L40	0.458	0.309	0.275	0.200	0.357	0.269	0.245	0.218	0.364	0.303	0.284	0.257
C150-L60	0.290	0.207	0.191	0.140	0.161	0.139	0.136	0.122	0.484	0.507	0.443	0.381
C200-L80	0.137	0.130	0.128	0.137	0.050	0.037	0.049	0.038	0.207	0.230	0.223	0.153
C50-L40		0.226	0.115	0.131		0.685	0.557	0.492		0.757	0.663	
C100-L80	0.212	0.215	0.189	0.155	0.466	0.404	0.376	0.326	0.773	0.554	0.523	0.421
C150-L120	0.298	0.201	0.198	0.178	0.387	0.382	0.353	0.326	0.763	0.838	0.707	0.579
C200-L160	0.210	0.192	0.135	0.121	0.225	0.198	0.171	0.184	0.323	0.347	0.355	0.335

Finally the density affection index (I_{De}) is calculated as:

$$I_{De} = \frac{q_{p28+Lime}}{q_{p28-Lime}} - 1 \qquad (4.17)$$

where $q_{p28+Lime}$ *is* defined as peak strength of samples with lime and silica fume at 28 days curing, and $q_{p28-Lime}$ is defined as peak strength of samples without lime at 28 days curing (Fig. 4.12).

Fig.4.11 shows the variation of pozzolanic reaction+Density index (I_{PR+De}),for different mixture of cemented Silica sand (50-200 kg/m^3 cement and 0 to 80% lime-silica fume). As seen in Fig.4.11, samples with 40 % lime and silica fume for different confining pressures

have an optimum value of Pozzolanic Reaction+Density index I_{PR+De} of 0.2 to 0.4 for 100 kg/m3 cement content samples. In samples with 80% lime and silica fume, there is a global decrease of I_{PR-De} with increasing cement content, but with a more complex pattern.

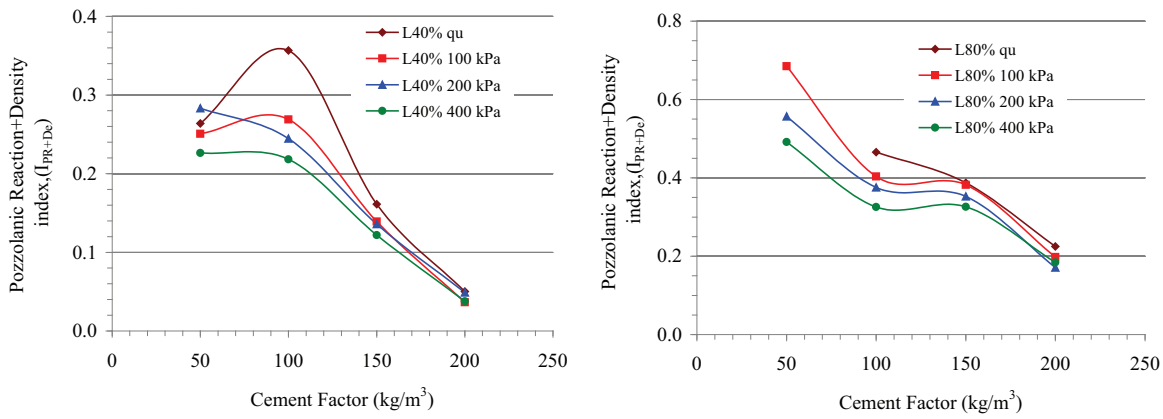

Figure 4.11 *Variation of Pozzolanic Reaction-Density index, I_{PR-De} =($q_{p180-Lime}$/$q_{p180-Lime}$)-1, for mixtures of cemented silica sand: 50-200 kg/m^3 cement and 0 to 80% lime-silica fume*

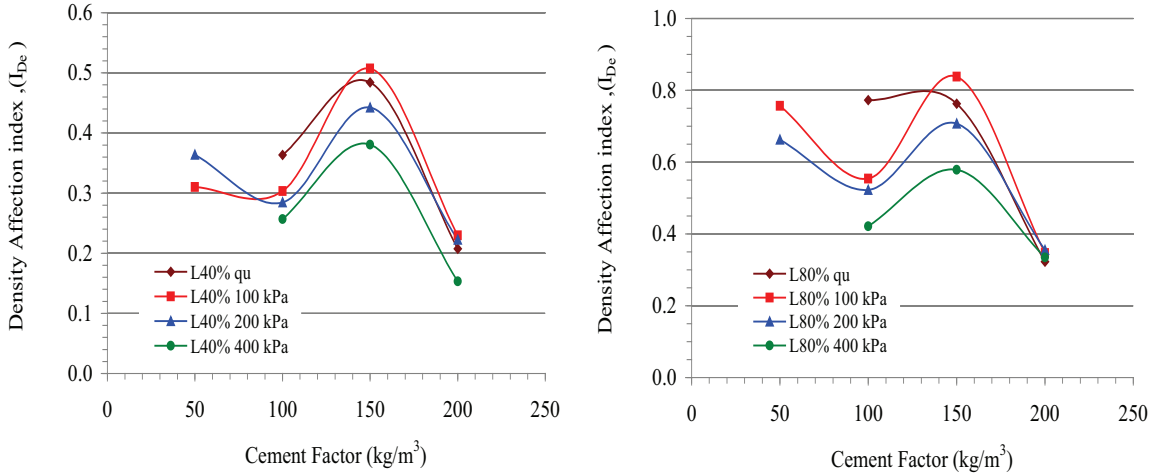

Figure 4.12 *Variation of the Density Affection index I_{De}=($q_{p28+Lime}$ /$q_{p28-Lime}$) -1, for mixtures of cemented silica sand: 50-200 kg/m^3 cement and 0 to 80% lime-silica fume*

4.7 Correlation Study of Results in triaxial and unconfined compressive strength

In the present study, an attempt has been made to develop empirical relationships to estimate certain parameters obtained from triaxial tests, such as deviator stress at failure q_p, as a function of unconfined compression strength at 28 days curing time q_{u-28}. The shear strength characteristics of cemented soils depend on a number of factors, and unconfined compressive

strength $q_{u\text{-}28}$ will be taken as the reference variable in estimating these factors since $q_{u\text{-}28}$ may contain their combined effects on the shear strength characteristics.

Fig. 4.13 shows that the deviator stress at failure q_p obtained from drained triaxial tests can be expressed as a power function of q_u for cemented sand modified with cement alone or in combination with lime and silica fume. The empirical relationships along with the values of the coefficient of determination R^2 are presented for varying confining pressures and curing times.

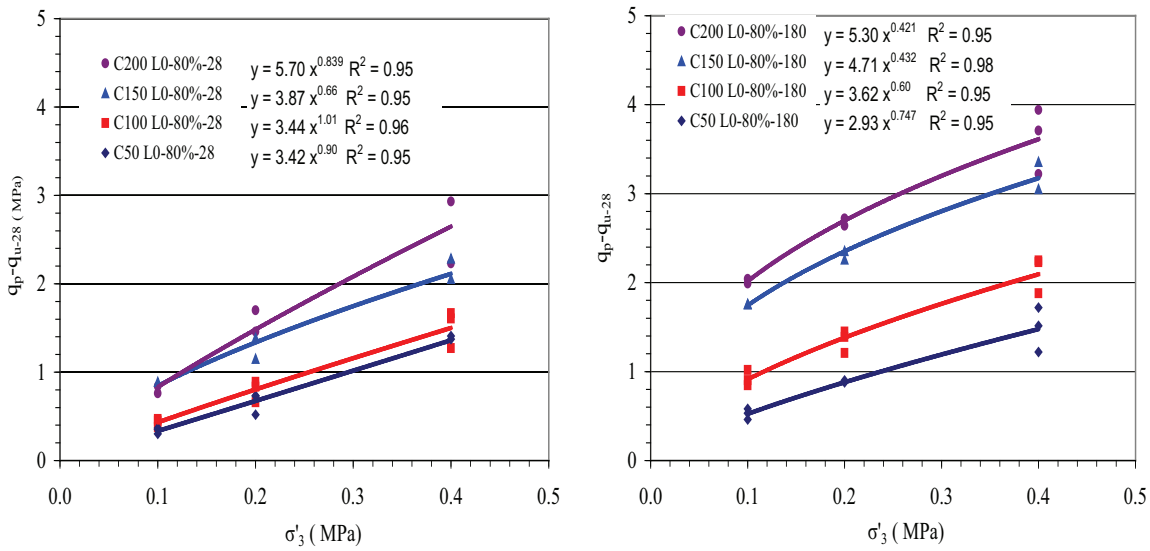

Figure 4.13 *Study of empirical relationships to estimate the parameters obtained from triaxial tests such as deviator stress at failure q_p as a function of unconfined compressive strength at 28 and 180 days curing*

It is shown from the Fig. 4.13 that q_p changes with curing time as well as with confining pressure σ'_3. The effect of curing time may be represented by the values of unconfined compressive strength. With this basis, a general empirical relationship for q_p is developed as function of $q_{u\text{-}28}$ and σ'_3. Using multiple regression analysis of the test results for all the 12 mixes, three curing periods 12, 28 and 180 days and three confining pressures 100, 200, and 400 kPa, the presentation of data obtained from triaxial tests according to ASTM-C 801 may take the following form:

$$q_p = q_{\text{u-28}} + K\,(\sigma'_3)^a \qquad (2.18)$$

Or, for the strength increase beyond the uniaxial strength (Fig 4.13):

$$q_p - q_{u\text{-}28} = K\,(\sigma'_3)^a \qquad (4.19)$$

where:

q_p = deviator stress at peak state,

σ'_3 = effective confining pressure,

$q_{u\text{-}28}$ = unconfined compressive strength at 28 days curing time,

K, a = empirical coefficients.

Chapter 5

SUMMARY OF RESULTS AND GENERAL CONCLUSION

5 Summary of Results and General Conclusion

The angle of shearing resistance and the cohesion intercept are the two important shear strength parameters of soils. In more details, static loads on soils are carried by the five components of their shear resistance, namely cohesion, basic mineral friction, dilatancy, particle crushing and particle rearrangement. Basic mineral friction, dilatancy, particle crushing and particle rearrangement are considered to constitute the frictional resistance of soils. According to studies by Wissa and Ladd (1965), Avramidis and Sexena (1985), Saxena and Reddy (1988) and Dano (2004), and according to findings in this study, the following points can be made:

- The gross shearing resistance of soils is increased greatly when they are mixed with small amounts of cementing agents such as Portland cement, lime, *etc*...
- The stress-strain response is greatly influenced by effective confining pressure $\sigma_3^{'}$ and cement content, and to a smaller degree by curing time and relative density D_r. Even a loose specimen cemented with a small amount of cement can exhibit brittle behavior
- The brittleness index, defined as the ratio of peak shear strength (q_{peak}) over residual shear strength q_{resid} is demonstrated to be larger at low $\sigma_3^{'}$ and large cement contents
- An increase in the angle of shearing resistance and the cohesion intercept with increasing cement content was observed consistently
- The strength ratio, defined as the ratio of cemented peak strength to uncemented peak strength, decreases as $\sigma_3^{'}$ increases and cement content decreases
- For uncemented sand the Mohr envelope at peak strength represents a condition where the maximum rate of volumetric expansion occurs, whereas for the cemented sand it represents a condition where the summation of all strength components becomes maximum
- The behavior of cemented sands presents the same features as other cement-treated soils, namely a contractive–dilatant and means stress-dependent behavior. Also, the stress–strain behavior of cemented sands is nonlinear, and stiffness and strength are greatly

improved by binder content. The Mohr–Coulomb failure envelope seems to represent reasonably well the failure envelope for compressive stresses.

The shear strength characteristics of silica sand and cemented sand with 50-200 kg/m^3 Portland cement plus 0 to 80% lime-silica fume, were studied through tensile, unconfined compression tests, direct shear and consolidated drained triaxial tests. The specimens were cured for up to 180 days. Empirical relationships were developed to estimate deviator stress at failure and cohesion as functions of unconfined compressive strength.

It was found that addition of 3.5 to 10 % of Portland cement (50 to 200 kg/m^3) alone or with lime and silica fume enhances the gain in shear strength at early curing periods (12 and 28 days) and develops with pozzolanic reaction for long curing periods (180 days).

Simple empirical relationships were found to estimate deviator stress at failure and unconfined compressive strength. The objective was to be able to use soils stabilized with a small percentage of cement along with lime and silica fume in potential applications in road and embankment constructions for their strength characteristics, durability and environmental safety. The cemented soils having low hydraulic conductivity may find use in construction of waste containment liners, cut off walls, and vertical barriers.

The stress–strain strength tests data imply that the cementing agent contributes to both stiffness and strength via two mechanisms, namely bonding between grains and additional dilation. Particle bonding and breakage can be seen to occur for instance through the stress–strain curves obtained for low cement content (50 kg/m^3), which show a brittle behavior, with the peak resistance mobilized at an axial strain of about 3 to 5 %.

The cementing agent always led to an increase in peak strength via an increase in dilatancy at failure. The higher dilatancy at a high stress ratio (and at failure) can be viewed as the remanence of bonding. According to Dano (2004) and Wang (2008), grouted sands present the general characteristics of cemented soils and can be considered as an intermediate material between soil and concrete.

In this study the underlying mechanisms of how cementation influences the strength and the stress– dilatancy behavior in cemented sand were investigated.

It was first shown that before yielding, the stress ratio rapidly increases but the dilatancy is hindered by the bonding network. The energy is either stored or dissipated by bond breakage. At peak state, the strength is governed by two competing processes: the bond breakage leads to a decrease in strength but create volumetric dilation, which increases the strength due to dilatancy. These findings and the fact that the dilatancy at the peak state increases with increasing cement content explain why the measured peak-state strength parameters, c' and ϕ'_p, depend on cement content. After the peak strength, numerous bond-breakage events have taken place, most of which are concentrated in the shear band. The strength loss due to decementation (bond breakage) outpasses the dilatancy effect and the strength is lower than at the peak value, even at the state of maximum dilatancy. Incidently, it was found that peak strength and maximum dilatancy do not occur at the same strain level in all the samples. At the ultimate state, most of the applied energy is consumed by friction as dilatancy and bond-breakage events are minimized.

The usual stress-dilatancy equations can overestimate the stress ratio q/p' in the case of lower confinement and higher dilatancy, when they are used to predict the stress dilatancy behavior in cemented sand. This finding implies that extra energy is available to dilate the specimen more than what can be produced by the applied stress.

The study of the influence of the dominant factors on behavior of cemented silica sand as summarized here, should allow a better overall understanding of cemented soil behavior, and help develop more efficient and cost effective methods of soil improvement, such as the deep mix method.

REFERENCES

REFERENCE

Ahnberg, H. (1996). Stress dependent parameters of cement and lime stabilized soils. *Proc. 2nd International Conference on Ground Improvement Geosystems – IS Tokyo'96*, Grouting and Deep Mixing, Tokyo 1996, Vol. 1, pp. 387-392

Åhnberg, H. (1996). Stress dependent parameters of cement and lime stabilized soils. *Proc. 2ndInternational Conference on Ground Improvement Geosystems IS Tokyo'96*. Grouting and Deep Mixing, Tokyo 1996, Vol. 1, pp. 387-392

Ahnberg, H. (2005)," Increase in strength with time in soils stabilized with different types of binder in relation to the type and amount of reaction products", *Proceedings of the International Conference on Deep Mixing, Stockholm 2005, Vol. 1.1.*

Ahnberg, H. (2006), "Strength of stabilized soils – A laboratory study on clays and organic soils stabilized with different types of binder", Doctoral Thesis, Lund University, Sweden

Åhnberg, H. (2006). Effects of consolidation stresses on the strength of some stabilized Swedish soils. *Ground Improvement*, Vol. 10, No. 1, pp. 1-13.

Ahnberg, H. and Holm, G. (1999), "Stabilization of some Swedish organic soils with different types of binder" Dry mix methods for Deep Soil Stabilization, Brendenberg, Holm and Broms, eds. Balkema, Rotterdam, 101-108

Ahnberg, H., Bengtsson, P.E. and Holm, G. (1989), Prediction of strength of lime columns, International Conference on Soil Mechanics and Foundation Eng., 12(2): 1327-1330.

Ahnberg, H., Holm, G., Holmqvist, L., and Ljungcrantz, C., 1994. "The use of different additives in deep stabilization of soft soils" International Conference on Soil Mechanics and Foundation Eng., 13(3): 1191-1194.

Airey, D.W. (1993), "Triaxial testing of naturally cemented carbonate soil", *J. Geotech. Eng.,* 119(9), 1379–1398

Al Mahmoud, M. (1997). "Etude en laboratoire du comportement des sables sous faibles contraintes", PhD dissertation, Univ. of Lille, Lille, France.

Andromalos, K. B. and Bahner, E. W. (2003) "The Application of Various Deep Mixing Methods for Excavation Support Systems" *Grouting and Ground Treatment*, ASCE, Geotechnical Special Publication No. 120, 515–526.

Asano, J., Ban, K., Azuma, K., and Takahashi, K. (1996), "Deep mixing method of soil stabilization using coal ash" *Grouting and deep mixing: Proc. IS Tokyo '96, 2nd Int. Conf. on Ground Improvement Geosystems*, 393–398.

ASTM C150, "Standard Specification for Portland Cement ".

ASTM D 1632-96," Standard Practice for Making and curing soil-cement compression and Flexure test Specimens in the Laboratory"

ASTM D 2166-98a," Standard Test Method for Unconfined Compressive Strength of Cohesive Soil"

ASTM D 3080-90, "Standard Test Method for Direct Shear Test of Soils under Consolidated Drained Conditions"

ASTM D 4767-95, "Standard Test Method for Consolidated Undrained Triaxial compression Test for Cohesive Soils"

ASTM C 801-98, "Standard Test Method for Determining the Mechanical Properties of Hardened Concrete under Triaxial Loads"

Avramidis, A. and Sexena, S.K., (1985) "Behavior of Cemented-stabilized sands under static and Dynamic loads," Report No. IIT-CE85-01, Department of Civil Engineering, Illinois Institute of Technology, Chicago

Babasaki, R. Terashi, M. Suzuki, T. Maekawa, A. Kawamura, M. and Fukazawa, E. (1996) JGS TC Report: Factors influencing the strength of improved soil, *In* Proceedings of the 2nd Int. Conference on Ground Improvement Geosystems – IS Tokyo'96, Grouting and Deep Mixing, Tokyo, 1996. Vol. 2, pp. 913-918

Babasaki, R., Terashi, M., Suzuki, T., Maekawa, A., Kawamura, M. & Fukazawa, E. (1996), JGS TC Report: Factors influencing the strength of improved soil. *Proc. 2nd Int. Conference on Ground Improvement Geosystems –IS Tokyo'96*.Grouting and Deep Mixing, Tokyo, 1996.Vol. 2, pp.913-918.

Baker, S. (2000). *Deformation behavior of lime/cement column stabilized clay,* Ph.D. Thesis, Department of Geotechnical Engineering, Chalmers University of Technology, Gothenburg.

Bengtsson, P.E. & Ahnberg, H. (1995), Settlement calculations for lime column stabilizations, Road E18 at Fiskvik kanal, SGI project 1-261/86

Biarez, J. and Ziani, F. (1991), "Introduction aux lois de comportement des sables très peu denses." *Revue Française de Géotechnique*, 54, 65–73.

Bishop, A. W. and Green, G. E. (1969), "Pore pressure measurement in the laboratory", Specialist session, Part II; *7th Int. Conf. on Soil Mechanics & Foundation Eng. Mexico,*

Bolton, M. D. (1986), "The strength and dilatancy of sand." *Géotechnique*, 3, 1, 65–78.

Boynton, R. (1980). Chemistry and technology of lime and limestone, John Wiley & Sons Inc

Brace, W. F. (1963) "Brittle Fracture of Rocks"*, proc. Int. Conf. on State of Stress in the Earth's crust,* Santa Monica, California, pp. 110-174.

Briaud, J. Nicholson P. Lee J. (2000) “Behavior of a Full–Scale VERT Wall in Sand.” *Journal of Geotechnical and Geoenvironmental Engineering*, 126(9), 808–818.

Bruce, D. & Bruce, M. (2003), "The Practitioner’s Guide to Deep Mixing,"

Bruce, D.A. Bruce, M.E.C. and DiMileo, A. (1998) “Deep Mixing Method: A Global Perspective.” ASCE, Geotechnical Special Publication No. 81, 1–15.

Carlsten, P. and Ekstrom, J., 1995. “Lime and lime/cement columns” Swedish Geotechnical Society Report 4:95E.

Case, J. and Chilver, A. H. (1959), Strength of Materials," an introduction to the analysis of stress and strain", Edward Arnold, London

Chew, S.H., Kamruzzaman, A. H. M. & Lee, F. H. (2004). "Physicochemical and engineering behavior of cement treated clays". Journal of Geotechnical and Geoenvironmental Engineering, Vol. 130, No. 7, pp. 696-706.

Chou, L., 1987 – “Lime Stabilization: Reactions, Properties, Design, and Construction” State of the Art Report 5, TRB, National Research Council, Washington D.C.

Clough, G. W. Sitar, B. (1981), "Cemented sands under static loading", *J. Geotech. Eng. Div. Amen. Soc. Civ. Eng.,* 107(6), 799–817

Clough, G.W., Sitar, N., Bachus, R.C. and Rad, N.S. (1981) Cemented sands under static

Consoli, N. C., Prietto, D.M., Ulbrich, L. A. (1998), "Influence of Fiber and Cement addition on Behavior of sandy soil ", Journal of Geotechnical and Geoenvironmental engineering, 1998

Coop, M. R. (1990), "The mechanics of uncemented carbonate sands", *Geotechnique, 40, No. 4, 607-626*

Coop, M. R. (1999), "The influence of particle breakage and state on the behavior of sands", *International workshop on soil crushability, IWSC ’99, Japan*

CRD-C 163-92, "Test Method for Water Permeability of Concrete Using Triaxial Cell"

Cresswell, A. & Powrie, W. (2004)," Triaxial tests on unbonded locked sand", *Geotechnique 54, No. 2, 107-115.*

Cuccovillo, T. and Coop, M. R. (1997) "Yielding and pre-failure deformation of structured sands", *Géotechnique*, 47(3), 491-508

Cuccovillo, T., and Coop, M. R. (1999), “On the mechanics of structured sands,” *Geotechnique*, 49(6), 741–760

Dano, C. (2001), "Mechanical Behavior of Soil Injected", Doctoral Thesis, l’Ecole Centrale de Nantes.

Dano, C. (2004), "Engineering Properties of Grouted Sands", 328 / Journal of Geotechnical

and Geo Environmental Engineering © ASCE / March 2004

Darcy, H. (1856). *Les fontaines publiques de la ville de Dijon*. Dalmont, Paris.

Davis, E.H. (1968)," Theories of Plasticity and the Failure of Soil Masses, in soil Mechanics, selected topics, ed. I.K. Lee, Butterworth

Eades, J.L. and Grim, R.E. (1960), "Reaction of Hydrated Lime with Pure Clay Minerals in Soil Stabilization", HRB, Bulletin 262

Eades, J.L. and Grim, R.E. (1966) "A Quick Test to Determine Lime Requirements for Lime Stabilization" Highway Research Record 139, HRB, NRC Washington, D.C.

Ekstrom, J.c. (1994), Kontroll av kalkcementpelare-slutrapport med redovisning av faltforsok I Ljungskile. Report B 1994:3, Goteborg.

Elias, V. Welsh, J. Warren, J. Lukas, R.(2001) "Ground Improvement Technical Summaries" FHWA Publication No. FHWA-SA-98-086R Vol. 2.

Esrig, M.I. (1999), "Keynote lecture: Properties of binders and stabilized soil", Dry mix methods for Deep Soil Stabilization, Brendenberg, Holm, and Broms, Eds, Balkema, Rotterdam. 67-72

Fakhimi, A., Riedel, J. J., and Labuz, J. F. (2006), "Shear banding in sandstone: Physical and numerical studies," *Int. J. Geomech*. 6(3), 185–194

Gallavresi, F. (1992), "Grouting improvement of foundation soils." *Proc., Grouting, soil improvement and geosynthetics, ASCE*, New York, vol. 1, 1–38,

Haan, E.J. (2000), "Laboratory Preparation of Test Samples of Soil Stabilized by Cement-Type Materials" Eurosoilstab Design Guide Chp. 6 Report no. 393220/6.

Haley & Aldrich, Inc. (2001) "Data Report on Soil Mix Design and Testing", I-95/Route 1 Interchange, Alexandria, VA. VDOT Project No. 0095-96A-106, PE-101

Hampton, M.B. and Edil, T.B. (1998), "Strength Gain of Organic Ground with Cement- Type Binders" Soil Improvement for Big Digs pp 135-148.

Head, K. H., MA (Cantab). C.Eng. FICE. FGS, (1988) "Manual of Soil Laboratory Testing", Volume 3, Effective Stress Tests, ELE international limited

Hoek, E. and Brown, E. T. (1980), "Empirical strength criterion for rock masses," *J. Geotech. Eng. Div. Am. Soc. Civ. Eng.* 106(9), 1013– 1035

Horpibulsuk, S. Miura, N. & Nagara, T. S. (2003)," Assessment of strength development in cement admixed high water content clays with Abrams' law as a basis", Géotechnique, Vol. 53, No. 4, pp. 439-444.

Horpibulsuk, S., Miura, N. & Nagara, T. S. (2003) Assessment of strength development in cement admixed high water content clays with Abrams' law as a basis. Géotechnique, Vol. 53, No. 4, pp. 439-444.

Houlsby, G.T. (1991), "How the Dilatancy of Soils Affects Their Behavior", Proceedings of the Tenth European Conference on Soil Mechanics and Foundation Engineering, Florence, May 27-30, Vol. 4, pp 1189-1202, ISBN 90-5410-005-2

Huang, J. T. Airey, D. W. (1998), "Properties of artificially cemented carbonate sand", *J. Geotech. Geoenviron. Eng.,* 124(6), 492–499.

Ingles, O.G. & Metcalf, J.B. (1972), *Soil stabilization*, Butter worth's Pty. Ltd, Australia.

Jacobson, j. (2002)**,"**Factors Affecting Strength Gain in Lime-Cement Columns and Development of a Laboratory Testing Procedure", Master Thesis, Virginia Polytechnic Institute and State University.

Kaushinger, J. L., Hankour, R., and Perry, E. B. (1992b), "Methods to estimate composition of jet grout bodies," *Proc., Grouting, soil improvement and geosynthetics, ASCE*, New York, vol. 1, 194–205,

Kawasaki, T. Saitoh, S., Suzuki, Y. & Babasaki, R. (1984), "Deep mixing method using cement slurry as hardening agent", *Seminar on Soil Improvement and Construction Techniques in Soft Ground*, Singapore 10-11 January 1984, pp. 17-38.

Kivelo, M. (1998), "Stabilization of embankments on soft soils with lime/cement columns", Doctoral Thesis 1023, Royal Institute of Technology, Sweden

Klotz, E. U. & Coop, M. R. (2001)," An investigation of the effect of soil state on the capacity of driven piles in sands", *Geotechnique 51, No. 9, 733-751.*

Konrad, J.-M., Flavigny, E., and Meghachou, M. (1991), "Comportement non drainé du sable d'Hostun lâche," *Revue Française de Géotechnique*, 54, 53–63.

Kukko, H. Ruohomaki, J. (1995), "Stabilization of clays with various binders in Finnish, VTT Research Notes 1682, Espoo. Technical Research Center of Finland

Kutzner, C. (1996)," *Grouting of rock and soil"*, Balkema, Rotterdam, The Netherlands

Lambe, T. W. (1960). "A mechanistic picture of shear strength of clay", Proc*., Soil Shear Strength Conf.*, 555–580

Lambe, T.W and Whitman, R. V. (1979), Soil Mechanic (SI version), Wiley, New York

Lambe, T.W. (1962), Soil stabilization, Foundation engineering, Leonards, G.A. ed. McGraw-Hill, New York, 351-437

Lancelot, L., Shahrour, I. and Al Mahmoud, M. (2004), "Instability and Static Liquefaction on Proportional Strain Paths for Sand at Low Stresses", Journal of Engineering Mechanics © ASCE / November 2004 / 1365

Lancelot, L., Shahrour, I. and Al Mahmoud, M. (2006), "Failure and Dilatancy Properties of Sand at Relatively Low Stresses ", Journal of Engineering Mechanics © ASCE / December 2006 / 1397

Larsson, R. Bengtsson, P.E. & Eriksson, L. (1997)," *Prediction of settlements of embankments on soft, fine-grained soils – calculation of settlements and their course with time*", Swedish Geotechnical Institute, Information No. 13E.

Lee, F. H., Lee, Y. Chew, S. H. and Yong, K. Y. (2005) "Strength and Modulus of Marine Clay-Cement Mixes **",** *JOURNAL OF GEOTECHNICAL AND GEOENVIRONMENTAL ENGINEERING © ASCE / FEBRUARY 2005*

Lee, K. L. & Seed, H. B. (1967)," Drained strength characteristics of sands", *Proceedings of the American Society of Civil Engineers, 93; SM6, Pages 117-141*

Leroueil, S., and Vaughan, P.R. (1990), "The general and congruent effects of structure in natural soils and weak rocks", Géotechnique, 40(3): 467–488.

Lo, S. C. R., Lade, P. V., and Wardani, S. P. R. (2003). "An experimental study of the mechanics of two weakly cemented soils." *Geotech. Test. J.*, 26(3), 1–14.

Lo, S.R. and Wardani, S.P.R. (2002) "Strength and dilatancy of a silt stabilized by a cement and fly ash mixture", Can. Geotech. J. Vol. 39: 77–89 (2002) loading, ASCE J. Geotech. Eng., 107(6), 799–817.

Luong, (1980), Phénomènes cycliques dans les sols pulvérulents. *Revue Française de Géotechnique*, No. 10, p. 39 – 53

Mántaras, F. M., and Schnaid, F. (2002), "Cylindrical cavity expansion in dilatant cohesive-frictional materials" *Geotechnique*, 52(5), 337– 348

Marclintock, F. A. and Walsh, J. B. (1962) "Friction on Griffith Cracks in Rocks under Pressure,"*proc.4th U.S. Nat. Cong. Appl. Mech., Vol. 2, PP. 1015-1022*

Matsuo, T., Nisibayashi, K., and Hosoya, Y. (1996), "Studies on Soil Improvement Adjusted at Low Compressive Strength in Deep Mixing Method." *Grouting and deep mixing: Proc. IS Tokyo '96, 2nd Int. Conf. on Ground Improvement Geosystems*, 521–526.

McGinn, A.J. and O'Rourke, T.D. (2003) "Performance of Deep Mixing Methods at Fort Point Channel." report prepared for Bechtel/Parsons Brinckerhoff, the Massachusetts Turnpike Authority, and the Federal Highway Administration at Cornell University, Ithaca, NY.

Mitchell, J. K. Baxler, C. D. P. and Munson, T. (1995) ‘‘Performance of improved ground during earthquakes’’ *Geotechnical Special Publication No. 49: Soil improvement for earthquake hazard mitigation*, ASCE, Reston, Va., 1–36.

Miura, N. Horpibulsuk, S., and Nagaraj, T.S. (2002) “Engineering Behavior of Cement Stabilized Clay at High Water Content” Soils and Foundations, Japanese Geotechnical Society, Vol. 41, No. 5, pg 33 – 45

Nagaraj, T.S., Miura, N., Yaligar P.P. & Yamadera A.(1996) Predicting strength development by cement admixture based on water content. *Proc. 2nd International Conference on Ground*

Porbaha, A. (1999). "Deep Mixing Technology For Liquefaction Mitigation" *Journal of Infrastructure Systems*, Vol. 5, No. 1, March, 1999.

Porbaha, A. Tanaka, H. and Kobayashi, M. (1998) ‘‘State of the art in deep mixing technology, Part II: Applications.’’ *Ground Improvement, J. ISSMGE*, 2(3), 125–139.

Porhaba, A. Shibuya, S. & Kishida, T. (2000)," State of the art in deep mixing technology", Part III Geomaterial characterization, Ground Improvement (2000) Vol.4, No. 3, pp. 91-110.

Pousette, K., Macsik, J., Jacobsson, A., Andersson, R., and Lahtinen, P., 1999. “Peat soil samples stabilized in the laboratory – Experiences from manufacturing and testing, Dry mix methods for Deep Soil Stabilization” Brendenberg, Holm, and Broms, eds. Balkema, Rotterdam. 85-92

Ratherford, c. j. (2004) "Design Manual for Excavation Support Using Deep Mixing Technology", Master Thesis, Texas A&M University

Roscoe, K. H., and Schofield, A. N. (1963), “Mechanical behavior of an idealized ‘wet’ clay.” *2nd European Conference on Soil Mechanics and Foundation Engineering (ECSMFE)*, Vol. 1, 47–54.

Roscoe, K.H., Schofield, A.N. and Wroth, C. P. (1958)," On the Yielding of soils" Geotechnique, 8:1:22

Rowe, P. W. (1962), “The stress-dilatancy relation for static equilibrium of an assembly of particles in contact.” *Proc. R. Soc. London*, 269, 500–527.

Rowe, P.W. (1969), " The Relation Between the Shear Strength of Sands in Triaxial Compression , Plane Strain and Direct Shear, Geotechnique , Vol. 19, No. 1, 75-86

Ruff, C.G. & Ho, C. (1966)," Time-temperature strength reaction product relationships in lime-bentonite-water mixtures" Highway Research Record No. 139, Highway Research Board, pp. 42-60

Saitoh, S., Suzuki, Y. & Shirai, K. (1985) Hardening of soil improved by the deep mixing method. Proc. 11th Int. Conference on Soil Mechanics and Foundation Engineering, Vol. 3 . pp. 1745-1748

Saxena. S.K, Reddy, K.R., Avramidis, A.S., (1988), " Static Behavior of Artificially Cemented Sand ", Indian geotechnical journal,18(2), 1988.

Scott. C R. (1980)," An Introduction to Soil mechanic and Foundations (third edition)", Applied Science Publishers

Shanley, F. R. (1957), Strength of Materials, McGraw-Hill

Skinner, A. (1969). "A note on the influence of interparticle friction on the shearing strength of a random assembly of spherical particles," *Geotechnique*, 19(1), 150–157

Tailliez, S. (1998), ''Etude expérimentale du comportement mécanique des sols granulaires injecte´s.'' PhD thèses, Ecole Centrale de Paris, Paris

Tanaka, Y. Nakajima, Y. and Tsuboi, H. (1991)"Liquefaction control works," *Symp. on control of soil liquefaction*, Japanese Soc. of Soil Mech. and Found. Engrg, Tokyo, 33–38

Taylor, H.F.W. (1997). Cement chemistry. Thomas Telford, London 1997.

Temiz, H., Karakeci, A.Y. (2002)," An investigation on microstructure of cement paste containing fly ash and silica fume ", Cement and Concrete Research 32 (2002) 1131–1132

Terashi, M. & Tanaka, H. (1983), Settlement analysis for deep mixing methods. *Proc. 8th European Conference on Soil Mechanics and Foundation Engineering*, Helsinki 1983, pp. 955-960.

Terashi, M. (1997) "Theme Lecture: Deep Mixing Method – Brief State of the Art", Proc. 14th ICSMFE, Vol. 4, pp.2475-2478

Thornton, C. (2000). "Numerical simulations of deviator shear deformation of granular media." *Geotechnique*, 50_1_, 43–53.

TRB (1987), Lime stabilization, "Reactions, properties, design, and construction", State of the Art Report 5, Transportation Research Board, Washington, D.C

Uddin, K., Balasubramaniam, A. S., and Bergado, D. T. (1997), "Engineering behavior of cement-treated Bangkok clay," *Geotech. Eng.*, 28(1), 89–119.Gallavresi (1992

Ventouras, k. (2005), "Engineering Behavior of Thanet Sand", Doctoral Thesis, Imperial College of Science, Technology & Medicine, University of London

Verdugo, R., Ishihara, K. (1996)," The steady state of sandy soils", *Soils and Foundations, Japanese Geotechnical Society, Vol. 36, No. 2, 81-91.*

Wang, Y. H., and Leung, S. C. (2008) "Characterization of Cemented Sand by Experimental and Numerical Investigations," *JOURNAL OF GEOTECHNICAL AND GEOENVIRONMENTAL ENGINEERING © ASCE / JULY 2008*

Wang, Y. H., and Leung, S. C. (2008), "A particulate scale investigation of cemented sand behavior," *Can. Geotech. J.*, 45(1), 29–44.

Wiggers, A.G. and Perzon, J. (2005) The Lekkerkerk trial: Mixed-in-place dike improvement in the Netherlands. *Proc.* Int. Conf. on Deep Mixing, Best Practice and Recent Advances, Stockholm, 1, 179-183

Wissa, A. E. Z., Ladd, C. C., and Lambe, T. W. (1965), "Effective stress strength parameters of stabilized soils," *Proc, Sixth Int. Conference of Soil Mechanics,* International Society of Soil Mechanics and Foundation Engineering, 1, 412-416.

Yang, D.S. (1997) "Chapter 2.5: Deep Mixing." In Situ Ground Improvement, Reinforcement and Treatment: A Twenty Year Update and a Vision for the 21st Century, Ground Reinforcement Committee, American Society of Civil Engineers, Geo-Institute Conference, Logan, UT, July 16-17. pp. 130-150.

Yang, D.S. (2003) "Soil–Cement Walls for Excavation Support" *Earth Retention Systems 2003: A Joint Conference presented by ASCE Metropolitan Section of Geotechnical Group, The Deep Foundations Institute, and The International Association of Foundation Drilling*, New York City, NY.

Yang, D.S. and Takeshima, S. (1994). "Soil Mix Walls in Difficult Ground" *In situ Ground Improvement Case Histories*, ASCE Convention, Atlanta, GA, 106–120

Yang, D.S. Scheibel, L.L. Lobedan, F. (2001) "Oakland Airport Roadway Project" Deep Foundations Institute Specialty Seminar–Soil Mixing, St. Louis, MI, 55–71

Yang, J. Li & X. S. (2004), State-dependent strength of sands from the perspective of unified modeling, *Journal of Geotechnical and Geoenvironmental Engineering, ASCE 1090-0241 pages 186-198.*

Yasuda, S. (1993) *Report on countermeasures used against liquefaction in Japan during 1985–1990*. Japanese Soc. of Soil Mech. and Found. Engrg, Tokyo

Zebovitz, S. Krizek, R. J. Atmatzidis, D. X. (1989), "Injection of fine sands with very fine cement grout", *J. Geotech. Eng.* 115(12), 1717–1733

Zelic, J., Radovanovic, I. and Jozic, D. (2006), "The Effect of Silica Fume Additions on the Durability of Portland Cement Mortars Exposed to Magnesium Sulfate Attack "